Stony Brook University

The Involvement of Metal Ions in Alzheimer's Disease Pathology and Implications for Diagnosis and Treatment

A Dissertation Presented

by

Andreana Charlotte Leskovjan

to

The Graduate School

in Partial Fulfillment of the

Requirements

for the Degree of

Doctor of Philosophy

in

Biomedical Engineering

Stony Brook University

December 2009

Stony Brook University

The Graduate School

Andreana Charlotte Leskovjan

We, the dissertation committee for the above candidate for the

Doctor of Philosophy degree, hereby recommend

acceptance of this dissertation.

Lisa M. Miller, Ph.D – Dissertation Advisor
Biophysicist, National Synchrotron Light Source, Brookhaven National Laboratory

Terry Button, Ph.D – Chairperson of Defense
Associate Professor, Departements of Biomedical Engineering and Radiology

Helene Benveniste, M.D., Ph.D
Professor and Vice Chair for Research, Department of Anesthesiology

Antonio Lanzirotti, Ph.D
Senior Research Associate, Consortium for Advanced Radiation Sources, University of Chicago

This dissertation is accepted by the Graduate School

Lawrence Martin
Dean of the Graduate School

Abstract of the Dissertation

The Involvement of Metal Ions in Alzheimer's Disease Pathology and Implications for Diagnosis and Treatment

by

Andreana Charlotte Leskovjan

Doctor of Philosophy

in

Biomedical Engineering

Stony Brook University

2009

Alzheimer's disease (AD) is an irreversible neurodegenerative disorder and is by far the most prevalent form of dementia in the U.S. Physically, it is characterized by cortical atrophy, neurodegeneration, and the accumulation of neurofibrillary tangles and amyloid beta (Aβ) plaques in the cortex and hippocampus. Imbalances of metal ions such as iron (Fe), copper (Cu), and zinc (Zn), which are present in the brain normally, have also been observed in AD brain, but the role of metal ions in the manifestation of the disease remains unclear. Therefore, the goal of this dissertation was to determine how metal homeostasis in the hippocampus, cortex, and in amyloid plaques is affected in a PSAPP transgenic mouse model of plaque formation in AD as a function of age.

We examined plaques in PSAPP at four time points representing four stages of plaque formation in AD, from pre-AD to late-AD. Results showed that Cu and Fe were not elevated in the mouse plaques at any time point, but were elevated in Zn at the late-AD time point. This is in contrast to endstage human AD plaques, which were enriched in all metals, but especially Cu. Since Cu can be neurotoxic, this finding may explain the lack of severe neurodegeneration in PSAPP mice that is a signature of human AD.

We then examined the metal ion content in the cortex and hippocampus, two regions affected by plaque formation in human AD, in PSAPP mice as they aged.

Results showed that in both the hippocampus and cortex Zn was elevated only at the late-AD time point. Since the plaques were also elevated in Zn only at the late-AD time point, this implies that Zn is not involved in plaque formation, but could hold a protective role.

Interestingly, even though Fe was absent from the PSAPP plaques, the Fe content in both the cortex and hippocampus was increased from early time points. Thus, the lack of Fe in plaques implies that the elevated Fe observed in non-plaque tissue arises not from an interaction with Aβ, but from some other mechanism. For example, increased Fe could result from disruption in the expression of other brain Fe regulatory, transport, or storage proteins. Since excess Fe can contribute to lipid peroxidation and damage to unsaturated lipids in the brain, we also examined the unsaturated lipid content of the hippocampus. We found that the changes in Fe content in the hippocampus were accompanied by reduced unsaturated lipid content in hippocampal white matter, which may be evidence for lipid peroxidation.

Taken together, these results suggest that early increases in Fe and damage to white matter reflect pathological changes related to plaque formation in PSAPP mice and that Fe deposition could be a promising biomarker to predict early plaque deposition. Moreover, the absence of Cu and Fe in PSAPP plaques, which are abundant in human plaques, provides a solid path to follow for future research to identify target for drug development or metal-targeted therapy.

TABLE OF CONTENTS

List of Abbreviations ..... *viii*
List of Figures ..... *x*
List of Tables ..... *xii*
Acknowledgements ..... *xiii*
Publications ..... *xv*

CHAPTER 1 ..... **1**

INTRODUCTION **1**

1.1 ALZHEIMER'S DISEASE 1
1.2 NEUROPATHOLOGY OF AD 2
1.3 GENETICS OF AD 3
1.4 HYPOTHESES ON THE CAUSES OF AD 4
1.5 Aβ STRUCTURE CHARACTERIZATION 5
1.6 POLYUNSATURATED FATTY ACIDS AND OXIDATIVE STRESS IN AD 6
1.7 INVOLVEMENT OF METAL IONS IN AD 7
1.8 TRANSGENIC MOUSE MODELS OF AD 9
1.9 OVERVIEW OF METHODS 10
1.9.1 Fourier Transform Infrared Imaging (FTIRI) *10*
1.9.2 Synchrotron X-ray Fluorescence Microscopy (XFM) *12*
1.9.4 Mice *12*
1.9.5 Euthanization *13*
1.9.6 Cryosectioning *13*
1.9.7 Thioflavin S *13*
1.10 SPECIFIC AIMS AND HYPOTHESES 14
1.10.1 Specific Aim 1: Metal Ion Content in PSAPP Plaques and Cortex as a Function of Aging and Relation to Human AD *14*
1.10.2 Specific Aim 2: Characterization of Metal Ion Content and Unsaturated Lipid in the Hippocampus of PSAPP Mice *15*

CHAPTER 2 ..... **17**

INCREASED BRAIN IRON IS INDICATIVE OF EARLY PLAQUE FORMATION IN AN ALZHEIMER'S DISEASE MOUSE MODEL **17**

2.1 ABSTRACT 17
2.2 INTRODUCTION 18
2.3 MATERIALS AND METHODS 19
2.3.1 Sample Preparation *19*

2.3.2 Synchrorton XFM *20*
2.3.3 Metal Content in Amyloid Plaques *20*
2.3.4 Statistical Analysis *21*
2.4 RESULTS 22
2.5 DISCUSSION 24
2.6 ACKNOWLEDGEMENTS 27

CHAPTER 3 28

AMYLOID PLAQUES IN PSAPP MICE BIND LESS METAL THAN PLAQUES IN HUMAN ALZHEIMER'S DISEASE 28

3.1 ABSTRACT 28
3.2 INTRODUCTION 29
3.3 MATERIALS AND METHODS 31
3.4 RESULTS 34
3.5 DISCUSSION 37
3.6 ACKNOWLEDGMENTS 41

CHAPTER 4 42

IRON, COPPER, AND ZINC IN THE HIPPOCAMPUS OF PSAPP MICE DURING THE PROGRESSION OF ALZHEIMER'S DISEASE 42

4.1 ABSTRACT 42
4.2 INTRODUCTION 43
4.3 MATERIALS AND METHODS 45
4.3.1 Sample Preparation *45*
4.3.2 Syncrhrotron XFM *46*
4.3.3 Data Analysis *47*
4.4 RESULTS 47
4.5 DISCUSSION 50
4.6 ACKNOWLEDGMENTS 54

CHAPTER 5 58

UNSATURATED LIPID CONTENT IS REDUCED IN THE HIPPOCAMPUS OF THE PSAPP TRANSGENIC MOUSE MODEL OF ALZHEIMER'S DISEASE 58

5.1 ABSTRACT 58
5.2 INTRODUCTION 59
5.3 MATERIALS AND METHODS 60
5.3.1 Tissue Preparation *60*
5.3.2 Fourier Transform Infrared Imaging (FTIRI) *61*
5.3.3 Separating Histological Structures of the Hippocampus *62*

5.3.4 Principal Components Analysis *62*
5.3.5 Integration Profiles *63*
5.4 RESULTS 63
5.5 DISCUSSION 67
5.6 ACKNOWLEDGMENTS 70

CHAPTER 6 ..... **71**

DISCUSSION, CONCLUSIONS, AND OUTLOOK **71**

6.1 IRON AND ZINC HOMEOSTASIS IN THE BRAIN 71
6.2 THE INVOLVEMENT OF METAL IONS IN AD 73
6.3 IMPLICATIONS FOR DIAGNOSIS AND TREATMENT 75
6.4 LIMITATIONS 76
6.5 CONCLUSION AND FUTURE DIRECTIONS 77

REFERENCES **80**

LIST OF ABBREVIATIONS

8-OHG	8-hydroxyguanosine
Aβ	Amyloid beta
Aβ40	Amyloid beta (1-40) fragment
Aβ42	Amyloid beta (1-42) fragment
AD	Alzheimer's disease
AFM	Atomic force microscopy
ANOVA	Analysis of variance
APOE	Apolipoprotein E
APP	Amyloid precursor protein
APS	Advanced Photon Source
BLAF	Brookhaven Laboratory Animal Facility
BNL	Brookhaven National Laboratory
Ca	Calcium
CA	Cornu ammonis
CaF_2	Calcium fluoride
CD	Circular dichroism
CNT	Control
CP	Choroid plexus
Cu	Copper
DG	Dentate gyrus
DHA	Docosahexaenoic acid
EM	Electron microscopy
Fe	Iron
FTIRI	Fourier transform infrared imaging
FTIRM	Fourier transform infrared microspectroscopy
H_2O_2	Hydrogen peroxide
HCA	Hierarchical cluster analysis
HNE	4-hydroxy-2-neonenal
IACUC	Institutional Animal Care and Use Committee

i.p.	Intraperitoneal
IR	Infrared
MCT	Mercury cadmium telluride
MRI	Magnetic resonance imaging
NFT	Neurofibrillary tangle
NMR	Nuclear magnetic resonance
NSLS	National Synchrotron Light Source
PBS	Phosphate buffered saline
PCA	Principal components analysis
PCL	Pyramidal cell layer
PIXE	Proton induced X-ray emission
PS	Presenilin
PSAPP	B6C3-Tg(APP_{swe},PSEN1dE9) 85Dbo/J (mouse model)
PUFA	Polyunsaturated fatty acid
ROI	Region of interest
ROS	Reactive oxygen species
SRM	Standard reference material
XAS	X-ray absorption spectroscopy
XFM	X-ray fluorescence microscopy
Zn	Zinc
ZnT	Zn transporter

LIST OF FIGURES

Figure 2.1 Fe (A), Cu (B), and Zn (C) content in non-plaque tissue in PSAPP mice (red bars) and CNT mice (blue bars). * = significantly different from 13 week-old PSAPP mice ($p < 0.05$); # = significantly different from CNT mice at the same time point ($p < 0.05$).

Figure 2.2 Thioflavin S-stained PSAPP mouse brain tissue and corresponding XFM images of Fe, Cu and Zn in plaques and surrounding non-plaque tissue. Units are mM. All scale bars are 25 μm.

Figure 2.3 (A) Ratio of metal content in plaque to non-plaque tissue. (B) Ratio of metal content in plaque to non-plaque tissue normalized to protein density. * = significantly different from 40 week-old mice ($p < 0.05$).

Figure 3.1 (A) Thioflavin S-stained PSAPP mouse brain tissue showing three plaques. (B) Infrared image of the same tissue showing the distribution of protein measured by the Amide II band. (C) Infrared spectra collected from the areas marked with asterisks in (A) and (B), showing the relative amount of protein in the center of a plaque (black) and the surrounding tissue (red). All scale bars are 5 μm.

Figure 3.2 (A) Thioflavin S-stained PSAPP mouse brain tissue, also shown in Fig. 1. XFM images of (B) Zn, (C) Cu, (D) Fe, and (E) Ca distribution in the same tissue. (F) XFM spectra collected from the areas marked with asterisks in (A) – (E), comparing the center of a plaque (black) to the surrounding tissue (red). All scale bars are 5 μm.

Figure 4.1 (A) Light micrograph of an unstained hippocampal brain section from a PSAPP mouse. XFM images of Fe (B), Cu (C), and Zn (D) in the same tissue section. Units are mM. Scale bar = 300 μm. (E) Hierarchical cluster analysis defining four distinct regions of the hippocampus based on metal content where the CA/DG is green, the PCL is blue, CA3 is turquoise, and the hilus is magenta. The yellow area corresponds

to the CP and was acquired manually.

Figure 4.2 Fe in the full hippocampus (A), CA/DG (B), the PCL (C), and the hilus (D) as a function of aging in PSAPP and CNT mice. (E) Zn in the hilus as a function of aging in PSAPP and CNT mice. * = PSAPP mice significantly different from 13 week-old PSAPP mice ($p < 0.01$). ** = PSAPP mice significantly different from 24 week-old PSAPP mice ($p < 0.01$). # = PSAPP mice significantly different from CNT mice at the same time point ($p < 0.01$).

Figure 5.1 (A) Light micrograph of an unstained hippocampal brain section from a PSAPP mouse. (B) Hierarchical cluster analysis defining three distinct regions of the hippocampus based on lipid content where the axonal layer is red, the somatic layer is green, and the dendritic layer is blue. Scale bar = 500 μm. (C) Average spectrum from each of the three regions illustrating differences in lipid content when normalized to protein content. Important peak frequencies are indicated. Inset shows the olefinic =CH stretching region (3012 cm^{-1}) from the axonal layer spectrum.

Figure 5.2 (A) Scores plot of average axonal layer spectra from 56 week-old PSAPP and CNT animals; (B) PC1 loadings of average axonal layer spectra from 56 week-old PSAPP and CNT animals.

Figure 5.3 Olefinic content as a function of age in CNT mice (top row) and PSAPP (bottom row) in the axonal layer. Red indicates very high olefinic content while purple represents very low olefinic content. * = median is significantly different from 13 and 24 week-old CNT mice ($p < 0.01$); ** = median is significantly different from CNT mice at the same time point ($p < 0.01$).

LIST OF TABLES

Table 3.1 Relative Metal and Protein Content in PSAPP AD Plaques

Table 3.2 Relative Metal and Protein Content in Human AD Plaques

Table 5.1 Fe Content in PSAPP and CNT Mice

Table 5.2 Cu Content in PSAPP and CNT Mice

Table 5.3 Zn Content in PSAPP and CNT Mice

ACKNOWLEDGEMENTS

It is my pleasure to acknowledge the wonderful people who have contributed to this dissertation over the years and who made completion of this work possible.

I would like to thank my advisor, Dr. Lisa Miller, for giving me the opportunity to conduct research in her laboratory, which allowed me to earn a PhD. Lisa not only provided excellent guidance, caring, and support, but also taught me how to question thoughts and express ideas. Her expert suggestions and commentary on everything I did and wrote made my work light years better. I am grateful to her for holding me to a high research standard and for teaching me how to do research.

Next, I would like to thank Dr. Tony Lanzirotti, without whom I would have gone insane. His patience, support, and friendship helped me to overcome many crisis situations and to finish this dissertation. I am also deeply grateful to him for the long discussions that helped me sort out the technical details of my work. I hope that one day I would become as good a mentor to my students as Tony has been to me.

I would also like to thank the other members of my dissertation committee, Dr. Terry Button and Dr. Helene Benveniste, who have provided critical insight and commentary, making sure everything I proposed to do was relevant and made sense.

I am indebted to Dr. Ariane Kretlow, a friend and former colleague, who inspired me to come up with most of the experiments in this work. Without her, finishing this dissertation would have been much more difficult.

My labmates in the Miller Research group, Alvin Acerbo, Imke Bodendiek, Megan Bourassa, Meghan Faillace, Randy Smith, and Ryan Tappero have provided non-stop support for everything. Whether it was assistance on experiments or listening to my complaining, they always took time out of their busy schedules to help me. Thanks also to my other NSLS/BME colleague, Matt Engel, who also came around to check on my progress.

I am also thankful to many people who enabled me to do my experiments: Bill Rao at NSLS Beamline X26A, Dr. Stefan Vogt at APS Beamline 2IDE, Dr. Raul Barrea at APS Beamline 18IDE, and Dr. Matt Newville at APS Beamline 13IDD for helping me before and after all of my beamtimes and for numerous other things in between. Also, to

Dr. Avraham Dilmanian for donating mice for my very critical pilot experiments; to Janelle Collins for helping me with the euthanizations, which she did with much kindness and respect to the mice; to Dr. Andrew Gifford for allowing me to use his laboratory and supplies; and, to the Brookhaven Animal Facility staff for providing my mice with a happy lab mouse life.

I could not have survived all these years without the support and understanding of all of my friends. Thank you so much especially to Kelly Bassett (who meticulously edited this dissertation), Dwan Gerido, Yu Xian Chen, Nikita Airen, Bjorg Larson, Sanjee Abeytunge, Angela Kim, and Sanjay Senanayake for providing hilarious moments, alcoholic beverages, Sunday football-watching marathons, shopping trips, gourmet cooking, and multiple reality checks which kept me in line and semi-normal. Thank you for still being my friends even though I've been a dud for the last few years! I promise to make it up to you. Thank you to many other friends who I don't see very much anymore, but still think about often. Thanks also to my volleyball girls, for lots of fun on Wednesdays and other days, and to my poker buddies for some extra cash.

Most importantly, none of this would have been possible without my family: my parents, Kathryn and Larry, have been a constant source of love, concern, support and strength all these years. I appreciate everything they have ever done for me; my brother, Mark, for being annoying, yet caring and willing to do what he can for me; and my boyfriend, Marco. His tolerance of my occasional bad moods is a testament in itself of his unyielding devotion and love. You mean more to me than I can express and you have made my life very special.

PUBLICATIONS

1. **Leskovjan, A.C.**, Kretlow, A., Miller, L.M. (2009). Unsaturated lipid content is reduced in the hippocampus of the PSAPP transgenic mouse model of Alzheimer's disease. *Analytical Chemistry*. (Submitted).

2. **Leskovjan, A.C.**, Lanzirotti, T., Miller, L.M. (2009). Amyloid plaques in PSAPP mice bind less metal than in human Alzheimer's disease. *NeuroImage*. 47, 1215-1220.

3. Zhong, Z., Bennett, D., Chapman, D., Chen, J., Connor, D., Dilmanian, A., Faulconer, L., Kao, T., **Leskovjan, A.C.**, Li, J., Liu, T., Miller, L.M., Muehleman, C., Parham, C., Pisano, E., Wu, A. (2008). Probing Alzheimer's Disease Pathology and Early Detection at the NSLS with Infrared, XRF, and DEI. *Synchrotron Radiation News*. 21, 11-16.

4. Zhang, L., Samaras, D., Alia-Klein, N., Tomasi, D., Cottone, L., **Leskovjan A.**, Volkow, N., Goldstein, R. (2005). Exploiting temporal information in functional magnetic resonance imaging brain data. *MICCAI*. 8, 679-687.

5. Goldstein, R.Z., Alia-Klein, N., **Leskovjan, A.C.**, Fowler, J.S., Wang, G.J., Gur, R.C., Hitzemann, R., Volkow, N.D. (2005). Dissociation of the lateral and medial orbitofrontal gyrus in cocaine addiction: involvement in anger and sadness. *Psychiatry Research: Neuroimaging*. 138, 13-22.

6. Goldstein, R.Z., **Leskovjan, A.C.**, Volkow, N.D., Hitzemann, R., Bashan, F., Khalsa, S.S., Wang, G.J., Fowler, J.S., Hoff, A.L. (2004). Severity of neuropsychological impairment in cocaine addiction: association with metabolism in the brain reward circuit. *Neuropsychologia*. 42, 1447-1458.

CHAPTER 1

INTRODUCTION

1.1 ALZHEIMER'S DISEASE

Alzheimer's disease (AD) is an irreversible, progressive neurodegenerative disorder affecting approximately 4.5 million Americans and is by far the most prevalent form of dementia [1]. Clinically, it is characterized by memory loss, changes in personality and behavior, cognitive decline, and eventually death [2]. Physically, it is characterized by cortical atrophy, cellular degeneration, neuronal loss, and the presence of intracellular neurofibrillary tangles and extracellular amyloid plaques [2, 3]. Despite significant advances in understanding the molecular mechanisms of the disease, the cause, a cure, or even a conclusive pre-mortem diagnosis, remains elusive.

AD is the third most common cause of death and the most common cause of dementia among people age 65 years and older with 3% prevalence for those 65-74 years old, 18.7% for those 75-84 years old, and 47.2% for those over 85 years old [4-6]. As a direct consequence of improved life expectancy and current trends, by 2050, an estimated 13 million Americans will be diagnosed with AD [7]. In addition, patient care is estimated to be over $100 billion [8] with individual costs estimated at $174,000, according the Alzheimer's Association. Thus, its effect on the individual as well as their families and the health system is devastating.

AD begins slowly with mild forgetfulness and loss of interest, energy, and ability to make decisions. During the mild stages of the disease, memory loss and confusion become more apparent, behavior may become inappropriate, and assistance to complete certain tasks may be required. At the final stage of the disease, the individual loses all ability to care for themselves and needs total assistance for daily activities. People with AD live an average of 8 years after diagnosis but may survive up to 20 years. Currently, diagnosis of AD is made by clinical, neuropsychological, and neuroimaging assessments

showing impairment in memory and cognitive decline and the absence of other diagnoses. However, these approaches are only 90% accurate in the mid- or late-stages of the disease [2]. A definitive diagnosis of AD must await microscopic examination of the brain upon autopsy.

There is no cure for AD and the only treatments available are palliative and aim to improve cognitive and behavioral symptoms associated with AD. Currently, four cholinesterase inhibitors have been approved for the symptomatic treatment of AD: tacrine (rarely prescribed now), donepezil, rivastigmine, and galantamine. These drugs work by blocking the breakdown of acetylcholine, a neurotransmitter important to cognitive function. Memantine, an NMDA receptor antagonist, works by inhibiting glutamate activity and has also been approved for the treatment of moderate to severe AD. However, none of these medications halt, delay, or reverse AD and appear to be effective only for about 6 months to a year.

1.2 NEUROPATHOLOGY OF AD

The primary neuropathological features of AD are gross cortical atrophy, widespread cellular degeneration, neuronal loss, and the presence of neurofibrillary tangles (NFTs) and amyloid plaques, found mainly in the hippocampus, entorhinal cortex, and some areas of the neocortex [3, 9]. Various other disorders are also characterized by NFTs (Kuf's disease, frontotemporal dementia) and amyloid plaques (Down's syndrome, Creutzfeldt-Jakob disease), but it is the appearance of both features that define AD. Although, the mechanism for the development of these abnormalities is unknown, they are presumed to be responsible for neuronal death and loss of brain function [10].

NFTs are composed of a protein called tau, a normal constituent in microtubules, which provides support and shape to cells and also transport routes for nutrients and other cellular components. In AD, tau is abnormally phosphorylated to form NFTs, which are most apparent in the hippocampus [2]. Though not always directly correlated to amyloid plaque burden, recent research has shown that NFTs may be related to severity of dementia, suggesting an integral role in AD [11]. It has also been shown that hyperphosphorylated forms of tau can aggregate and prevent binding to microtubules, leading to degradation of the cytoskeleton and neuronal death [12].

Amyloid plaques are primarily composed of a small 39-43 amino acid protein called amyloid beta (Aβ), which is derived from the proteolytic cleavage of a larger transmembrane glycoprotein, the amyloid precursor protein (APP), by β and γ secretases [3]. β-secretase first cleaves APP extracellularly, forming the N-terminus, and γ-secretase then cleaves APP in the intramembrane domain, creating the C-terminus. The two most frequently produced peptides are Aβ40, composed of 40 residues and found mostly in cerebrospinal fluid and vasculature, and Aβ42, composed of 42 residues and the main component of amyloid plaques [13]. However, both Aβ40 and Aβ42 are capable of aggregation, but through different pathways [14]. One suggestion is that Aβ42 is deposited first as diffuse plaques, which then acts as a seed for Aβ40 accumulation [15].

Another protein, apolipoprotein E, has also been shown to be involved in AD and interacts directly with Aβ. While in its normal form it protects against oxidative damage and is involved in neuronal repair mechanisms [16]. The presence of the ε4 allele, accounting for 15% of all allelic variants, has been shown to increase the risk of AD by four times [2, 17] and is also associated with increased risk of cell death [18].

1.3 GENETICS OF AD

Most AD cases occur sporadically and develop after age 60, but about 5% of cases are early-onset and develop before age 60. Though far less common, the early-onset form shows strong genetic linkage and could provide insight into disease etiology [19]. To date, mutations in three genes have been linked to familial autosomal dominant AD: the APP gene, the presenilin 1 (PS1) gene, and the presenilin 2 (PS2) gene [20]. Apolipoprotein E (ApoE) with the ε4 allele has been identified as a genetic risk factor for late-onset sporadic AD [17]. All four of these genes have been linked to increased production and accumulation of Aβ peptides, even before AD symptoms arise [3].

The function of APP is not known, but a significant amount of work suggests a role in cell signaling copper homeostasis [21, 22]. Mutations of the APP gene are located either before the β-secretase cleavage site, after the α-secretase cleavage site, or near the γ-secretase site, demonstrating a direct effect on APP processing and Aβ formation [3]. For example, the “Swedish” mutation occurs at the two amino acids immediately before

the β-secretase cleavage site and makes APP a better substrate for β-secretase. This decreases APP processing by the α-secretase pathway and increases production of both Aβ40 and Aβ42 [3].

Presenilin knock-out mice have shown that the presenilin protein is involved in γ-secretase activity [23] and could actually be γ-secretase itself [24]. Mutations in the PS1 and PS2 genes occur on chromosomes 14 and 1, respectively [25] and the earliest and most aggressive form of AD is thought to be caused by PS1 mutations [3]. These mutations lead to subtle changes in γ-secretase cleavage specificity that increases Aβ42 production.

ApoE is normally a lipid carrier protein involved in the transport of cholesterol and phospholipids. The ApoE gene is encoded on chromosome 19 and exists in three allelic variants. The ε4 variant is thought to be a major genetic risk factor for the more common late-onset AD and may also be involved in oxidative damage in the brain [17, 26]. It is thought that this isoform enhances the deposition of Aβ, particularly Aβ40, in the cerebral cortex as well as the microvasculature [3].

1.4 HYPOTHESES ON THE CAUSES OF AD

Although, the exact cause of AD is unknown, a number of theories have been proposed to explain the pathogenesis of AD. The *Amyloid Cascade Hypothesis* [27, 28] is the dominant theory and states that the pathological changes observed in AD, such as synaptic dysfunction, microgliosis and inflammation, and neuronal loss are a result of aberrant APP processing which leads to an imbalance between the production and removal of Aβ [2]. This theory has been supported by genetic data indicating that four different genes associated with Aβ production are involved in the pathology of AD [29]. These include APP gene mutations on chromosome 21, presenilin 1 and 2 mutations on chromosomes 14 and 1, respectively [25, 30], which all lead to increased levels of Aβ in the brain [2]. In addition, individuals with Down's syndrome also develop amyloid plaques and exhibit AD-like pathology [31].

More recently, the *Dual Pathway Model* was introduced [32], which suggests an additional mechanism linking Aβ and tau in late-onset AD. Specifically, it is

hypothesized that common upstream drivers cause both elevation in Aβ and tau hyperphosphorylation through independent but parallel mechanisms.

Finally, the *Metals Hypothesis of Alzheimer's Disease* describes a theory in which it is the interaction of Aβ with specific metal ions, such as Cu and Zn, that drives Aβ toxicity and AD pathogensis [33].

1.5 Aβ Structure Characterization

The formation of Aβ, even the deposition of diffuse plaques, is a normal cellular process, but in AD the peptide misfolds and aggregates to form dense plaques in specific regions of the brain [2]. Exactly how and why this misfolding occurs is still unknown. It was initially assumed that insoluble Aβ fibrils were the neurotoxic agent in AD [34]. Although all Aβ fibrils and their precursors are assumed to be toxic to some extent, diffusible, soluble Aβ oligomers rich in β-sheet, but not monomers or insoluble fibrils, have been shown to be most toxic to cultured neurons and are thought to be responsible for the neurotoxicity and synaptic dysfunction present in AD [35, 36]. However, the inhomogeneity and metastable nature of the Aβ species makes identification of pathogenic states difficult [37].

Aβ structure characterization has primarily been accomplished through the use of electron microscopy (EM) and atomic force microscopy (AFM). EM has shown that amyloid fibrils are composed of multiple protofibrils wrapped around each other, forming a crossed beta-pleated sheet [38]. Recently, high resolution AFM was used to characterize Aβ42 dimers and tetramers [39]. This study proposed a model in which the Aβ monomer is a β-hairpin, which forms dimers with dimensions of 2 nm x 6 nm x 1 nm by inter-strand hydrogen bonding. However, nearly all studies investigating the structure of Aβ fibrils are done *in vitro* and it is widely accepted that the solution conditions are critical to the experiment. This means that Aβ acquires different structures depending on the solution environment [40-42]. In addition, although the fibril structure has been well characterized, the mechanism of the conformational transition is not fully understood and it is also still not known what the role of each Aβ assembly is *in vivo* [43].

Other studies have shown how pH can affect the structure of Aβ. For example, Aβ40 forms tetramers and dimers at physiological pH, while at pH 5 it forms protofibrils and fibrils [44]. This suggests the role of an acidic environment in the brain in AD.

1.6 Polyunsaturated Fatty Acids and Oxidative Stress in AD

Polyunsaturated fatty acids (PUFAs) synthesized from ω-3 and ω-6 essential fatty acids are key structural components of phospholipid membranes and are critical for brain growth, membrane fluidity, signal transduction, and visual and cognitive development [45]. Normal brain function depends on maintaining homeostatic concentrations of PUFAs both during development and throughout life [45]. However, impairments in PUFA metabolism have been implicated in many neurological diseases, including Alzheimer's disease (AD). For example, blood levels of the ω-3 PUFA docosahexaenoic acid (DHA) were found to be lower in AD patients compared to control subjects without cognitive impairment [46]. Levels of DHA and arachidonic acid in the brains of AD patients were also shown to be lower than in control patients [47]. Furthermore, lower levels of DHA were associated with the loss of post-synaptic proteins in dendrites in a transgenic mouse model of AD [48]. DHA also reduced amyloid burden in cell culture [49] and in transgenic mouse models of AD [50, 51], possibly by inhibiting the amyloidogenic pathway or by upregulating Aβ clearance mechanisms.

The brain is particularly vulnerable to oxidative attack because it has a high rate of oxygen consumption, it contains a relatively poor level of antioxidants, and neuronal cell membranes are enriched in polyunsaturated lipids, which are readily attacked by free radicals, becoming oxidized into lipid peroxides [52]. Both *in vitro* and *in vivo* studies have shown that oxidative stress to neurons induced by reactive oxygen species (ROS) such as hydrogen peroxide, nitric oxide, superoxide, and hydroxyl radicals, is presumed to be a key event in the pathology of AD and might contribute to amyloidogenesis and neuronal degeneration. In fact, oxidative damage is one of the earliest events in AD [53]. Oxidative stress in AD is demonstrated by increases in protein oxidation marked by elevated protein carbonyls and nitrotyrosine; lipid peroxidation, marked by elevated levels of thiobarbituric acid, isoprostanes, and 4-hydroxy-2-neonenal (HNE); DNA and RNA oxidation marked by increased 8-hydoxy-2-deoxyguanosine and 8-

hydroxyguanosine (8-OHG); sugar modification, marked protein glycation and glycoxidation; and reactive oxygen species formation [54, 55]. Lipid membrane peroxidation is caused by the conversion of the superoxide anion to hydrogen peroxide, inducing continuous cellular damage over time [56]. Damage to lipid membranes is highly correlated with amyloid plaque and NFT formation in AD [57]. Oxidative stress may also contribute to Aβ accumulation by generating modified Aβ species prone to aggregate and resistant to clearance [56, 58-60]. On the other hand, plaque formation may be a protective response to free radical generation and serve to trap reactive products of oxidative stress [55].

Neuronal damage and death can also induce glial activation and a localized, detrimental cycle of neuroinflammation by the release of toxic products by these cells, including reactive oxygen species [61, 62]. Immunohistochemical studies have revealed clusters of activated microglia located around amyloid plaques [63] and similar results were found in Tg2576 and APP23 transgenic mice [64, 65]. Soluble Aβ itself has also been shown to induce reactive alterations in astroglial cells, which causes secretion of inflammatory cytokines [66].

1.7 Involvement of Metal Ions in AD

Metal ions such as iron (Fe), copper (Cu), and zinc (Zn), are present in the body under normal conditions, but are increased in regions of the brain involved in AD [67, 68]. It is thought that metal imbalance is involved in protein misfolding and leads to oxidative damage and neuron degeneration, however the exact mechanism remains unknown [69]. *In vitro* experiments have shown that Aβ possesses specific binding sites for Zn, Cu, and to a lesser extent, Fe [70-73] although only Zn and Cu co-purify with Aβ extracted from human AD brain [74]. Metal binding to Aβ may increase toxicity and tendency to form plaques [67, 72, 75-77]. High-affinity binding of Cu^{2+} to Aβ42 has been shown to slowly modify the peptide and promote precipitation [78]. Interestingly, this same study also showed that while most proteins lose metal ions with decreasing pH, Aβ accepts Cu^{2+} under mildly acidic conditions and can displace Zn^{2+}, which loses affinity at low pH, suggesting a combined role of Cu^{2+} and acidic environments in the pathophysiology of AD. In addition, there is evidence that Aβ42 promotes oxidative

lipid damage in the presence of Cu [79] and this may initiate the misfolding of Aβ [80], increasing its neurotoxic effects [59].

It is also thought that metal dyshomeostasis is involved in the oxidative stress mechanism of Aβ, induced by peroxide formation and causing neuron degeneration in AD [81]. Cu^{2+} and Fe^{3+} are strongly redox-reactive and generate hydroxyl radicals, via Fenton chemistry, and peroxide (H_2O_2) species, via the Haber-Weiss reaction, upon the interaction with Aβ, which may cause oxidative stress [82]. One study has demonstrated that Aβ42 promotes oxidative lipid damage in the presence of Cu, which in turn induced misfolding and fibrillization of Aβ42 [79]. Another study suggested that RNA oxidation of vulnerable neurons, marked by 8-OHG production, is caused by hydroxyl radicals, formed from a reaction of H_2O_2 with reduced Cu or Fe bound to nucleic acid bases [83]. On the other hand, another study determined that Zn inhibits H_2O_2 production from Aβ42 by competing with Cu^{2+} for a redox-active binding site on the Aβ peptide and preventing its reduction [59]. Antioxidant properties of Aβ have also been suggested. For example, amyloid plaque density in the cerebral cortex was found to be inversely correlated to levels of 8OHG, indicating that diffuse plaque formation may be a response to reduce oxidative stress [59]. In cell culture, monomeric, but not oligomeric, forms of Aβ40 have been shown to have a protective effect against neuronal death caused by reduction of Cu and Fe [84].

There are two ways in which metal ions can bind Aβ, either intermolecularly or intramolecularly, and different structural models involving different numbers of histidine residues have been suggested [85]. Recently, it was found that Cu is bound via the histidine imidazole rings in isolated senile plaques using Raman spectroscopy [86]. Later, using nuclear magnetic resonance (NMR) it was found that Cu^{2+} specifically binds to the N terminus of Aβ and the imidazole rings of His^{6}, His^{13}, and His^{14} [87].

Another recent NMR study showed that Zn shares the same binding sites on Aβ as Cu [70]. However, Zn also has a concentration-dependent effect, either increasing aggregation at high concentrations, or decreasing it at low concentrations [88, 89]. In contrast to Cu, the ability of Aβ to bind Zn also appears to be pH dependent; while Zn can easily bind to Aβ under physiological conditions, no binding occurs under acidic

conditions [90]. This provides evidence of a pathogenic mechanism in which Zn may protect against Cu-induced toxicity under physiological conditions, but this protection is reduced under acidic conditions [91]. On the other hand, some studies have indicated a deleterious role of Zn, causing rapid aggregation of Aβ [77]. Thus, the functional relationship of metal ions and misfolded Aβ species is not clear.

In vivo, Zn ions are released into the neocortex during neurotransmission by glutamatergic neocortical fibers, achieving extracellular concentrations of 300 μM, while Cu is released by hippocampal neurons at about 15 μM [92]. In AD plaques, concentrations of up to 0.4 mM Cu and 1 mM Fe and Zn have been observed [68]. Studies involving Swedish mutant APP transgenic mice have shown that Zn is elevated in dense senile plaques and similar results were found in end-stage human AD plaques [93-95]. Elevated Zn has also been found in the cortex [96]. However, other studies have found decreased levels of Zn and Cu in AD brains [97, 98]. Like the *in vitro* studies, the effect of these metal ions is also not clear and several studies have indicated conflicting results for the roles of different metal ions. For example, some studies have suggested that Cu, Fe, and Zn are toxic and increase the aggregation potential of Aβ [76, 96]. Other studies have shown a protective role for Zn, possibly quenching Aβ activity in cell culture [59] and that Cu can reduce Aβ levels in transgenic mice [99]. But the question of whether the metals accumulate first, followed by amyloid production or vice versa still remains.

1.8 TRANSGENIC MOUSE MODELS OF AD

Transgenic animal models have become important research tools because they can provide insight into the pathological and biochemical processes involved in the pathogenesis of AD and also into the effectiveness of possible treatments. Although the fruit fly (*Drosophila melanogaster*), the nematode (*Ceanorhabditis elegans*), and the sea lamprey (*Petromyzon marinus*) are commonly used invertebrate model organisms in studies of AD, mice are more accurate reproductions of AD pathology and have a more similar brain anatomy to other mammals [100]. Various transgenic mouse models that express one or more mutant forms of human proteins associated with AD, including APP, presenilin, and tau, have been developed [19].

Overexpression of human APP with familial AD-associated mutations in mouse models such as PDAPP, Tg2576, APP23, and TgCRND8 can mimic much of the amyloid pathology seen in AD [19, 101]. These mice develop cognitive deficits and plaque deposition in a pattern similar to human AD at approximately 8-12 months of age. Double transgenic PSAPP mice express a chimeric mouse/human amyloid precursor protein gene (APP695swe) and a mutant human presenilin 1 (PS1) gene and exhibit markedly accelerated amyloid deposition compared to singly transgenic mice, demonstrating the involvement of presenilin 1 in early onset AD [102-104]. However, none of these models develop severe neuronal loss or neurofibrillary tangles. In contrast, neurofibrillary pathology as well as significant neuronal loss has been observed in models such as JNPL3 and rTg4510 through the overexpression of mutant tau transgenes [105, 106]. More recently, a triple transgenic mouse expressing mutant APP, tau, and PS1 transgenes (3×Tg-AD) has been developed [107]. This model accumulates amyloid plaques, neurofibrillary tangles, and synaptic dysfunction in an age-dependent manner. Although neurofibrillary pathology in this model has not yet been fully characterized it is hypothesized that Aβ accumulation can accelerate or initiate tangle formation and that early tau aggregates lead to neurodegeneration [108].

These models have resulted in valuable progress in understanding AD pathology, but have certain limitations because they only partially reproduce the progression, severity, and range of cognitive deficits such as those found in human AD. Moreover, there is no single model that reliably reproduces amyloid plaques, neurofibrillary tangles, and neuronal loss – three key histopathological features of AD. However, the deficits in these mice are greatly beneficial to the understanding of the complex disease mechanisms associated with human AD [109].

1.9 Overview of Methods

1.9.1 Fourier Transform Infrared Imaging (FTIRI)

FTIR spectroscopy is a measurement of the absorbance of infrared light as a function of wavelength in a sample. Depending on the atoms in the molecule, their binding forces, masses and orientation, the molecule will absorb light of specific wavelengths which amplifies the natural characteristic vibrations of the molecule by

stretching, bending, wagging, and/or deforming the bonds. In general, bonds with bending modes vibrate at lower frequencies, bonds to lighter atoms have higher stretching frequencies, and single bonds vibrate at lower frequencies than double or triple bonds. For example, C-O vibrates at ~1100 cm^{-1}; C=O vibrates at ~1650 cm^{-1}; C-C vibrates at ~1400 cm^{-1}; and, C-H vibrates at ~2950 cm^{-1}. The approximate frequency of molecular vibrations can be calculated using Hooke's Law:

$$\nu = \frac{1}{2\pi c}\sqrt{\frac{k}{\mu}},$$

where k is the bond force constant which varies from one bond to another, c is the velocity of light (3 x 10^{10} cm/sec), and μ is the reduced mass given by:

$$\mu = \frac{m_1 m_2}{m_1 + m_2},$$

where m_1 and m_2 are the masses of the two atoms within the bond. The intensity of a peak in an absorption spectrum is directly proportional to its concentration in a sample, as defined by the Lambert-Beer Law:

$$A = \varepsilon \cdot b \cdot c,$$

where A is absorbance intensity, ε is the absorption constant, b is the sample thickness, and c is the concentration. Thus, FTIR can be used to determine the chemical composition of a sample.

An infrared spectrum of a biological sample is composed of characteristic absorption bands originating from all the macromolecules it contains: proteins, lipids, nucleic acids, and carbohydrates. Variations in these molecules can provide important details about the chemistry of diseased states and the utility of FTIRI in studies of biological tissue has been demonstrated [110]. For example, FTIR has been used to detect subtle biochemical changes in diseases such as AD [95], cancer [111], heart

disease [112] bone diseases [113, 114], and multiple sclerosis [115], among others. One of the main advantages of using FTIR for studies of biological tissue is that the quantitative evaluation of multiple chemical components can be examined in intact, native tissue without the use of labels, stains, or dyes which may disrupt cells, damage the tissue, or distort the chemical composition. In addition, unlike other techniques which require tissue homogenization, FTIR is sensitive and non-destructive allowing the chemical composition in different structures within the tissue to be differentiated.

1.9.2 SYNCHROTRON X-RAY FLUORESCENCE MICROSCOPY (XFM)

XFM is a non-destructive method of measuring the elemental composition of a material. The technique relies on the principle of X-ray fluorescence in which an incident photon is absorbed by an atom and inner shell electron is ejected, creating an electron hole. The resulting vacancy is filled by an outer shell electron and the excess energy is emitted as a characteristic X-ray with energy equal to the difference between the energy of the incoming photon and the binding energy of the shell. In most cases the innermost K and L shells are involved in X-ray fluorescence detection. Characteristic X-rays are unique for each element and its intensity is proportional to the concentration of that element in the sample. Using a synchrotron source allows trace metal ion concentration and distribution in the sample to be measured with a resolution of 5-10 μm and a sensitivity of less than 10 ppm (in 30 μm sections). Synchrotron XFM experiments were carried out at beamlines X26A at the NSLS and 18-ID at the Advanced Photon Source (APS), Argonne National Laboratory (Chicago, IL).

1.9.4 MICE

Female B6C3-Tg(APP_{swe}, PSEN1dE9)85 Dbo/J (PSAPP) and age-matched non-transgenic B6C3F1/J control (CNT) mice were obtained from Jackson Laboratory (Bar Harbor, ME). PSAPP mice over-express both human presenilin (PS1) and Swedish mutation amyloid precursor protein (APP_{swe}) and are bred with B6C3F1/J mice to develop amyloid plaques. These double transgenic mice show markedly accelerated amyloid pathology over single transgenic mice, developing plaques at approximately six to seven months of age. PSAPP mice do not develop neurofibrillary tangles or widespread neuronal loss, making them an appropriate animal model to determine the

effect of overproduction and deposition of Aβ on the brain. In this work, PSAPP mice were separated into one of four groups representing four stages of plaque formation in AD: pre-AD (13 weeks) early-AD (24 weeks), intermediate-AD (40 weeks), and late-AD (56 weeks). Age- and gender-matched CNT mice were also used at each time point. All mice were treated in accordance with the guidelines set by the BNL Institutional Animal Care and Use Committee (IACUC protocol #338). The mice were housed at the Brookhaven Laboratory Animal Facility (BLAF) where they underwent no surgeries or experimental procedures until they were euthanized.

1.9.5 EUTHANIZATION

At 13, 24, 40, and 56 weeks of age, the mice were deeply anesthetized with 100 mg/kg 1:10 ketamine:xylazine administered by intraperitoneal (i.p.) injection. Afterwards, they were perfused transcardially with phosphate buffered saline (PBS), resulting in exsanguination and death. Paraformaldehyde or formalin was not used for fixation because it interferes with analysis of oxidative lipid and protein modifications [116] and may denature zinc binding sites, artificially lowering zinc levels [96]. The brains were then surgically removed, placed on dry ice until frozen, and stored at -80 °C until further processing.

1.9.6 CRYOSECTIONING

Sequential coronal sections of each brain were cut with a cryo-microtome (Leica, Germany) at a temperature of -17 °C. Ten micron thick whole brain sections, which include the hippocampus (Bregma: ~-1.28 – -2.12), were mounted on IR-transparent calcium fluoride (CaF_2) slides (Korth Kristalle, Altenholz, Germany) for the FTIR experiments and 30 μm thick cryosections on Ultralene® film (SPEX CertiPrep, Metuchen, NJ) for the XFM experiments. This substrate is free of trace elements that interfere with the XFM measurements and is also sufficiently IR-transparent. All sections were kept in a desiccator until use.

1.9.7 THIOFLAVIN S

Amyloid plaques were visualized with the fluorescent dye, Thioflavin S. Thioflavin is a sulfur-containing fluorescent dye, commonly used to detect amyloid in

tissue sections. Compared to Congo red, crystal violet, and van Gieson, it has been shown to be a superior method for identifying amyloid [117]. Although the specific binding mode of Thioflavin is not known, it has been suggested that it interacts with the specific quaternary structure of the β-pleated sheet fibril and not the monomeric peptides. However, one drawback is that it is not fully specific and may bind other structures such as fibrin or collagen [118]. Fortunately, background staining is minimal and appears to require large arrays of β-sheet structure to bind [119].

1.10 Specific Aims and Hypotheses

Despite significant advancements in understanding the pathogenesis of AD [2, 3, 10], the study of their putative molecular mechanisms is still evolving: the role of metal ion accumulation during disease progression remains unknown and we do not have a complete timeline for these events. To date, the majority of AD studies have been performed on post-mortem human brain tissue and much less is known about the processes that occur throughout the course of the disease. Analysis of earlier stages of AD is necessary in determining the sequence of events that may lead to AD. In addition, most current techniques used to study metal content and chemical composition require tissue homogenization and do not provide spatial information (e.g. inductively coupled plasma [ICP] spectroscopic methods) or are destructive to the sample (e.g. proton induced X-ray emission [PIXE]). Therefore, the goal of this dissertation was to determine how metal homeostasis in the hippocampus, cortex, and in amyloid plaques is affected in a PSAPP transgenic mouse model of AD as a function of age.

1.10.1 Specific Aim 1: Metal Ion Content in PSAPP Plaques and Cortex as a Function of Aging and Relation to Human AD

It is still not well understood how metal affects the brain in earlier stages of AD. From our pilot study investigation of plaques in a 73 week-old PSAPP mouse, we found that Zn and β-sheet content increases towards the center of the plaque, suggesting a specific role of Zn in plaque formation. Cu and Fe were not elevated in the plaques, but may bind earlier or may be elevated in non-plaque cortical tissue. Therefore, **Chapter 2** will address a time-course study using XFM to analyze the metal ion content in PSAPP cortex and plaques at different stages of AD. We hypothesize that dense, mature plaques

will be particularly associated with Zn, while other metal ions may have a different, earlier role and contribute to neurotoxicity or propensity towards aggregation. Moreover, the ability to identify elevations of specific metal ions at early stages of the disease could have implications for prevention, diagnosis, or treatment of AD.

We have also previously shown that endstage human AD is characterized by the accumulation of Fe, Cu, Zn, and Ca that are co-localized with areas of high β-sheet protein and that the concentrations of metal inside the plaque are much higher than outside of the plaque [95]. Transgenic mouse models of AD also exhibit amyloid plaques, but fail to develop the high degree of neurodegeneration observed in humans. It is still unknown how metal content in endstage PSAPP mice compares to human AD plaques or how metal accumulates in plaques throughout the duration of the disease. **Chapter 3** will examine difference between mouse and human plaque that could account for the absence of neurodegeneration. We hypothesize that differences in plaque metal content may explain the differences in neurodegeneration in human and mouse brain.

1.10.2 Specific Aim 2: Characterization of Metal Ion Content and Unsaturated Lipid in the Hippocampus of PSAPP Mice

The hippocampus is one of the first and most severely affected regions of the brain by amyloid pathology in AD [120] and imbalances of metals have also been observed in the hippocampus during AD [121]. For example, Deibel and colleagues [98] found a decrease in Cu, and an increase in Zn and Fe in the hippocampus in AD. However, how metal ion content in specific regions of the hippocampus changes over time remains to be determined. Thus, **Chapter 4** will examine the distribution and concentration of Fe, Cu, and Zn in the hippocampus of PSAPP mice during the progression of AD using synchrotron XFM. We hypothesize that PSAPP mice will show changes in hippocampal metal ion content as the mice age, while the content in CNT mice will remain constant. In addition, previous studies have suggested a loss of unsaturated lipids in this region [47, 122]. However, most investigations of unsaturated lipid content in the brain employ biochemical techniques that require homogenization, eliminating the ability to study and visualize specific brain regions. Therefore, **Chapter 5** will examine the unsaturated lipid content in the hippocampus of PSAPP mice during the progression of AD using FTIRI. Since unsaturated lipids are highly vulnerable to

oxidative stress, a key feature of AD, we hypothesize that regions rich in unsaturated lipid content (i.e. white matter) will be predominantly affected, while those with lower unsaturated lipid content will be less affected.

CHAPTER 2

INCREASED BRAIN IRON IS INDICATIVE OF EARLY PLAQUE FORMATION IN AN ALZHEIMER'S DISEASE MOUSE MODEL

2.1 ABSTRACT

Elevated levels of metal ions such as copper, iron, and zinc in the brain and in amyloid plaques are proposed to be key mediating factors in the pathophysiology of Alzheimer's disease (AD). However, the role of metal ions in the manifestation of the disease remains unclear. Using a mouse model of plaque formation in AD, we found that zinc was associated with late-stage plaques, but that iron was increased in non-plaque tissue at an early stage, corresponding to the commencement of plaque formation in these mice. Since plaque formation in human AD is presumed to occur years before the first cognitive symptoms appear, quantification of iron could be useful for identifying the early pathological changes in AD.

2.2 INTRODUCTION

Alzheimer's disease (AD) is an irreversible, progressive neurodegenerative disorder affecting approximately 4.5 million Americans and is by far the most prevalent form of dementia [1]. Clinically, it is characterized by memory loss, changes in personality and behavior, cognitive decline, and eventually death [2]. Physically, it is characterized by cortical atrophy, cellular degeneration, neuronal loss, and the presence of neurofibrillary tangles and amyloid beta (Aβ) plaques found mainly in the hippocampus, entorhinal cortex, and some areas of the neocortex [2, 3, 9].

Metal ions of zinc (Zn), copper (Cu), and iron (Fe) are present in the brain under normal conditions, each very tightly regulated and with specific roles in brain function. For example, Zn is involved in brain excitability and synaptic transmission [92]; Cu has a role in brain metabolism and the regulation of certain enzymes such as CuZn superoxide dismutase, ceruloplasmin, and cytochrome c oxidase [123]; Fe is involved in neural development, myelination of axons and neurotransmitter synthesis [124]. The concentrations of these metal ions may increase slightly with age normally, but in AD the brain is even further enriched and it is thought that metal ion dyshomeostasis contributes to Aβ aggregation and toxicity leading to oxidative damage and neuron degeneration [67, 69]. In addition, previous studies have shown that amyloid plaques in human AD [68, 95] and transgenic mice [94, 125, 126] are characterized by hot spots of Fe, Cu, and Zn.

Currently, AD is typically diagnosed only after cognitive symptoms have appeared and most accurately in the mid- or late-stages, which may be too late for effective treatment [2]. However, formation of plaques is estimated to occur years earlier [127]. Thus, early identification of pathological changes in AD may allow for treatment strategies to be implemented at pre-clinical stages when they are more likely to be effective. For example, metal concentrations can be measured in serum and cerebrospinal fluid, while interest in optimizing magnetic resonance imaging (MRI) sequences to non-invasively detect and quantify Fe in the brain has increased [128-130]. For example, Thomas and colleagues demonstrated a relationship between the transverse relaxation rate, R_2, measured *in vivo* and Fe content in autopsied brains [131], while a better correlation with brain Fe was achieved using different MRI parameters, R_2' [132], and $T_2\rho$ [133]. It is, therefore, possible that MRI could be used to assess disease-relevant

changes in Fe content before neuropathological symptoms occur in AD [134].

In this study, we examined the possibility of using abnormal brain metal ion content as a diagnostic marker of pre-clinical AD. In order to determine metal ion content prior to the onset of symptoms, we used a PSAPP transgenic mouse model of AD to measured metal ion content in plaque and non-plaque tissue at different stages of plaque accumulation using synchrotron X-ray fluorescence microscopy (XFM). This technique is superior to histochemical methods, which are not quantitative and only identify free or loosely-bound metals or to bulk techniques, which require tissue homogenization and loss of spatial orientation. Analysis of metal content in PSAPP mouse brain from the earliest stages of plaque formation may provide insight into quantitative measurements for early diagnosis and assessment of treatment strategies in human AD.

2.3 MATERIALS AND METHODS

2.3.1 SAMPLE PREPARATION

Sixteen female B6C3-Tg(APP_{swe}, PSEN1dE9)85 Dbo/J (PSAPP) mice and twenty-eight age- and gender-matched B6C3F1/J control (CNT) mice were obtained from Jackson Laboratory (Bar Harbor, ME). The mice were cared for in accordance with the guidelines set by the BNL Institutional Animal Care and Use Committee and were housed at the Brookhaven Laboratory Animal Facility under standard conditions. At time points representing pre-AD (13 weeks; PSAPP=7, CNT=7), early-AD (24 weeks; PSAPP =2, CNT=7), intermediate-AD (40 weeks; PSAPP =3, CNT=7), and late-AD (56 weeks; PSAPP =4, CNT=7) the mice were deeply anesthetized with 100 mg/kg 1:10 ketamine:xylazine administered by intraperitoneal (i.p.) injection. Afterwards, they were perfused transcardially with phosphate buffered saline, resulting in exsanguination and death. The brains were removed, frozen on dry ice, and stored at -80°C until processing. For each sample, 30 μm thick whole brain cryosections were mounted onto Ultralene® film (SPEX CertiPrep, Metuchen, NJ) and dried at room temperature. This substrate is free of trace elements that interfere with the XFM measurements and is also sufficiently IR-transparent.

2.3.2 SYNCHRORTON XFM

The distributions of Fe, Cu, and Zn in a 1024 μm^2 healthy, plaque free area in the cortex in both PSAPP and CNT mice were imaged with the XFM at beamline X26A at the National Synchrotron Light Source (NSLS), Brookhaven National Laboratory (BNL, Upton, NY). The synchrotron X-ray beam was tuned to 12 keV using a Si(111) channel-cut monochromotor. The monochromatic beam was then collimated to 350 μm × 350 μm and then focused to approximately 6 μm × 10 μm using Rh-coated silicon mirrors in a Kirkpatrick-Baez (KB) geometry. The sample was placed at a 45° angle to the incident X-ray beam and X-ray fluorescence was detected with an energy dispersive, 9 element germanium array detector (Canberra, Meriden, CT) oriented at 90° to the incident beam. The sample was approximately 6 cm from the detector. A light microscope objective (Mitutoyo, M Plan Apo 5X) was coupled to a digital CCD camera for sample viewing. Thioflavin S fluorescence was viewed using a commercially available epifluorescence module (Navitar, Rochester, NY). Energy dispersive spectra were collected by raster scanning the sample through the X-ray beam using a dwell time of 30 s/pixel and a step size of 4 μm to provide oversampling. Fe Kα, Cu Kα, and Zn Kα, fluorescence counts were then extracted from background-corrected energy dispersive spectra. All data were normalized to variations in incident photon flux by normalizing to changes in I_0 measured by ion chamber upstream of the KB optics. NIST thin-film standard reference materials (SRM) 1832 and 1833 were used for calibration and quantification. The counts per second for each element were then converted into $\mu g/cm^3$ by comparing the differences in X-ray absorption between the sample and the thin film standards. Finally, the concentrations in $\mu g/cm^3$ were converted into molar concentrations and means and standard deviations were calculated.

2.3.3 METAL CONTENT IN AMYLOID PLAQUES

Amyloid plaques were also imaged using XFM and were visualized with the fluorescent dye, Thioflavin S. In order to minimize tissue disruption and optimize visualization on Ultralene film, a modified procedure based on the method used by [135] was developed. In short, the tissue sections were first rehydrated with 50% ethanol and allowed to dry completely. A 0.006% solution of Thioflavin S in 50% ethanol was placed on the tissue sample and allowed to stand for two minutes. The sample was then

rinsed with 50% ethanol and then carefully rinsed with nanopure water to remove the excess Thioflavin S solution. The sections were dried in air, and the locations of the plaques were visualized by their green fluorescence using epifluorescence microscopy (filter cube excitation: 430 nm, emission: 550 nm). All plaques imaged were 30 – 50 μm in size to ensure that the plaque extended through the whole volume probed by the X-ray beam. Approximately two plaques per sample were analyzed. To confirm that Thioflavin S staining did not cause redistribution or leaching of metal ions in the sample, we scanned several areas of a tissue prior to staining with Thioflavin S. We subsequently stained the tissue and then scanned the sample again in the same area. We did not observe any substantial alterations in the Fe, Cu, or Zn abundance or distribution. XFM data from the plaques was normalized to tissue protein density using FTIRM at beamline U10B at the NSLS using previously described methods [125]. Briefly, a Thermo Nicolet Magna 860 FTIR spectrometer, coupled to a Continuum IR microscope (Thermo Nicolet, Madison, WI), was used with synchrotron light as the infrared source. The regions to be imaged were the same as those imaged using XFM and the stage was raster scanned through this area with a step size of 4 μm. At each point, an absorbance spectrum was collected in transmission mode in the mid-infrared spectral range (4000–800 cm^{-1}) with a spectral resolution of 8 cm^{-1} and 128 scans co-added. To examine the relative protein content in the plaques compared to the non-plaque tissue, the Amide II protein band of each spectrum was integrated from 1490 – 1580 cm^{-1}. A Matlab routine was then used to mask out the plaque area based on the Zn Kα fluorescence, which corresponded well with the Thioflavin S staining. These elevated Zn regions were used to create a mask that would define the plaque area for the Cu Kα and Fe Kα images. A similar procedure was followed to create the FTIRM protein images. There were approximately 50-100 pixels per plaque. To normalize the plaques to protein density, a ratio of metal/protein content for each sample was then calculated.

2.3.4 Statistical Analysis

A Kruskal-Wallis test was performed using SPSS v.14.0 to test for significant differences between PSAPP and CNT at each time point, and differences between time points. Post-hoc analyses on significant Kruskal-Wallis tests were performed using Mann-Whitney U tests. Wilcoxon signed-rank tests were performed for pair-wise

comparisons. A significance level of 0.05 was used for all analyses.

2.4 RESULTS

The metal content in healthy (non-plaque) cortex in both CNT and PSAPP mice over time is shown in **Figure 2.1**. Results show that the Fe, Cu, and Zn contents in CNT mice do not vary as the animal ages. In contrast, the Fe content in the PSAPP mice significantly increased by 71.2% ($p < 0.05$) from 13 weeks-old to 40 weeks-old and by 33.9% ($p < 0.05$) from 13 weeks-old to 56 weeks-old (**Figure 2.1A**). Fe content was also significantly higher in PSAPP mice than CNT mice at 24 (PSAPP = 0.79 ± 0.18; CNT = 0.57 ± 0.05), 40 (PSAPP = 1.01 ± 0.26; CNT = 0.60 ± 0.07), and 56 weeks-old (PSAPP = 0.79 ± 0.18; CNT = 0.60 ± 0.04). Cu remained constant in the PSAPP mice (**Figure 2.1B**). Zn content in PSAPP mice increased significantly by 162.2% ($p < 0.05$) from 13 weeks-old to 56 weeks-old and was also 160.5% ($p < 0.05$) higher than CNT mice at 56 weeks-old (**Figure 2.1C**).

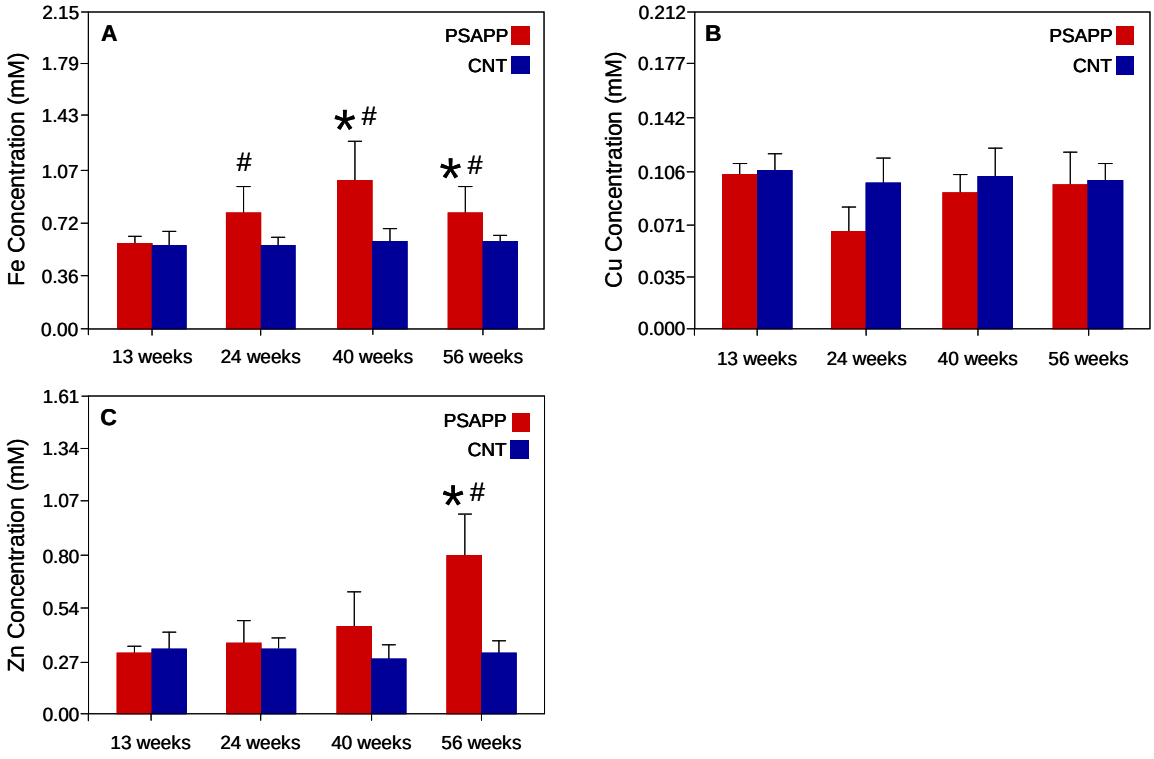

Figure 2.1 Fe (A), Cu (B), and Zn (C) content in non-plaque tissue in PSAPP mice (red bars) and CNT mice (blue bars). * = significantly different from 13 week-old PSAPP mice ($p < 0.05$); # = significantly different from CNT mice at the same time point ($p < 0.05$).

Figure 2.2 shows the XFM images of the Cu, Fe, and Zn distributions in representative plaques at 24, 40, and 56 weeks-old in the PSAPP mice. There were no plaques observed at the 13 week-old time point. From these images, it can be seen that the Fe and Cu distributions increased only slightly and were quite homogeneous, indicating that plaque and surrounding tissue levels were similar, whereas Zn content in the plaque area increased dramatically at 56 weeks-old and can easily be distinguished from the surrounding tissue. **Figure 2.3A** shows that the ratio of Fe, Cu, and Zn concentrations in the plaque compared to the surrounding normal tissue was increased by14.2%, 17.3%, and 48.8%, respectively, higher from 40 to 56 weeks-old ($p < 0.05$). At 56 weeks-old, the concentrations of Fe, Cu, and Zn were 29.1%, 30.0%, and 90.0% higher in the plaque than the surrounding normal tissue.

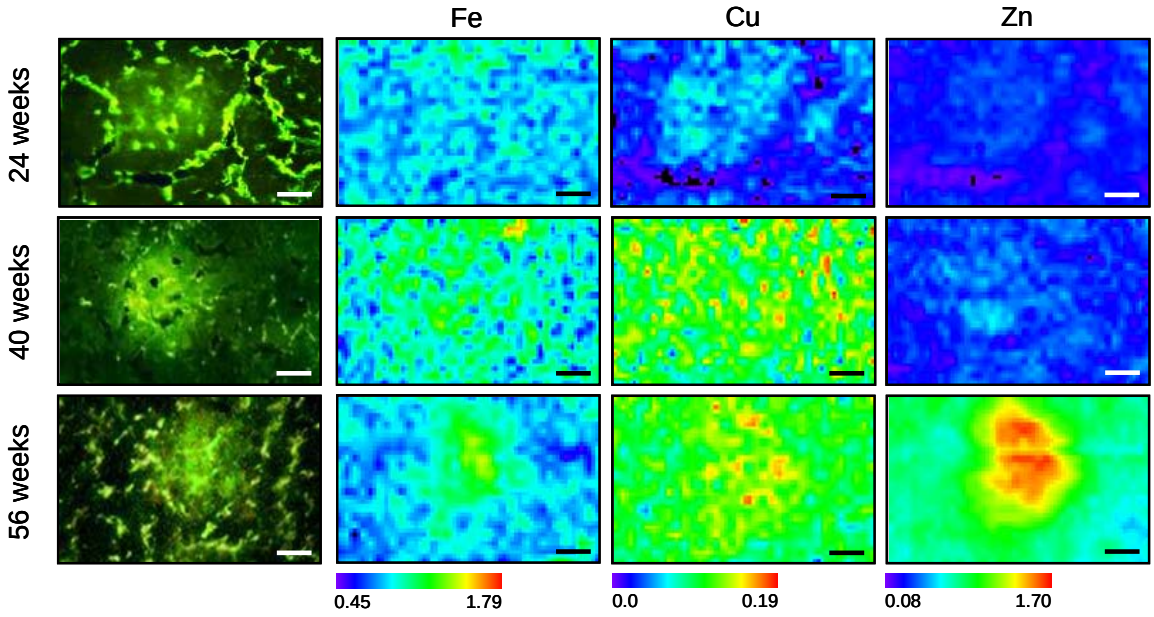

Figure 2.2 Thioflavin S-stained PSAPP mouse brain tissue and corresponding XRF microprobe images of Fe, Cu, and Zn in plaques and surrounding non-plaque tissue. Units are mM. All scale bars are 25 μm.

In order to attain a relationship between metal content and protein concentration and to ensure that any changes in protein density within the plaque are taken into account, we normalized the metal content to the amount of protein in the amyloid plaque. We have approximated the increase in tissue density in the plaque by measuring the relative

increase in protein in the plaque compared to the non-plaque area using the Amide II IR band. Results showed that, when normalized to protein content, there was less Cu, Fe, and Zn in the plaque than normal tissue at 24 and 40 weeks-old and less Cu and Fe at 56 weeks-old (**Figure 2.3B**). In contrast, Zn content in the plaque at 56 weeks-old was still 37.8% higher ($p < 0.05$) than in the normal tissue and the ratio increased from 40 weeks-old to 56 weeks-old by approximately 50.0% ($p < 0.05$).

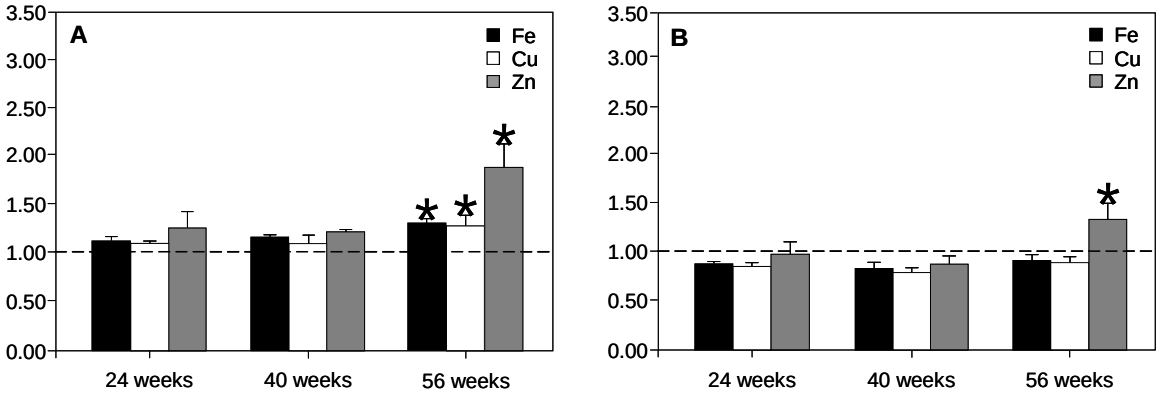

Figure 2.3 (A) Ratio of metal content in plaque to non-plaque tissue. (B) Ratio of metal content in plaque to non-plaque tissue normalized to protein density. * = significantly different from 40 week-old mice ($p < 0.05$).

2.5 DISCUSSION

There is growing evidence to suggest that dyshomeostasis of Fe, Cu, and Zn and their accumulation in amyloid plaques play an important role in AD pathology [68, 93, 95]. Moreover, recent research implies that elevated brain Fe could be used as a diagnostic tool in AD [136, 137]. However, despite evidence that certain metal ions are elevated in AD, it remains unclear how early in the disease process do alterations in metal ion content occur. Our goal in this study was to examine the Fe, Cu, and Zn content in plaque and non-plaque tissue as a function of aging in PSAPP mice. Metal ion content in age-matched CNT mice was also examined. The present results showed that plaques were elevated only in Zn and only at the latest time point, but concentrations of Fe in non-plaque tissue in PSAPP mice were already increased over CNT animals from an early time point.

Zn has previously been shown to be elevated in AD brain [98, 138] and to be an

integral component of both human and PSAPP plaques [68, 95, 125, 139]. Though not statistically significant, there is a trend that increasing Zn coincides with amyloid deposition since plaques start to accumulate at around 24 weeks-old and increase as the animal ages. However, at 56 weeks-old Zn was significantly elevated in both the plaque and non-plaque tissue in PSAPP mice. This supports previous research by Religa and colleagues indicating that elevated Zn levels are associated with Aβ burden since significantly elevated Zn was found only in advanced AD patients with high plaque burden and severe dementia whereas tissue with few or no plaques was not associated with elevated Zn [96].

Cu is strongly redox-active and interaction of excess Cu with Aβ contributes to the generation of toxic hydrogen peroxide and hydroxyl radicals, which can lead to neurodegeneration [74, 82]. In addition, Cu homeostasis appears to be affected in AD. For example, extracellular Cu was shown to increase with normal aging, while subcellular levels appear to be deficient in AD [76] and intracellular Cu deficiency is thought to be exacerbated by Cu accumulation in plaques [140]. The present results showed that there was no Cu in the plaques. Moreover, there was no evidence of Cu dyshomeostasis since Cu content remained similar in both PSAPP and CNT mice at all time points. Since no Cu was found in the plaques, this implies that intracellular Cu content in the PSAPP mice most likely remained at a similar level to the CNT mice.

Fe is also redox active and when bound to Aβ produces hydrogen peroxide and hydroxyl radicals, similarly to Cu [82]. Like Cu, we did not observe an increase in Fe in the plaques. Previous research has suggested that Zn binding to Aβ may act as an antioxidant by preventing Cu or Fe binding [59]. It is therefore possible that Cu and Fe have minimal interaction with Aβ in PSAPP mice and could be one reason why these mice do not show neurodegeneration. However, in contrast to Cu, we found that Fe content in non-plaque tissue was significantly higher in the PSAPP mice than in the CNT mice starting from 24 weeks of age and progressively increased as the mice aged. Since Fe was not found in the plaques, this suggests that the observed increase in Fe in PSAPP mice arises not from an interaction with Aβ, but from some other mechanism. For example, increased Fe could result from disruption in the expression of other brain Fe metabolism, transport, or storage proteins.

The observed increases in Fe at the beginning stages of plaque formation may have direct clinical relevance for early detection of the pathological symptoms of AD. Currently, AD is most accurately diagnosed in the mid or late stages, which may be too late for effective treatment [2]. However, there is considerable interest in optimizing MRI sequences to non-invasively detect and quantify excessive Fe in the brain for the purposes of early diagnosis and treatment monitoring [128-130]. In addition, XFM measurements of Fe concentration have already been shown to correlate well with susceptibility weighted MR in the tgCRND8 mouse model of AD [141]. Recently, the parietal cortex was determined to be more sensitive than other brain regions at detecting Fe deposition using phase-corrected MRI in mild AD cases [142]. Though previous studies have shown elevated Fe in AD, they have not indicated when the excess Fe begins to accumulate. The present results showed that Fe is not only higher in the PSAPP mice than in the CNT mice, but that this difference was already evident at 24-weeks of age, i.e. at the first signs of plaque formation, as well as spatial working memory impairments, in these mice [143]. This implies that if Fe is in sufficient quantity to be identified by MRI, an increase in Fe could be indicative of a disease state. Our results indicate that Fe concentration in PSAPP cortical tissue increased 41.6% to within reported values detected by MRI [137, 142, 144].

Taken together, these results suggest that early Fe accumulation reflects pathological changes related to plaque formation in PSAPP mice, making Fe deposition a promising biomarker to predict the presence of early amyloid plaque deposition. Further advancement of MRI techniques in conjunction with other imaging techniques to identify amyloid plaques (e.g. positron emission tomography) may allow for early diagnosis through sensitive quantification of brain Fe deposition at pre-clinical or early stage AD and related diseases so that more effective treatments can be developed and monitored. However, understanding the significance of increased Fe the AD brain is critical in determining if Fe is a primary cause of AD or a secondary consequence of disease progression. Future work should involve disentangling elevated Fe in AD brain from other possible causes of excess Fe in the brain and longitudinal examinations of brain Fe in human patients should be conducted.

2.6 ACKNOWLEDGEMENTS

The authors would like to thank Janelle Collins for her skillful technical assistance with the animal dissection. We are also grateful to Bill Rao at beamline X26A for his support with beamline operation and data collection. This work is funded by the National Institutes of Health Grant R01-GM66873. The National Synchrotron Light Source is funded by the U.S. Department of Energy, Office of Science, Office of Basic Energy Sciences, under Contract DE-AC02-98CH10886.

CHAPTER 3

AMYLOID PLAQUES IN PSAPP MICE BIND LESS METAL THAN PLAQUES IN HUMAN ALZHEIMER'S DISEASE [125]

3.1 ABSTRACT

Amyloid beta (Aβ) is the primary component of Alzheimer's disease (AD) plaques, a key pathological feature of the disease. Metal ions of zinc (Zn), copper (Cu), iron (Fe), and calcium (Ca) are elevated in human amyloid plaques and are thought to be involved in neurodegeneration. Transgenic mouse models of AD also exhibit amyloid plaques, but fail to exhibit the high degree of neurodegeneration observed in humans. In this study, we imaged the Zn, Cu, Fe, and Ca ion distribution in the PSAPP transgenic mouse model representing end-stage AD (N = 6) using synchrotron X-ray fluorescence microscopy (XFM). In order to account for differences in density in the plaques, the relative protein content was imaged with synchrotron Fourier transform infrared microspectroscopy (FTIRM) on the same samples. FTIRM results revealed a 61% increase in protein content in the plaques compared to the surrounding tissue. After normalizing to protein density, we found that the PSAPP plaques contained only a 29% increase in Zn and there was actually *less* Cu, Fe, and Ca in the plaque compared to the surrounding tissue. Since metal-binding to Aβ is thought to induce redox chemistry that is toxic to neurons, the reduced metal-binding in PSAPP mice is consistent with the lack of neurodegeneration in these animals. These findings were in stark contrast to the high metal ion content observed in human AD plaques, further implicating the role of metal ions in human AD pathology.

3.2 INTRODUCTION

One of the key clinical features of Alzheimer's disease (AD) is the extracellular deposition of amyloid plaques primarily composed of a 39-43 amino acid protein called amyloid beta (Aβ). Aβ is derived from the proteolytic cleavage of a larger transmembrane glycoprotein, the amyloid precursor protein (APP), by β and γ secretases [3]. β-secretase first cleaves APP extracellularly, forming the N-terminus, and γ-secretase then cleaves APP in the intramembrane domain, creating the C-terminus. The two most frequently produced peptides are Aβ40, composed of 40 residues and found mostly in cerebrospinal fluid and vasculature, and Aβ42, composed of 42 residues and the main component of amyloid plaques [13]. The formation of Aβ, even the deposition of diffuse plaques, is a normal cellular process, but in AD the peptide aggregates to form dense plaques in specific regions of the brain [2]. But exactly how and why this misfolding occurs is still unknown.

Zinc (Zn), copper (Cu), iron (Fe), and calcium (Ca) ions are all present in the body under normal conditions, but their abundances are elevated in regions of the brain that are involved in AD [67, 68]. The observation that human Aβ can bind to certain metal ions *in vitro* may indicate these ions play a role in increasing the protein's toxicity and the tendency to form plaques [67, 72, 75-77]. Nuclear magnetic resonance (NMR) and X-ray absorption spectroscopy (XAS) studies of metal binding to human Aβ have revealed the presence of a low and high affinity binding site for both Cu and Zn via three N-terminal histidine imidazole rings and that the stoichiometry for Cu:Aβ is 1:1 and for Zn:Aβ ranging from 1:1 to 3:1 [71, 78, 145].

The affinity for the Zn binding sites were measured as 100 nM and 5 μM [77] and 10^{-10} M for Cu [78]. These affinities are well below physiological levels (~100-150 μM [146]), supporting the possibility that Zn and Cu are likely to bind human Aβ *in vivo*, especially in AD where brain metal levels are known to be increased [94]. Indeed, elevated levels of Zn, Cu, and Fe ions have been observed in amyloid plaques in human AD brain [68, 94, 95] and studies involving Swedish mutant APP transgenic mice have shown that Zn is elevated in dense senile plaques [93]. It has also recently been shown that Zn transporter proteins, which transport Zn ions into different intracellular

compartments when intercellular Zn is elevated, are increased in AD and are abundantly expressed in human senile amyloid plaques [147, 148]. Increased Fe was also found within the glial cells surrounding the plaques [149]. Excess Fe is typically sequestered by the iron storage protein ferritin and it was found that expression of ferritin is associated with degeneration of microglia in AD brain [150]. However, those previous studies primarily utilized histochemical methods, which can only detect free and loosely bound metal ions and cannot be accurately compared to the metal content in the surrounding healthy (non-plaque) tissue. In addition, previous studies that quantified metal content using proton and X-ray methods [68, 95] did not consider the elevated protein density in the plaque compared to the surrounding tissue. Thus, the observed increase in metal ions within the plaques may simply be attributed to an increase in protein density within the plaque and not an "accumulation" of excess metal ions or metalloproteins.

A number of mouse models have been developed to mimic one or more neuropathological features of AD, which has resulted in valuable progress in understanding AD progression. However, there is some evidence that they are not a complete representation of human AD [151]. While mice overexpressing mutant AD related genes exhibit many of the same neuropathological and behavioral features of human AD, including amyloid plaques, neurofibrillary tangles, motor impairments, and memory deficits [152, 153], most transgenic models lack the widespread neuronal loss and severity of symptoms present in human AD pathology [154]. Additionally, the surrounding neurons appeared displaced by the plaques rather than damaged by them [151]. Exactly why this occurs is not known; however, mouse Aβ lacks a histidine at position 13. This residue has been shown to be critical in coordinating Cu and inducing aggregation in human Aβ, where wild-type mice show no aggregation [87, 91]. Transgenic mice develop amyloid plaques that contain both endogenous murine Aβ and transgene-derived human Aβ [155, 156]. Since both types are found in transgenic mouse plaques, this mixture may alter the metal-binding characteristics of the peptide [109].

We have previously shown that endstage human AD is characterized by the accumulation of Zn, Cu, Fe, and Ca that are co-localized with areas of high β-sheet protein and that the concentrations of metal inside the plaque are much higher than

outside of the plaque [95]. Here, those results are compared to analogous studies from the end stage of a PSAPP transgenic mouse model of AD, which overexpresses the presenilin (PS) 1 gene and the amyloid precursor protein (APP) gene. Synchrotron X-ray fluorescence microscopy (XFM) was used to image the metal content in the plaques and surrounding non-plaque tissue. In order to normalize to plaque protein density, synchrotron Fourier transform infrared microspectroscopy (FTIRM) was used on the same samples. Results revealed a dramatic decrease in metal binding in the PSAPP plaques compared to the human plaques. When normalized to protein density, human plaques showed elevated Zn, Cu, Fe, and Ca, whereas the PSAPP aggregates contained only elevated Zn. The differences in both neurodegeneration and metal accumulation between human AD and the PSAPP mouse model provide more evidence of the involvement of metal ions in AD.

3.3 MATERIALS AND METHODS

Six female B6C3-Tg(APP_{swe}, PSEN1dE9)85 Dbo/J (PSAPP) mice were obtained from Jackson Laboratory (Bar Harbor, ME). The mice were cared for in accordance with the guidelines set by the BNL Institutional Animal Care and Use Committee and were housed at the Brookhaven Laboratory Animal Facility under standard conditions. At 56 weeks of age the mice were deeply anesthetized with 100 mg/kg 1:10 ketamine:xylazine administered by intraperitoneal (i.p.) injection. Afterwards, they were perfused transcardially with phosphate buffered saline (PBS), resulting in exsanguination and death.

The mouse brain specimens were prepared in a similar manner to the human brain specimens described previously [95]. The brains were removed, frozen on dry ice, and stored at -80°C until processing. For each sample, 30 μm thick whole brain cryosections were mounted onto Ultralene® film (SPEX CertiPrep, Metuchen, NJ) and dried at room temperature. This substrate is free of trace elements that interfere with the XFM measurements and is also sufficiently IR-transparent. Amyloid plaques were visualized with the fluorescent dye, Thioflavin S. In order to minimize tissue disruption and optimize visualization on Ultralene film, a modified procedure based on the method used by [135] was developed. In short, the tissue sections were first rehydrated with 50% ethanol and allowed to dry completely. A 0.006% solution of Thioflavin S in 50%

ethanol was placed on the tissue sample and allowed to stand for two minutes. The sample was then rinsed with 50% ethanol and then carefully rinsed with nanopure water to remove the excess Thioflavin S solution. The sections were dried in air, and the locations of the plaques were visualized by their green fluorescence using epifluorescence microscopy (filter cube excitation: 430 nm, emission: 550 nm). All plaques imaged were 30 – 50 μm in size to ensure that the plaque extended through the whole volume probed by the X-ray beam. Approximately 2-4 plaques per sample were analyzed.

The relative content and distribution of Zn, Cu, Fe, and Ca in PSAPP mouse plaques were imaged with the XFM at beamline X26A at the National Synchrotron Light Source, Brookhaven National Laboratory (Upton, NY). The synchrotron X-ray beam was tuned to 12 keV using a Si(111) channel-cut monochromotor. The monochromatic beam was then collimated to 350 μm × 350 μm and then focused to approximately 6 μm × 10 μm using Rh-coated silicon mirrors in a Kirkpatrick-Baez geometry. The sample was placed at a 45° angle to the incident X-ray beam and X-ray fluorescence was detected with an energy dispersive, 9 element germanium array detector (Canberra, Meriden, CT) oriented at 90° to the incident beam. The sample was approximately 6 cm from the detector. A light microscope objective (Mitutoyo, M Plan Apo 5X) was coupled to a digital CCD camera for sample viewing. Thioflavin S fluorescence was viewed using a commercially available epifluorescence module (Navitar, Rochester, NY). Energy dispersive spectra were collected by raster scanning the sample through the X-ray beam using a dwell time of 30 s/pixel and a step size of 4 μm to provide oversampling. Zn Kα, Fe Kα, Cu Kα, Ca Kα fluorescence counts were then extracted from background-corrected energy dispersive spectra. NIST thin-film standard reference materials (SRM) 1832 and 1833 were used for calibration. All data were normalized to variations in incident photon flux by normalizing to changes in I_0 measured by an upstream ion chamber. To confirm that Thioflavin S staining did not cause redistribution or leaching of metal ions in the sample, we scanned several areas of a tissue prior to staining with Thioflavin S. We subsequently stained the tissue and then scanned the sample again in the same area. We did not observe any substantial alterations in the Zn, Fe, or Cu abundance or distribution.

For all plaques that were analyzed with the XFM, the protein distribution was determined using FTIRM at beamline U10B at the National Synchrotron Light Source, Brookhaven National Laboratory (Upton, NY). A Thermo Nicolet Magna 860 FTIR spectrometer, coupled to a Continuum IR microscope (Thermo Nicolet, Madison, WI), was used with synchrotron light as the infrared source. The microscope was equipped with a matching 32x Schwarzschild objective/condenser pair, a motorized x–y mapping stage, an adjustable rectangular aperture, and a mercury cadmium telluride (MCT) detector. The regions to be imaged were the same as those imaged using XFM and were identified as Aβ aggregates by Thioflavin S fluorescence. The IR microscope stage was raster scanned through this area with a step size of 4 μm. At each point, an absorbance spectrum was collected in transmission mode in the mid-infrared spectral range (4000–800 cm^{-1}) with a spectral resolution of 8 cm^{-1} and 128 scans co-added. The IR beam size was 10 x 10 μm. A background spectrum was collected from an area with no substrate or sample in the beam.

The FTIRM data were analyzed using Thermo Nicolet's software Omnic 7.3. To examine the relative protein content in the plaques compared to the non-plaque tissue, each spectrum was integrated from 1490 – 1580 cm^{-1}. This region represents the Amide II absorption band, which arises from the N–H bending and C–N stretching modes of the peptide backbone and is proportional to protein concentration. A linear baseline from 1480 – 1800 cm^{-1} was applied. Both the FTIRM and XFM maps were then normalized by dividing the entire map by the average background intensity of the non-plaque (healthy) tissue. A Matlab routine was then used to mask out the plaque area based on the Zn Kα fluorescence, which corresponded well with the Thioflavin S staining. On average, these areas gave Zn fluorescence intensity about 1.8 times higher than non-plaque tissue. These elevated Zn regions were used to create a mask that would define the plaque area for the Cu Kα, Fe Kα, and Ca Kα images. A similar procedure was followed to create the FTIRM protein images. There were approximately 150 pixels per plaque. Although a faster method would have been to obtain a few individual spectra from the plaque and non-plaque regions, we chose the current procedure because we have previously observed a heterogeneous distribution of metal in plaques. Therefore, a single spectrum or even an average of a few spectra may overestimate or underestimate the

amount of metal observed depending on where the spectrum was taken. Once all of the appropriate pixels from each image were masked out, the data were checked for normality with a Kolmogorov-Smirnov test using SPSS v.14.0 and means and standard deviations were calculated. The final data represented a ratio of the intensity in the plaque to the non-plaque area. The percentage increase in metal within the plaque compared to the non-plaque area was also determined. A ratio of metal/protein content for each sample was then calculated. To compare the actual change in metal content once the plaques were normalized for protein density, the percentage difference was determined.

3.4 RESULTS

The distribution of protein, as measured by the Amide II FTIRM band, in three plaques from a PSAPP mouse representing endstage AD is shown in **Figure 3.1**. Also shown are representative spectra illustrating the increase in protein in the plaque compared to the surrounding normal tissue. The protein distribution showed that the protein density was highest in the center of the plaque and decreased toward the periphery. On average, the protein density was 61% higher within the PSAPP plaques than the surrounding area (**Table 3.1**).

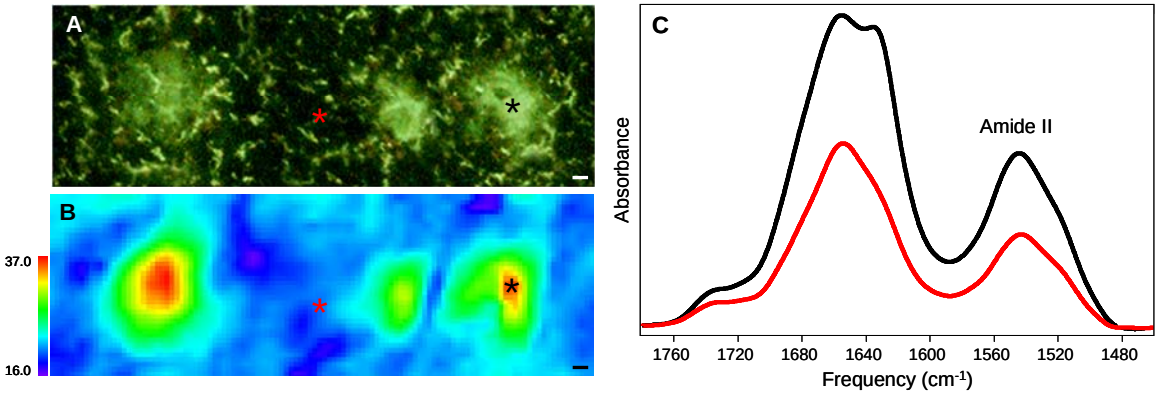

Figure 3.1 (A) Thioflavin S-stained PSAPP mouse brain tissue showing three plaques. (B) Infrared image of the same tissue showing the distribution of protein measured by the Amide II band. (C) Infrared spectra collected from the areas marked with asterisks in (A) and (B), showing the relative amount of protein in the center of a plaque (black) and the surrounding tissue (red). All scale bars are 5 μm.

TABLE 3.1 Relative Metal and Protein Content in PSAPP AD Plaques

	Zinc	Copper	Iron	Calcium	Protein
Measured (inside/outside plaque)	2.07 ± 0.34	1.25 ± 0.11	1.33 ± 0.14	1.50 ± 0.23	1.61 ± 0.18
% Difference	*+107.0*	*+25.0*	*+33.0*	*+50.0*	*+61.0*
Normalized	1.29 ± 0.12	0.79 ± 0.07	0.83 ± 0.09	0.94 ± 0.16	
% Difference	*+29.0*	*-22.0*	*-17.0*	*-7.0*	

Figure 3.2 shows the XFM images of the Zn, Cu, Fe, and Ca distributions from the same plaques as shown in **Figure 3.1.** Representative spectra from the plaque and non-plaque regions are also shown. Results show that the relative Zn, Fe, and Ca contents are preferentially concentrated in the core of the plaque, with about 1.8, 1.7, and 1.5 times more, respectively, in the center than the edge of the plaque. In contrast, the relative distribution of Cu was more homogeneous: no central core was observed and, although there were a few elevated spots in some areas, the plaque was generally only about 1.2 times elevated above the background. When compared to the surrounding non-plaque tissue, there was approximately a 107% increase in Zn, 25% increase in Cu, 33% increase in Fe, and a 50% increase in Ca (**Table 3.1**). Although Zn, Cu, and Fe have all been implicated in AD plaques, this is the first known study to show elevated Ca in PSAPP plaques. Since Aβ does not have any known binding sites for Ca, this result implies there are other proteins or physiological processes using Ca in the plaques.

In order to attain a relationship between metal content and protein concentration and to ensure that any changes in protein density within the plaque are taken into account, we normalized the metal content to the amount of protein in the amyloid plaque. We have approximated the increase in tissue density in the plaque by measuring the relative increase in protein in the plaque compared to the non-plaque area using the Amide II IR band. We have approximated the increase in tissue density in the plaque by measuring the relative increase in protein in the plaque compared to the non-plaque area using the Amide II IR band. A ratio of relative metal content to the relative protein content

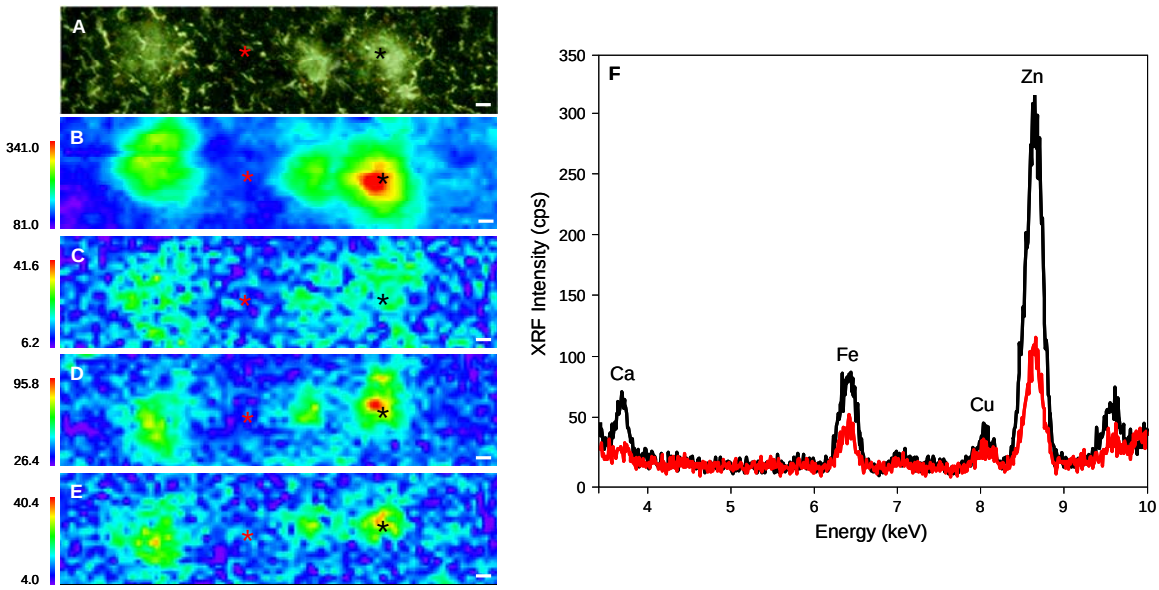

Figure 3.2 (A) Thioflavin S-stained PSAPP mouse brain tissue, also shown in Fig. 1. XFM images of (B) Zn, (C) Cu, (D) Fe, and (E) Ca distribution in the same tissue. (F) XFM spectra collected from the areas marked with asterisks in (A) – (E), comparing the center of a plaque (black) to the surrounding tissue (red). All scale bars are 5 μm.

measured by Amide II was calculated for each element and sample (**Table 3.1**). Results showed that, when normalized to protein content, there was approximately a 29% increase in Zn compared to protein in the plaque, while there was actually 22% less Cu, 17% less Fe, and 7% less Ca in the plaque.

In order to compare these findings to human AD, the same procedure was applied to the data used in our previous human AD study [95]. In contrast to PSAPP mouse plaques, human AD plaques are highly enriched in Zn, Cu, Fe, and especially Ca (**Table 3.2**). Specifically, when compared to the surrounding tissue, there was approximately a 908% increase in Zn, 1171% increase in Cu, 573% increase in Fe, 9838% increase in Ca. Human plaques showed a 107% increase in protein, so when normalized to protein density, there was still a 339% increase in Zn, a 466% increase in Cu, a 177% increase in Fe, and a 4653% increase in Ca.

TABLE 3.2 Relative Metal and Protein Content in Human AD Plaques

	Zinc	Copper	Iron	Calcium	Protein
Measured (inside/outside plaque)	9.09 ± 0.20	11.72 ± 1.24	5.74 ± 3.31	98.40 ± 31.56	2.07 ± 0.18
% Difference	*+908*	*+1171*	*+573*	*+9839*	*+107*
Normalized	4.42 ± 0.38	5.70 ± 0.49	2.79 ± 0.24	47.85 ± 4.10	
% Difference	*+339*	*+466*	*+177*	*+4653*	

3.5 DISCUSSION

There is growing evidence to suggest that the accumulation of metals ions in amyloid plaques plays an important role in AD pathology [68, 93, 95]. However, previous studies used non-quantitative histochemical techniques or did not normalize to increased plaque density, the former of which only identify free metal ions. Our goal in this study was to analyze the distribution of Zn, Cu, Fe, and Ca in PSAPP mouse plaques normalized to the density of the tissue and to compare the results to previous results from our laboratory examining human AD plaques [95]. Like the human plaques, the present results showed that PSAPP mouse plaques were elevated in Zn, Cu, Fe, and Ca. Interestingly, however, we found that the abundance of metal in the PSAPP plaques was considerably lower than in the human plaques. Even though human plaques are more dense (i.e. showed approximately 30% more protein) than the PSAPP plaques, it is not enough to account for the large increase in metal content. This suggests that metals may not have the same effect in transgenic mouse models of AD as in human AD.

Double transgenic PSAPP mice express a chimeric mouse/human amyloid precursor protein gene (APP695swe) and a mutant human presenilin 1 (PSEN1) gene allowing them to secrete a human Aβ peptide, which can be detected by antibodies specific for human sequence within this region [102]. PSAPP mice exhibit markedly accelerated amyloid deposition demonstrating the involvement of presenilin 1 in early onset AD [102]. However, it was recently shown that both human and mouse Aβ are deposited in the plaques of these mice [156] as well as in the plaques of transgenic mice expressing the London APP mutation [155]. On the other hand, wild-type mice express

only rodent Aβ and do not develop plaques nor any other AD-like pathology [87, 157].

In vitro experiments have shown that Aβ possesses specific binding sites for Zn, Cu, and to a lesser extent, Fe [70-73] although only Zn and Cu co-purify with Aβ extracted from human AD brain [74]. In contrast, rodent Aβ is not aggregated by Zn, Cu, or Fe [91]. Rodent Aβ is different from human Aβ in that it contains three amino acid substitutions at positions 5, 10, and 13 [157], but it appears to be the histidine substitution for arginine at position 13 in the rodent Aβ that minimizes metal-induced aggregation [158]. Since PSAPP plaques contain a fraction of rodent Aβ, the metal coordination within these plaques is likely different from human plaques.

In human Aβ, high-affinity binding of Cu^{2+} to Aβ has been shown to slowly modify the peptide and promote precipitation [78]. Moreover, while most proteins lose metal ions with decreasing pH, Aβ accepts Cu under mildly acidic conditions and can displace Zn, which loses affinity at low pH, suggesting a combined role of Cu and acidic environments in the pathophysiology of AD. Alternatively, Cu may bind to Aβ first and Zn may act as an antioxidant by displacing non-specific Cu^{2+} binding [59].

We have previously shown that human AD plaques accumulated high amounts of Cu compared to the surrounding normal tissue [95], while the present study showed negligible Cu accumulation in PSAAP mouse plaques. Mildly acidic pH is a common occurrence in the aged human brain and also in response to inflammation [91]. Since Cu^{2+} coordination is highly pH dependent [87], the low level of Cu binding in the present study suggests that in PSAPP mice either the pH in the brain remains at a physiological level and, therefore, not low enough to allow Cu binding or that Zn binding displaced Cu that was previously bound. Moreover, it appears that Zn may change the conformation of Aβ so that Cu or Fe cannot access its metal binding sites [75]. Aβ is strongly redox-reactive and generates hydroxyl radicals via Fenton chemistry, and peroxide (H_2O_2) species via the Haber-Weiss reaction, upon the reduction of Cu^{2+} and Fe^{3+}, which may cause oxidative stress [82]. Our human AD study showed nearly equivalent accumulation of Zn, Cu, and Fe, while in PSAPP mice we have shown clearly less Cu and Fe accumulation in the plaques than Zn. This suggests that Cu or Fe binding is important in causing the widespread neuronal damage observed in human AD, which does not occur in PSAPP mice. It is possible that Zn may act as an antioxidant by

inhibiting Cu and Fe binding and preventing peroxide formation in these mice.

Although it has been shown that metal binding can form plaques *in vitro*, it is not known if Aβ *in vivo* is metal bound under normal physiological conditions. However, Aβ:Cu and Aβ:Zn stoichiometry has been shown to be 1:2 and 1:3 respectively *in vitro* with apparent binding affinities in the atto- and picomolar range, indicating that these metals could be bound to Aβ under normal physiological conditions [78]. While we have shown that there appears to be an increase in metal content in plaque versus surrounding tissue, these differences disappear once we consider the amount of protein in the plaque. We have made the assumption that the plaques we analyzed were largely composed of Aβ based on previous findings using HPLC, laser capture microdissection, and Raman spectroscopy that plaque cores are primarily composed of Aβ and that other proteins are localized to the periphery or present in minute amounts [13, 86, 159, 160]. Thus, since Aβ is presumed to bind at least 2-3 metal ions per peptide, we expected a minimum of 2-3 times more metal than protein in the plaque. However, this was not the case. We observed an increased accumulation of Zn in the plaque, while Cu, Fe, and Ca were decreased in the plaque when normalized to protein content. One explanation is that once mature plaques have formed, Aβ may lose affinity for metal ions and this would therefore account for the decrease in metal. It is also possible that the metal binding modes of Aβ *in vivo* are different from those shown in Aβ *in vitro*. This is a likely explanation because previous FTIRM studies have shown that amyloid plaques in AD tissue have an elevated β-sheet structure that is different than the Aβ structure found *in vitro* [95, 161]. The different structure of Aβ in the tissue may contribute to different metal binding modes than those observed *in vitro*. This difference may be even greater in PSAPP mice considering that the amyloid that accumulates in plaques of transgenic AD mice was found to be chemically distinct from that found in human AD [162]. In addition, Cu is abundant in human plaques, while lacking in PSAPP plaques. This is an important finding because Aβ and Cu-bound histidine have been shown to be involved in the generation of neurotoxic H_2O_2 [86] and the presence of Cu in the plaques could be one reason why human AD exhibits such severe neurodegeneration, which is not observed in the mice.

Calcium disruption has also been postulated to play a role in AD [163] and has

gained even more interest lately [164-166]. It is thought that Aβ is involved in Ca regulation by forming ion channels in the cell membrane allowing Ca to flow into the cell [167]. More recently, it was shown that transgenic mice expressing both mutant APP and PSEN1 exhibited calcium overload while mice expressing only one of the transgenes or mice that did not yet have plaques did not [166]. To the best of our knowledge, this is the first study in transgenic AD mice that has examined Ca distribution in plaques. Ca was found to be extremely elevated in human AD plaques and just slightly elevated in PSAPP plaques. Since Aβ does not have any known binding sites for Ca, this result implies there could be other physiological processes using Ca in the plaques.

In summary, we have found that PSAPP mice accumulate much less metal in their plaques compared to human AD plaques, suggesting that PSAPP mice are affected differently by metals. These results together indicate that PSAPP mice are only a limited representation of human AD plaque pathology. However, the deficits in these mice are extremely beneficial in that they give insights into potential disease mechanisms of human AD. Why AD in PSAPP mice is different than in humans may be due to a number of factors including differences in Aβ structure and distribution, as well as species differences such as life span, duration of illness, and other pathologic features (e.g. the absence of neurofibrillary tangles in PSAPP mice). Nevertheless, the lack of metal in PSAPP plaques, while abundant in human plaques, indicates that metals may be related to the detrimental neurotoxicity observed in human AD, which is nearly absent in PSAPP mice.

3.6 ACKNOWLEDGMENTS

The authors would like to thank Ariane Kretlow and Janelle Collins for their skillful technical assistance with the animal dissection and tissue preparation. We are also grateful to Bill Rao at beamline X26A for his support with beamline operation and data collection. This work is funded by the National Institutes of Health Grant R01-GM66873. The National Synchrotron Light Source is funded by the U.S. Department of Energy, Office of Science, Office of Basic Energy Sciences, under Contract DE-AC02-98CH10886.

CHAPTER 4

IRON, COPPER, AND ZINC IN THE HIPPOCAMPUS OF PSAPP MICE DURING THE PROGRESSION OF ALZHEIMER'S DISEASE

4.1 ABSTRACT

Approximately 4.5 million people in the U.S. suffer from Alzheimer's disease (AD), a neurodegenerative disorder characterized by neurofibrillary tangles and amyloid plaques in the cortex and hippocampus. Accumulating evidence suggests a role of zinc, copper, and iron, in the pathology of the disease, but the function of these metal ions and their origin remains unclear. It is thought that metal homeostasis is altered in AD and contributes to plaque formation, oxidative damage, inflammation, and neuron degeneration. We used X-ray fluorescence microscopy at beamline 18ID to examine the metal ion distribution and concentration in the hippocampus of PSAPP mice (N=28), a model for human AD, and age-matched control (CNT) mice (N=20) at four stages of plaque formation. Results showed that for both PSAPP and CNT mice Fe was highest in the pyramidal cell layer (PCL) of CA1; Zn was highest in the hilus of the dentate gyrus (DG); Cu was uniformly distributed throughout the hippocampus but was high in regions corresponding to the choroid plexus outside the hippocampus. No significant changes in metal ion content were observed in the CNT mice over time. In PSAPP mice, Fe content was increased by 31.2% in the hippocampus ($p < 0.01$) and by 51.7% specifically in the PCL ($p < 0.01$) from 13 to 24 weeks-old. It decreased by 14.7% and 51.7% in the hippocampus and PCL, respectively ($p < 0.01$) from 24 to 56 weeks-old. Fe content was also lower than CNT mice at 56 weeks-old in both regions ($p < 0.01$). Zn content in the hilus increased by 49.8% ($p < 0.01$) from 13 to 56 weeks-old in the PSAPP mice. These results provide evidence for a general increase in brain Fe during plaque formation, but a more specific involvement of Zn. It is possible that these fluctuations are important in increasing the oxidative stress and neurodegeneration implicated in AD.

4.2 INTRODUCTION

Alzheimer's disease (AD) is an irreversible neurodegenerative disorder affecting approximately 5.3 million Americans and is by far the most prevalent form of dementia [1]. Clinically, it is characterized by memory loss, changes in personality and behavior, cognitive decline, and eventually death [2]. Physically, it is characterized cortical atrophy, cellular degeneration, neuronal loss, and the presence of intracellular neurofibrillary tangles and extracellular amyloid beta (Aβ) plaques found in the hippocampus, entorhinal cortex, and some areas of the neocortex [2, 3, 9]. In addition, metal ions such as zinc (Zn), copper (Cu), and iron (Fe) are present in the brain under normal conditions and each has a specific role in the brain. For example, Zn is involved in brain excitability and synaptic transmission [92]; Cu has a role in brain metabolism and the regulation of certain enzymes such as CuZn superoxide dismutase, ceruloplasmin, and cytochrome c oxidase [123]; Fe is involved in neural development, myelination of axons and neurotransmitter synthesis [124]. The concentration of these metal ions may increase slightly with age normally, but in AD it is thought that metal imbalance contributes to AD pathology leading to oxidative damage and neuron degeneration [69].

The hippocampus is of neuropathological interest because it is important for long-term memory storage and neurogenesis and one of the first and most severely affected brain regions in AD [120]. Anatomically, the hippocampus can be divided into the dentate gyrus (DG), the cornu ammonis (CA), and the subiculum. The DG is composed of granule cells that project to the CA3 field via mossy fiber projections. Pyramidal neurons in CA3 then project to CA1 via Schaffer collaterals and the pyramidal neurons of CA1 project to the subiculum. Finally, CA1 and the subiculum both project back to the deep layers of the entorhinal cortex [168]. Data from human AD patients show that the CA1 region loses more neurons than any other subregion of the hippocampus [169]. Furthermore, this result appears to be disease-related since only minor neuron losses have been observed with aging [170]. In addition, the hippocampus has been shown to be more sensitive to metal perturbation than other brain regions and has unique regulatory demands for Fe, Cu, and Zn since they are involved in synaptic plasticity [171].

Fe, Cu, and Zn are involved brain function under normal physiological conditions,

but the levels of these metal ions must be tightly regulated and naturally occurring variation is relevant to behavior [171]. Imbalances of these metals have also been shown to be associated with AD (for review [121]). For example, Deibel et al. [98] found a decrease in Cu, and an increase in Zn and Fe in the hippocampus in human AD. It has been suggested that this decrease in intracellular Cu may be due partly to Cu bound in extracellular plaques which leads to a reduction in important metabolic mechanisms and thus, neuronal damage [123]. In addition, Zn bound in plaques might interfere with Zn trafficking pathways and lead to depleted intracellular Cu levels [123]. Regulation of Fe and Cu are particularly important because of their propensity to interact with Aβ and to reduce, causing reactive oxygen species to form. There is also evidence that Aβ promotes oxidative lipid damage in the presence of Cu [79] and this may initiate the misfolding of Aβ [80], increasing its neurotoxic effects [59]. Finally, it has been recently suggested that Cu imbalance in the hippocampus may be related to susceptibility to APP-related death in transgenic mice [171].

Zn has been shown to be particularly important in the hippocampus. For instance, Zn is stored in synaptic vesicles within the mossy fiber axons of the dentate granule neurons which extend to the CA3 and CA1 pyramidal neurons [172]. Glutamatergic synapses are abundant in this area and normally release Zn and Cu into the extracellular space at concentrations of up to 300 μM and 15 μM, respectively [126, 173-175]. This system is involved in processes related to learning and memory and one of the main roles of Zn in this region is to protect neurons from the exictotoxicity of glutamate [175]. In AD, Zn transporter (ZnT) proteins, which serve to regulate Zn in normal and pathological conditions the brain, are also affected in the hippocampus. For example, elevated expression of ZnT3, ZnT4, and ZnT6 have been observed in the hippocampi of human AD patients and transgenic mice [147, 176]. Furthermore, ZnT3 is primarily found in synaptic vesicles within the mossy fiber boutons, particularly in the hilus of the dentate gyrus to the CA3 pyramidal neurons [177]. Experiments in the Tg2576 mouse model lacking ZnT3 showed a drastic reduction in Zn in the hippocampal mossy fiber area, where the concentration is normally as high as 300 μM, as well as a reduction in plaque formation [126, 178].

Since maintenance of metal homeostasis in the hippocampus appears to be critical

in AD, the aim of the present study was to evaluate the distribution and concentration of these metal ions during normal aging in the hippocampus and how they are affected in AD. Previous studies utilized histochemical methods or bulk methods such as inductively coupled plasma mass spectrometry (ICP-MS) to measure metal ion content. However, histochemistcal techniques can only detect free and loosely bound metal ions and are not quantitative. ICP-MS can examine multiple metal ions simultaneously, but information on the spatial distribution of metal ions within cells and tissues is lost. X-ray fluorescence microscopy (XFM) is a highly sensitive technique that can be used to visualize and quantify multiple metal ions simultaneously in a tissue. XFM also measures the total amount of metal ions, not only the histochemically reactive, loosely bound, or free metal ions. The technique relies on the principle of X-ray fluorescence in which an incident photon is absorbed by an atom and inner shell electron is ejected, creating an electron hole. The resulting vacancy is filled by an outer shell electron and the excess energy is emitted as a characteristic X-ray. Characteristic X-rays are unique for each element and their intensities are proportional to the concentration in the sample. Using a synchrotron source allows trace metal ion concentration and distribution in the sample to be measured with a resolution of 5-10 μm and a sensitivity of less than 10 ppm (in 30 μm sections). In this study, we used synchrotron XFM to examine Fe, Cu, and Zn concentration and spatial distribution in the hippocampus of a PSAPP transgenic mouse model of plaque formation in AD as a function of aging. The evaluation of the spatial distribution and the local concentration in the hippocampus of trace elements involved in AD will help understand how different anatomical areas are affected in this critical brain region and may provide insight into the metal imbalances previously observed in AD.

4.3 Materials and Methods

4.3.1 Sample Preparation

Twenty-two female B6C3-Tg(APP_{swe}, PSEN1dE9)85 Dbo/J (PSAPP) mice and 26 age- and gender-matched B6C3F1/J control (CNT) mice were obtained from Jackson Laboratory (Bar Harbor, ME, USA). The mice were cared for and euthanized in accordance with the guidelines set by the Brookhaven National Laboratory (BNL) Institutional Animal Care and Use Committee and were housed at the Brookhaven

Laboratory Animal Facility under standard conditions. At time points representing pre-AD (13 weeks; PSAPP=6, CNT=6), early-AD (24 weeks; PSAPP=5, CNT=6), intermediate-AD (40 weeks; PSAPP=6, CNT=7), and late-AD (56 weeks; PSAPP=5, CNT=7), the mice were deeply anesthetized with 100 mg/kg 1:10 ketamine:xylazine administered by intraperitoneal injection. Afterwards, they were perfused transcardially with phosphate buffered saline, resulting in exsanguination and death. The brains were removed, frozen on dry ice, and stored at -80°C until further processing. For each sample, 30μm thick whole brain cryosections, which included the hippocampus, were mounted onto 3μm thick Ultralene film (SPEX CertiPrep, Metuchen, NJ) and dried at room temperature. The samples were kept in a dessicator until the XFM experiments were carried out.

4.3.2 SYNCRHROTRON XFM

The concentration and distribution of Fe, Cu, and Zn in the hippocampus were measured with XFM at the Biophysics Collaborative Access Team (BioCAT) beamline 18-ID-D at the Advanced Photon Source, Argonne National Laboratory (Argonne, IL). The synchrotron X-ray beam was tuned to 12 keV using a Si(111) double crystal monochromator. The incident beam was then collimated to 600 μm × 600 μm and then focused to 30 μm using Kirkpatrick-Baez focusing mirrors. This provided an X-ray flux to the sample of approximately 1.0×10^{12} photons/s. The sample was placed at a 45° angle to the incident X-ray beam, and X-ray fluorescence was detected with a Ketek single-element silicon drift detector (80 mm^2 active area) oriented at 90° to the incident beam. A light microscope objective (infinity K2/S long distance video microscope with CVF-12/3/4 objectives) was coupled to a Hitachi digital CCD camera for sample viewing in transmission geometry. Energy dispersive spectra were collected by raster scanning the sample using a dwell time of 1 s/pixel and a step size of 30 μm. Fe Kα, Cu Kα, and Zn Kα fluorescence counts were then extracted from background-corrected energy dispersive spectra. NIST thin-film standards NBS 1832 and 1833 were used for calibration and quantification. All data were normalized to variations in incident photon flux by normalizing to changes in I_0 measured by an upstream ion chamber.

4.3.3 DATA ANALYSIS

Elemental maps were created by fitting the full fluorescence spectrum at each pixel to modified Gaussians using MAPS software v.1.6.4.3 [179]. Area concentrations for each element were calculated by normalizing integrated fluorescence peak intensities to fitted spectra from the thin film standards NBS 1832 and 1833 and converting the fluorescence signal to a two-dimensional concentration in $\mu g/cm^2$. In order to partition the maps into different histological structures, cluster analysis was used to create unsupervised regions of interest (ROIs) in the hippocampus based on Fe, Cu, and Zn content. Two additional ROIs were created based on light microscopy to encompass the entire CA and DG areas to analyze the total metal ion content of the hippocampus and a small region corresponding to the choroid plexus (CP) outside of the hippocampus. The concentrations were converted from $\mu g/cm^2$ to molar units by first divding by the sample thickness (0.003 cm) and density, which was assumed to be 1 g/cm^3. That value was then divided by the molecular weight of the element. For each ROI, the concentrations of Fe, Cu, and Zn were determined and are presented in molar units (mean ± standard deviation). A Kruskal-Wallis test was performed using SPSS v.14.0 to test for significant differences between time points. Mann-Whitney U tests were used for post-hoc analyses on significant Kruskal-Wallis tests and to test for significant differences between PSAPP and CNT at each time point. Since regional regulation is complex and may involve interactions between the metal ions [171], we also performed a correlational analysis comparing each metal ion to another in specific regions of the hippocampus using Spearman ρ analysis. A significance level of 0.01 was used for all analyses.

4.4 RESULTS

The hippocampal formation consists of the subiculum, CA, and the DG. A visible image of an unstained hippocampal section can be seen in **Figure 1A**. XFM showed that the distributions of Fe, Cu, and Zn are higher in specific regions of the hippocampus **(Figure 1B-D)**. For example, the Zn concentration is highest in the region corresponding to the DG and CA3 **(Figure 1B)**, whereas the Fe concentrations is highest in the region corresponding to the pyramidal cell layer of the CA1 region **(Figure 1C)**. Cu appears to be uniformly distributed in the hippocampus but is high near the dorsal and lateral ventricles, most likely corresponding to the CP **(Figure 1D**). These trends were the same

for both PSAPP and CNT mice and across all time points. Four hippocampal anatomical ROIs were consistently identified using cluster analysis based on their Fe, Cu, and Zn content and are shown in **Figure 1E**. The green area corresponds to the the combined CA and DG regions (CA/DG) containing mainly granule and pyramidal cells and their dendrites, the blue area corresponds to the pyramidal cell layer of CA1 (PCL), the turquoise area corresponds to CA3, the magenta area corresponds to the hilus of the DG, and the yellow area corresponds to the CP.

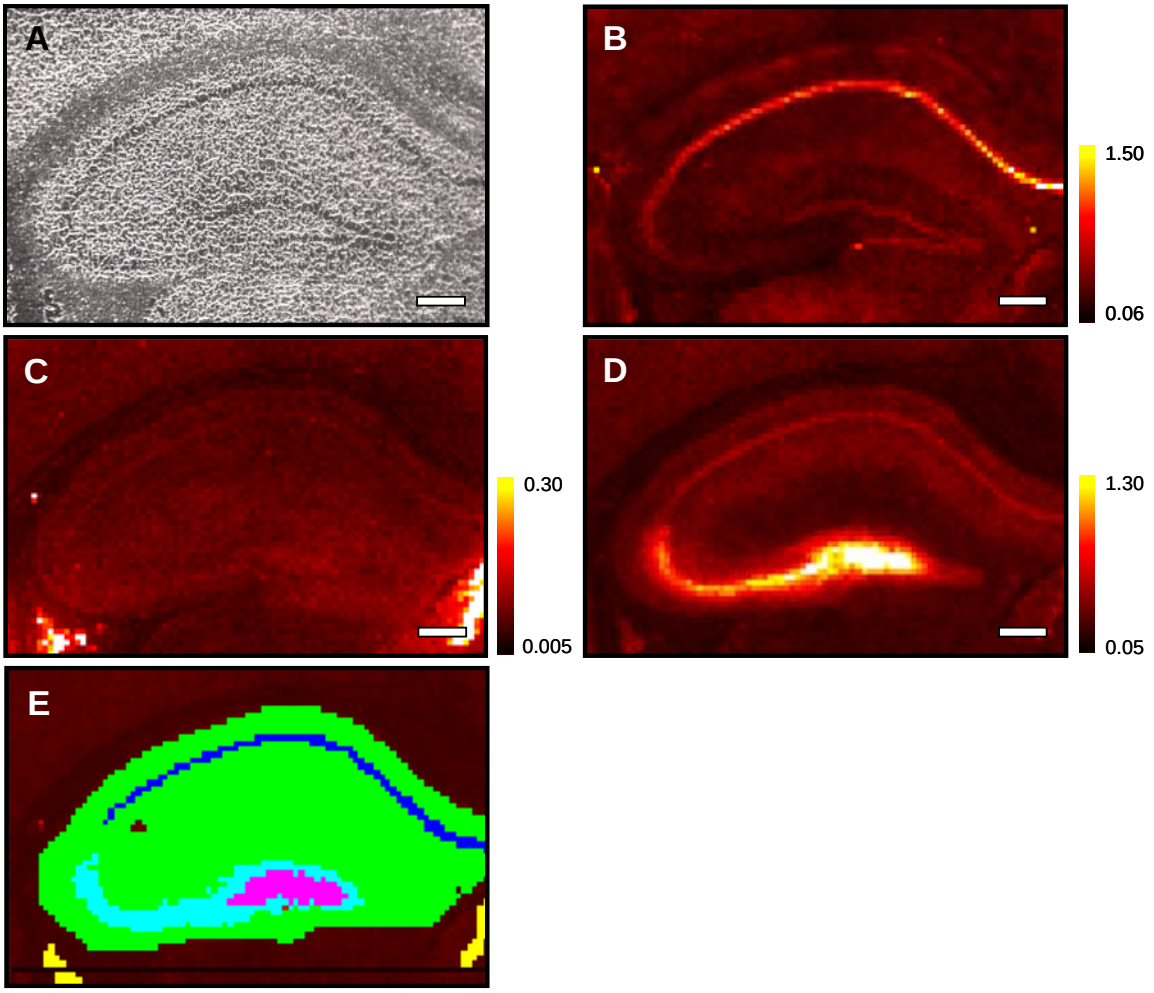

Figure 4.1 (A) Light micrograph of an unstained hippocampal brain section from a PSAPP mouse. XFM images of Fe (B), Cu (C), and Zn (D) in the same tissue section. Units are mM. Scale bar = 300 µm. (E) Hierarchical cluster analysis defining four distinct regions of the hippocampus based on metal content where CA/DG is green, the PCL is blue, CA3 is turquoise, and the hilus is magenta. The yellow area corresponds to the CP and was acquired manually.

The means and standard deviations of Fe content in each ROI at each time point for PSAPP mice and age-matched CNT mice are shown in **Table 1**. Results for all time points showed that Fe was highest in the PCL compared to the other ROIs. Specifically, the average Fe content in the full hippocampus was approximately 324 ± 43 μM, but was 642 ± 142 μM in the PCL. No significant changes were observed in the CNT mice as they aged Fe content in the full hippocampus in PSAPP mice significantly increased by 31.2% from 13 to 24 weeks-old, but significantly decreased from 24 to 56 weeks old by 14.7%, **(Figure 4.2A)**. In addition, the content in PSAPP mice (291 ± 15 μM) was significantly lower than in CNT mice (354 ± 21 μM) at 56 weeks old. The same trend was observed for the CA/DG and the PCL. For example, Fe content in the CA/DG **(Figure 4.2B)** in the PSAPP mice increased significantly by 30.1% from 13 to 24 weeks-old, but significantly decreased from 24 to 56 weeks old by 13.6% and was significantly lower than in the CNT mice at 56 weeks old (PSAPP: 280 ± 13 μM; CNT: 342 ± 21 μM). In the PCL **(Figure 4.2C)**, Fe content in the PSAPP mice increased significantly by 51.7% from 13 to 24 weeks-old and significantly decreased from 24 to 56 weeks old by 34.1% and was significantly lower than in the CNT mice at 56 weeks old (PSAPP: 291 ± 15 μM; CNT: 354 ± 21 μM). In the hilus, Fe content increased significantly by 37.6% from 13 to 56 weeks-old and was significantly higher than CNT mice at 56 weeks-old (PSAPP: 326 ± 31 μM; CNT: 270 ± 19 μM) **(Figure 4.2D)**.

The means and standard deviations of Cu content in each ROI at each time point for PSAPP mice and age-matched CNT mice are shown in **Table 2**. No significant changes were observed in Cu content, but, as expected, Cu content was highest outside the hippocampus in the region corresponding to the CP where the average Cu content was approximately 504 ± 297 μM, but was 79 ± 7 μM in the full hippocampus. The means and standard deviations of Zn content in each ROI at each time point for PSAPP mice and age-matched CNT mice are shown in **Table 3**.

Finally, Zn content was highest in the hilus of the DG (1435 ± 232 μM) compared to the full hippocampus (418 ± 47 μM) and increased significantly in the hilus by 44.9% from 13 to 40 weeks-old in the PSAPP mice only **(Figure 4.2E)**. Zn content in the PSAPP mice was also significantly higher than CNT mice at 56 weeks-old (PSAPP: 1757 ± 540 μM; CNT: 1150 ± 98 μM).

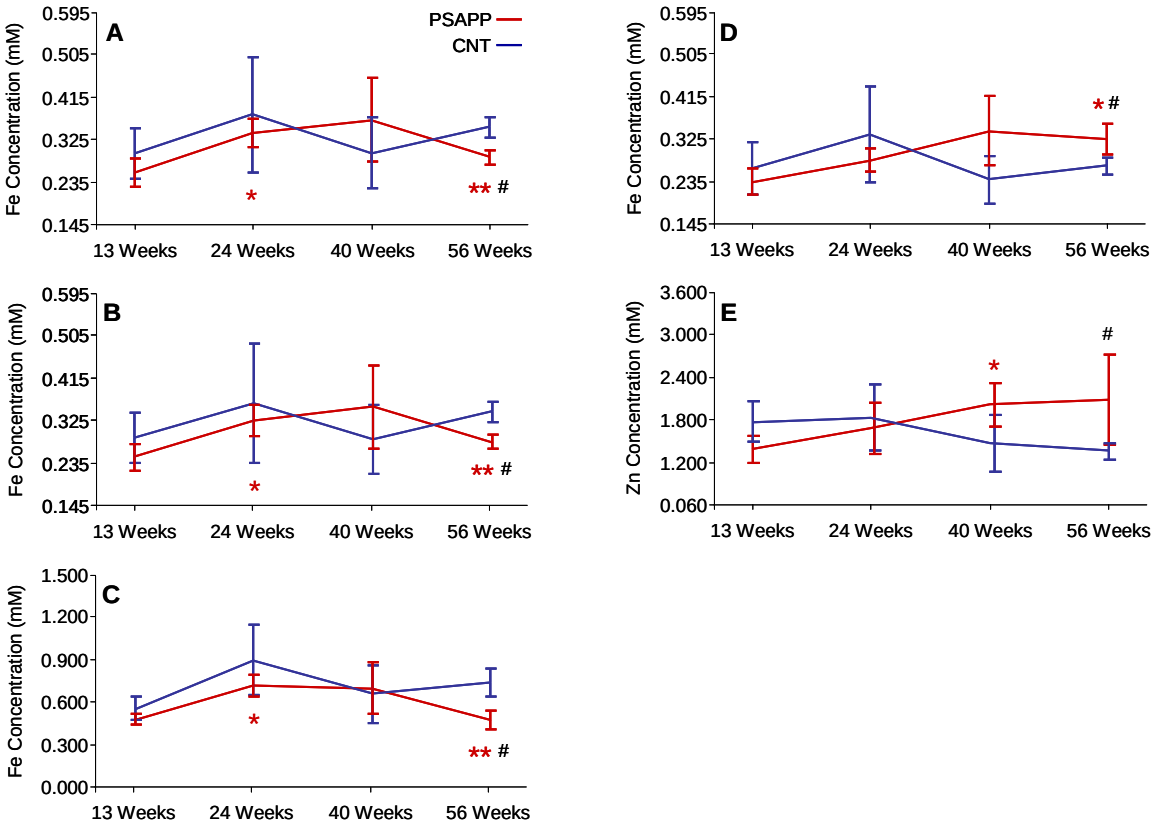

Figure 4.2 Fe in the full hippocampus (A), CA/DG (B), the PCL (C), and the hilus (D) as a function of aging in PSAPP and CNT mice. (E) Zn in the hilus as a function of aging in PSAPP and CNT mice. * = PSAPP mice significantly different from 13 week-old PSAPP mice ($p < 0.01$). ** = PSAPP mice significantly different from 24 week-old PSAPP mice ($p < 0.01$). # = PSAPP mice significantly different from CNT mice at the same time point ($p < 0.01$).

4.5 Discussion

There is growing evidence to suggest that dyshomeostasis of Fe, Cu, and Zn plays an important role in AD pathology [68, 93, 95, 146]. However, little is known about metal ion distribution in the hippocampus or if there are fluctuations in metal ion content over time. The goal of this study was to assess metal ion homeostasis in the hippocampus as a function of aging by investigating changes in the concentration and distribution of physiologically relevant metal ions in PSAPP mice and age-matched CNT mice. We examined the concentration and distribution of Fe, Cu, and Zn in the hippocampus at four time points representing pre-AD to late-AD using XFM. We observed significant fluctuations in Fe content in the PSAPP mice only. We also found that Zn content in the hilus was significantly higher in PSAPP mice than CNT mice at 40

weeks-old. No significant alterations in Cu were observed.

The hippocampus is a critical structure in the brain responsible for certain aspects of learning and declarative memory and is one of the first and most severely affected regions of the brain by amyloid pathology in AD [120]. Fe concentration in the hippocampus has been studied previously in human AD brain using atomic absorption spectroscopy [180]. However, this technique requires tissue homogenization and the spatial distribution of Fe in the hippocampus has not been imaged at a cellular level. The present results showed that Fe content in both PSAPP and CNT mice was highest in the PCL compared to other regions of the hippocampus. This is in contrast to a previous study that examined non-heme Fe content in the hippocampus and found the highest concentration of Fe to be in the CA2 and adjacent CA3 regions [181]. However, that study used a histochemical technique which mainly identifies Fe associated with the Fe storage protein, ferritin. The XFM technique used in the present study quantifies all forms of bound and unbound Fe. In addition, since the animals were perfused with PBS it is unlikely that the Fe observed in this region is heme iron associated with hemoglobin in blood.

Increased Fe in the brain has been consistently observed in AD and a number of studies suggest that Fe homeostasis is altered in AD [98, 137, 182]. The present results also showed fluctuations in Fe content in the PSAPP mice in all hippocampal ROIs. For example, Fe content in the full hippocampus, the CA/DG, and the PCL significantly increased from 13 weeks-old to 24 weeks-old and then significantly decreased from 24 weeks-old to 56 weeks-old. In addition, Fe content in CA3 and the hilus was also increased from 13 to 40 and 56 weeks-old, respectively. In contrast to the PSAPP mice, no significant alterations in Fe were observed in the CNT mice.

The early increase in Fe is consistent with previous studies in human AD showing Fe was increased in the hippocampus of patients with mild cognitive impairment, a condition thought to be an early precursor to AD [183]. On the contrary, another study using double transgenic APP/PS1 mice did not find any significant changes in Fe content with age in any brain region except the dorsal striatum [184]. However, that study examined mice in two different age ranges: young (27 to 45 weeks) and old (60-86 weeks). Based on previous research indicating Fe accumulation in the mouse brain

reaches a plateau at around 17 weeks [185], the authors concluded the mice were already too old to observe fluctuations in Fe. It is also possible that the large age range of the two groups masked any changes in Fe content. The mice in the current study were not only younger in the early-AD group (13 weeks), but the mice in each group were of the same age. The exact role of the alterations in Fe found in this study is unknown and could result from a number of factors. For example, the Fe storage protein ferritin is found in all areas of the hippocampus [186]. However, in contrast to normal aging, the ferritin level in human AD brain is thought to remain constant even though Fe content increases. For example, ferritin isolated from AD and Parkinson's patients had higher Fe content than that from control brains [187, 188]. *In vitro* studies have shown that excess iron leads to free radical formation, lipid peroxidation, and neuronal damage [189] and increased loading of ferritin provided a source for Fe-related free radical generation. Since Fe was increased in CA3 and in the hilus of PSAPP mice and not in the CNT mice, it is possible that this increase represents overloaded ferritin related to plaque pathology and not age.

Our results have also shown that PSAPP mice have 41.8% higher Zn content in the hilus than CNT mice. Zn content was also significantly increased by 44.9% from 13 to 40 weeks-old in PSAPP mice. The Zn transporter protein ZnT3 is localized in this region of the hippocampus and serves to sequester Zn ions into synaptic vesicles [177]. Previous studies have indicated a role for ZnT3 and synaptic Zn in AD. For example, in the same PSAPP mouse strain Zhang et al. showed that ZnT3 was 398.6% increased in the hippocampus compared to wild-type mice [190]. Furthermore, Tg2576 mice lacking ZnT3 are devoid of Zn in the hilus and also have reduced plaque load [126, 191]. While Fe in the present study was altered in all ROIs suggesting a global fluctuation in Fe content as a result of plaque pathology, increased Zn was confined to the hilus and implies a more specific defect. For example, Zn is co-localized with the neurotransmitter glutamate in the synaptic vesicles [192] and excess Zn may impede the reuptake of glutamate [193], which is toxic in excess [175]. In addition, Zn reuptake after synaptic release is a rapid and energy dependent process and it is possible that energy depletion could cause pooling of extracellular Zn [67, 76].

There are a few limitations associated with this study. First, the spatial resolution

was about 30 μm, which is on the order of the size of some cells in the hippocampus (e.g. mossy and pyramidal basket cells), but is much larger than others (e.g. dentate gyrus granule cells). Though changes were observed on a cellular scale, it is possible that that are extensive subcellular changes taking place, which could not be visualized and should be examined in the future in order to fully understand the involvement of metal ions in the disease process. Second, the measurements were acquired over the course of three beamtimes. Though beamtime to beamtime analysis should be consistent, we attempted to minimize possible inconsistencies by using non-parametric statistics with a small p value. In this way, we considered only the most robust results.

In summary, these studies have revealed that Fe and Zn homeostasis in the hippocampus is affected in a PSAPP mouse model of AD as a function of age. For example, Fe showed changes in all regions of the hippocampus, while Zn was elevated only in the hilus. These results provide further evidence for a general increase in brain Fe during plaque formation, but a more specific involvement of Zn, perhaps related to excess synaptic Zn. While it remains to be determined if altered metal ion levels are a cause or consequence of plaque pathology, it is possible that these fluctuations are important in increasing the oxidative stress, excitoxicity, and neurodegeneration implicated in AD.

4.6 ACKNOWLEDGMENTS

The authors would like to thank Janelle Collins for her skillful technical assistance with the animal dissection and tissue preparation. This work is funded by the National Institutes of Health Grant R01-GM66873. The NSLS and APS are supported by the United States Department of Energy, Office of Science, Office of Basic Energy Sciences, under contracts DE-AC02-98CH10886 and W-31-109-Eng-38, respectively.

Table 1. Fe Content in PSAPP and CNT Mice

ROI	13 weeks	24 weeks	40 weeks	56 weeks
Full Hippocampus				
PSAPP	260 ± 29	341 ± 31*	369 ± 89	291 ± 15**, ‡
CNT	299 ± 54	380 ± 122	300 ± 74	354 ± 21
CA/DG Layer				
PSAPP	249 ± 27	324 ± 32*	352 ± 85	280 ± 13**, ‡
CNT	288 ± 53	360 ± 122	285 ± 70	342 ± 21
PCL				
PSAPP	468 ± 37	710 ± 71*	688 ± 181*	468 ± 68**, ‡
CNT	546 ± 81	880 ± 246	649 ± 200	726 ± 96
CA3				
PSAPP	225 ± 29	294 ± 22*	346 ± 88*	291 ± 43
CNT	265 ± 69	345 ± 117	244 ± 57	395 ± 19
Hilus				
PSAPP	237 ± 28	281 ± 24	343 ± 71*	326 ± 31*, ‡
CNT	265 ± 55	335 ± 98	242 ± 50	270 ± 19
CP				
PSAPP	316 ± 162	382 ± 176	338 ± 111	242 ± 28
CNT	254 ± 49	306 ± 93	272 ± 72	309 ± 61

* = significantly different from 13 weeks

** = significantly different from 24 weeks

‡ = significantly different from CNT

Table 2. Cu Content in PSAPP and CNT Mice

ROI	13 weeks	24 weeks	40 weeks	56 weeks
Full Hippocampus				
PSAPP	72 ± 10	74 ± 10	91 ± 15	80 ± 13
CNT	76 ± 14	87 ± 23	70 ± 16	78 ± 12
CA/DG Layer				
PSAPP	76 ± 10	76 ± 11	95 ± 16	82 ± 14
CNT	77 ± 14	88 ± 23	71 ± 16	79 ± 13
PCL				
PSAPP	56 ± 7	62 ± 12	68 ± 9	66 ± 11
CNT	66 ± 14	77 ± 24	52 ± 13	58 ± 9
CA3				
PSAPP	58 ± 9	66 ± 6	77 ± 11	71 ± 6
CNT	70 ± 18	81 ± 22	66 ± 17	75 ± 13
Hilus				
PSAPP	66 ± 10	72 ± 9	81 ± 12	78 ± 12
CNT	75 ± 12	89 ± 21	81 ± 025	101 ± 32
CP				
PSAPP	387 ± 148	395 ± 178	1078 ± 350	702 ± 584
CNT	376 ± 181	300 ± 234	664 ± 70	728 ± 223

* = significantly different from 13 weeks

** = significantly different from 24 weeks

‡ = significantly different from CNT

Table 3. Zn Content in PSAPP and CNT Mice

ROI	13 weeks	24 weeks	40 weeks	56 weeks
Full Hippocampus				
PSAPP	378 ± 40	427 ± 85	462 ± 104	410 ± 80
CNT	472 ± 105	467 ± 79	349 ± 65	376 ± 23
CA/DG Layer				
PSAPP	294 ± 33	334 ± 68	360 ± 83	312 ± 59
CNT	366 ± 79	370 ± 65	270 ± 54	297 ± 20
PCL				
PSAPP	374 ± 36	401 ± 48	438 ± 084	411 ± 114
CNT	452 ± 64	463 ± 103	320 ± 57	345 ± 29
CA3				
PSAPP	752 ± 91	814 ± 142	950 ± 178	868 ± 207
CNT	893 ± 193	979 ± 198	762 ± 160	774 ± 53
Hilus				
PSAPP	1173 ± 161	1415 ± 303	1700 ± 266*	1757 ± 540‡
CNT	1497 ± 238	1547 ± 393	1244 ± 345	1150 ± 98
CP				
PSAPP	245 ± 50	264 ± 18	310 ± 66	228 ± 43
CNT	299 ± 57	301 ± 63	245 ± 44	268 ± 24

* = significantly different from 13 weeks

** = significantly different from 24 weeks

‡ = significantly different from CNT

CHAPTER 5

UNSATURATED LIPID CONTENT IS REDUCED IN THE HIPPOCAMPUS OF THE PSAPP TRANSGENIC MOUSE MODEL OF ALZHEIMER'S DISEASE [194]

5.1 ABSTRACT

Polyunsaturated fatty acids are essential to brain function and are reduced in the brains of Alzheimer's disease (AD) patients. However, it is not known how they are affected in different regions of the hippocampus, which is a primary target of AD pathology. In this study, we used Fourier Transform Infrared Imaging (FTIRI) to visualize the unsaturated lipid content in specific regions of the hippocampus in the PSAPP mouse model of AD as a function of disease severity. Specifically, the axonal, dendritic, and somatic layers of the hippocampus were examined in the mice at 13 weeks, 24 weeks, 40 weeks and 56 weeks old. Results showed that lipid unsaturation in the axonal layer is significantly increased with normal aging in control (CNT) mice ($p < 0.01$), but remained low and relatively constant in PSAPP mice. Thus, these findings indicate that unsaturated lipid content is reduced in hippocampal white matter during amyloid pathogenesis and that maintaining unsaturated lipid content early in the disease may be critical in avoiding progression of the disease.

5.2 INTRODUCTION

The brain contains the highest lipid content of any other organ in the body, with the exception of adipose tissue. However, adipose tissue utilizes lipids for energy storage, while nearly all lipids in the brain have a role in modifying the structure, fluidity, and function of cellular and subcellular membranes and in myelin [195]. These membrane lipids are comprised of saturated, monounsaturated, and polyunsaturated fatty acids including gangliosides, phospholipids, and cholesterol [195].

Polyunsaturated fatty acids (PUFAs) synthesized from ω-3 and ω-6 essential fatty acids are key structural components of phospholipid membranes and are critical for brain growth, membrane fluidity, signal transduction, and visual and cognitive development [45]. Normal brain function depends on maintaining homeostatic concentrations of PUFAs both during development and throughout life [45]. Indeed, impairments in PUFA metabolism have been implicated in many neurological diseases, including Alzheimer's disease (AD). For example, blood levels of the ω-3 PUFA docosahexaenoic acid (DHA) were found to be lower in AD patients compared to control subjects without cognitive impairment [46]. Levels of DHA and arachidonic acid in the brains of AD patients were also shown to be lower than in control patients [47]. Furthermore, lower levels of DHA were associated with the loss of post-synaptic proteins in dendrites in a transgenic mouse model of AD [48] while DHA reduced amyloid burden in cell culture [49] and in transgenic mouse models of AD [50, 51], possibly by inhibiting the amyloidogenic pathway or by upregulating amyloid beta (Aβ) clearance mechanisms.

Unsaturated lipids are highly vulnerable to oxidative attack because of their double bond content and the increased degradation of PUFAs in AD may be evidence of lipid peroxidation [196]. Lipid peroxidation is marked by elevated levels of thiobarbituric acid reactive substances, isoprostanes, and chemically reactive, diffusible aldehydes, such as 4-hydroxy-2-neonenal, malondialdehyde, and acrolein [54]. Under normal conditions, the brain is generally protected from oxidative damage through a careful balance of physiological amounts of reactive oxygen species and antioxidant defenses [57]. However, these mechanisms may be impaired in AD and increasing evidence shows elevated lipid peroxidation products and protein carbonyl formation in human AD brain [197, 198] and in transgenic AD mice [199, 200], particularly in regions

of high amyloid plaque density such as the hippocampus and inferior parietal lobule [201]. For example, protein carbonyl content was 42% higher in AD hippocampus relative to the cerebellum, while control hippocampus and cerebellum levels were similar [201].

The hippocampus is of pathological relevance to AD and previous studies have suggested neuronal loss [120] and loss of unsaturated lipids in this region [47, 122]. However, previous investigations of unsaturated lipid content in the brain employ biochemical techniques that require homogenization, eliminating the ability to study and visualize specific brain regions. Fourier Transform Infrared Imaging (FTIRI) is an analytical technique that is used to examine the chemical composition of multiple biological components simultaneously in unfixed, unstained, thin sections of biological tissue. Its usefulness in imaging biological tissue [110] and specifically monitoring unsaturated lipid content by utilizing the olefinic =CH stretching mode (3012 cm^{-1}) has been demonstrated previously [202-204].

In this study, we used FTIRI to visualize unsaturated lipid content in specific areas of the hippocampus in a PSAPP mouse model of AD as a function of animal age. This mouse model expresses a mutant human presenilin 1 (PS1) gene and a chimeric mouse/human amyloid precursor protein gene (APP), developing amyloid plaques in the same brain regions as human AD by around 6 months of age [103, 104]. The evaluation of unsaturated lipid content and distribution in individual regions of the hippocampus will help understand how different anatomical areas are affected in this critical brain region and how accumulation of unsaturated lipid may be impaired in AD.

5.3 Materials and Methods

5.3.1 Tissue Preparation

Twenty female B6C3-Tg(APP_{swe}, PSEN1dE9)85 Dbo/J (PSAPP) mice and twenty age- and gender-matched B6C3F1/J control (CNT) mice were obtained from Jackson Laboratory (Bar Harbor, ME, USA). The mice were cared for and euthanized in accordance with the guidelines set by the Brookhaven National Laboratory (BNL) Institutional Animal Care and Use Committee and were housed at the Brookhaven Laboratory Animal Facility under standard conditions. Animals were fed the standard

Mouse Diet 5015 (PMI Nutrition International, St. Louis, MO, USA). At time points representing pre-AD (13 weeks; PSAPP=5, CNT=5), early-AD (24 weeks; PSAPP=5, CNT=5), intermediate-AD (40 weeks; PSAPP=5, CNT=5), and late-AD (56 weeks; PSAPP=5, CNT=5) the mice were deeply anesthetized with 100 mg/kg 1:10 ketamine:xylazine administered by intraperitoneal injection. Afterwards, they were perfused transcardially with phosphate buffered saline, resulting in exsanguination and death. The brains were removed, frozen on dry ice, and stored at -80°C until further processing. For each sample, 10 μm thick coronal, whole brain cryosections, which included the hippocampus, were mounted onto IR transparent calcium fluoride (CaF_2) slides (Korth Kristalle GmbH, Altenholz, Germany) and dried at room temperature. The CaF_2 slides were kept in a dry and dark environment until the FTIRI experiments were carried out.

5.3.2 Fourier Transform Infrared Imaging (FTIRI)

FTIR spectroscopy is a measurement of the absorbance of infrared light as a function of wavelength in a sample. If a specific functional group in a molecule is subjected to infrared light of its specific vibrational frequency, it will absorb that frequency of light, creating a peak in the absorption spectrum [205, 206]. Moreover, the size of the peak is proportional to its concentration in the sample according to the Beer-Lambert Law. For example, lipids have characteristic C-H stretching vibrations between 2700 – 3000 cm^{-1} [207]. Specifically, the asymmetric and symmetric C-H stretching vibrations of the aliphatic $–CH_2$ functional group fall at ~2920 and 2850 cm^{-1}, respectively. For $–CH_3$ functional groups, the asymmetric and symmetric C-H stretching vibrations are found at ~2957 and 2872 cm^{-1}, respectively. In this study, we are examining the unsaturated olefinic $=CH_2$ stretching vibration, which has a unique vibrational frequency of 3012 cm^{-1} and is well-separated and distinguishable from the saturated aliphatic peaks. Thus, FTIR spectroscopy provides a quantitative chemical footprint of the composition of a sample without the need for stains or probe molecules.

The FTIRI data were collected using a Bruker imaging system (Bruker Optics, Billerica, MA, USA) consisting of a Vertex 80v Rapid Scan FTIR spectrometer, coupled to a Hyperion 3000 IR microscope, equipped with a 128 × 128 mercury cadmium telluride focal plane array detector (Santa Barbara Focalplane, Goleta, CA, USA). For

each sample, an area approximately 2.5 mm × 2 mm encompassing the hippocampus was imaged. At each pixel, absorbance spectra in the mid-infrared spectral range (4000–800 cm^{-1}) were collected using a 15X objective in transmission mode with a spectral resolution of 8 cm^{-1}, 64 scans co-added, and 8 × 8 pixel binning, resulting in a final pixel resolution of 21.6 μm. A background spectrum was collected from clean CaF_2 and ratioed to each of the sample spectra. All spectra then underwent quality tests to remove spectra with poor signal-to-noise in the absorbance-free region of the spectrum from 1900 – 2200 cm^{-1}. The remaining spectra were subsequently converted into first derivative spectra using a 9-point Savitzky-Golay algorithm.

5.3.3 Separating Histological Structures of the Hippocampus

In order to partition the spectra into different histological structures, i.e. regions of interest (ROIs), unsupervised reduced hierarchical cluster analysis (HCA) was performed on the first derivative spectra in the 1620 – 1680 cm^{-1} (i.e. protein) and 2750 – 3020 cm^{-1} (i.e. lipid) spectral regions. This is a technique that clusters IR spectra together based on their similarity to each other. D-values based on Pearson's correlation coefficient were used to calculate the distance matrix, which determines the similarity of the spectra. Hierarchical clustering was subsequently performed using Ward's algorithm, which searches the distance matrix for clusters of similar spectra. On average, five clusters were required to separate the images into histological ROIs. For each ROI, an average spectrum was calculated. In addition, binary masks were created for each ROI. This was done by converting each ROI pixel in the matrix to ones and the remainder of the pixels in the matrix to zeroes, then repeating the procedure for each ROI separately.

5.3.4 Principal Components Analysis

Principal components analysis (PCA) is a technique used to reduce the dimensionality of a large dataset without decreasing the variance. It is used to determine if one sample set is different from another and which variables (absorption frequency in the present case, i.e. cm^{-1}) contribute most to the difference. The first principal component (PC) is the combination of variables that accounts for the greatest amount of the total variation, while the second PC accounts for most of the remaining variation and is orthogonal to the first PC. In order to identify spectral regions as possible sources of

maximum variance associated with AD mice and CNT mice, the average spectra from each ROI for each sample that were derived from HCA analysis were subjected to PCA using The Unscrambler 9.8 (CAMO, Norway). All average spectra were converted into second derivative spectra using a 7-point Savitzky-Golay smoothing algorithm. PSAPP mice were analyzed with their corresponding age-matched controls at each time point in each ROI using a Norris Gap algorithm and a fully cross-validated model. Scores plots were created to identify any clustering of the sample groups, which would indicate variability between the sample groups. If group clusters were identified, a loadings plot of the most influential PC was created to assess the contribution of each wavenumber to the total variance.

5.3.5 INTEGRATION PROFILES

The degree of unsaturation was investigated by examining the olefinic =CH stretching vibration at 3012 cm^{-1}. The peak intensity at 3012 cm^{-1} is proportional to the amount of unsaturated lipid in the tissue [202, 204]. The olefinic content was calculated as a ratio of the integrated area from 3000 – 3020 cm^{-1} normalized to the total lipid content, i.e. the integrated area of the total C-H stretching region (2750 – 3020 cm^{-1}). A linear baseline in the same spectral region was applied. The total lipid (2750 – 3020 cm^{-1}) to protein (1620 – 1680 cm^{-1}) ratio was also calculated.

After the chemical images for olefinic content were created, the masks for each of the three ROIs described above were applied to each image separately and the resulting images contained only the data points (approximately 1000-4000 pixels) from each ROI. For each ROI, the median olefinic content was determined. The median values were then obtained for PSAPP and CNT mice at each time point. A Kruskal-Wallis test was performed using SPSS v.14.0 to test for significant differences between PSAPP and CNT at each time point, and differences between time points. Post-hoc analyses on significant Kruskal-Wallis tests were performed using Mann-Whitney U tests. A significance level of 0.01 was used for all analysis.

5.4 RESULTS

The hippocampal formation consists of the subiculum, CA, and the DG. A visible image of an unstained hippocampal section can be seen in **Figure 5.1A**. Using HCA,

three hippocampal anatomical ROIs were consistently identified based on their lipid and protein content and are shown in **Figure 5.1B**. The red area corresponds to the alveus and fimbria which are rich in axons (axonal layer), green corresponds to the dendrites of the hippocampus (dendritic layer), and blue corresponds to the cell somata of the granule cells of the DG and pyramidal cells of the CA (somatic layer). The subiculum was not included in the area imaged and was therefore not part of the analysis. Also, the fimbria and alveus are generally not considered part of the "hippocampal formation", but they carry many subcortical afferent and efferent fibers through the hippocampus and are also highly enriched in lipids. Moreover, previous research shows that despite primarily being considered a disease of the grey matter, white matter alterations have also been observed in AD [208, 209]. Therefore, we included this region in the analyses. Also shown in **Figure 5.1C** are representative spectra from each ROI, illustrating the differences in lipid content. The axonal layer spectrum (red) has a strong intensity in the area of the spectrum mainly attributed to lipids (2750 – 3020 cm^{-1}) and corresponds to the high myelin content in this region. The dendritic layer spectrum (green) is intermediate in lipid content, but contains a higher proportion of protein (1620 – 1680 cm^{-1}) relative to the axonal layer spectrum. The somatic layer spectrum (blue) contains the least amount of lipid but a similar amount of protein as the axonal layer spectrum.

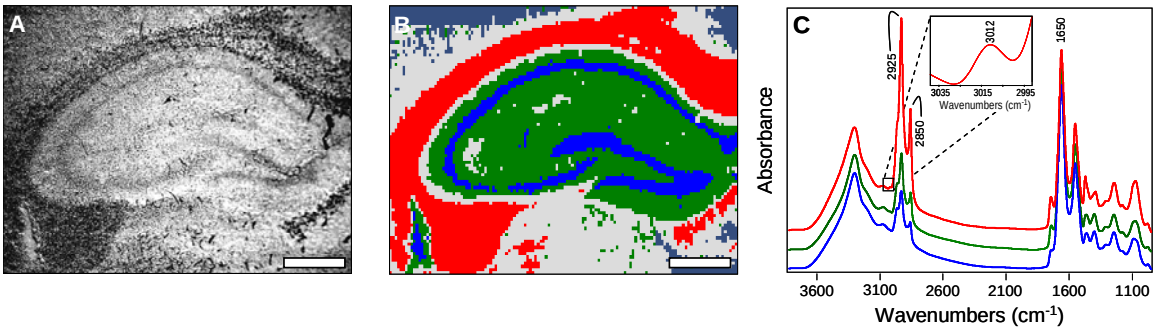

Figure 5.1 (A) Light micrograph of an unstained hippocampal brain section from a PSAPP mouse. (B) Hierarchical cluster analysis defining three distinct regions of the hippocampus based on lipid content where the axonal layer is red, the somatic layer is green, and the dendritic layer is blue. Scale bar = 500 µm. (C) Average spectrum from each of the three regions illustrating differences in lipid content when normalized to protein content. Important peak frequencies are indicated. Inset shows the olefinic =CH stretching region (3012 cm^{-1}) from the axonal layer spectrum.

Our first goal was to use PCA to identify the specific regions of the FTIR spectra that contributed to the observed variance in the data. The PCA scores plot of the average axonal layer spectra from the endstage animals (**Figure 5.2A**) shows that PSAPP mice are easily discriminated from CNT by using the first two components, PC1 and PC2, which account for 95% and 2% of the variance, respectively. Interestingly, the earlier time points or other ROIs did not show such discrimination (data not shown). To visualize the spectral regions displaying the most variability, loadings plots were used to highlight the contribution of each spectral frequency to each PC. In the PC1 loadings plots (**Figure 5.2B**), the major contributions to spectral variation between PSAPP and CNT endstage mice were the olefinic (=CH) stretching vibration (3012 cm^{-1}), the asymmetric and symmetric C-H stretching vibrations from CH_2 and CH_3 groups (2865 – 2960 cm^{-1}), the C=O stretching vibration of carbonyl esters (1740 cm^{-1}), the Amide I (1654 cm^{-1}) and Amide II (1550 cm^{-1}) protein bands, and the symmetric C-H scissoring of CH_2 (1465 cm^{-1}). However, the C-H stretching region showed the largest differences.

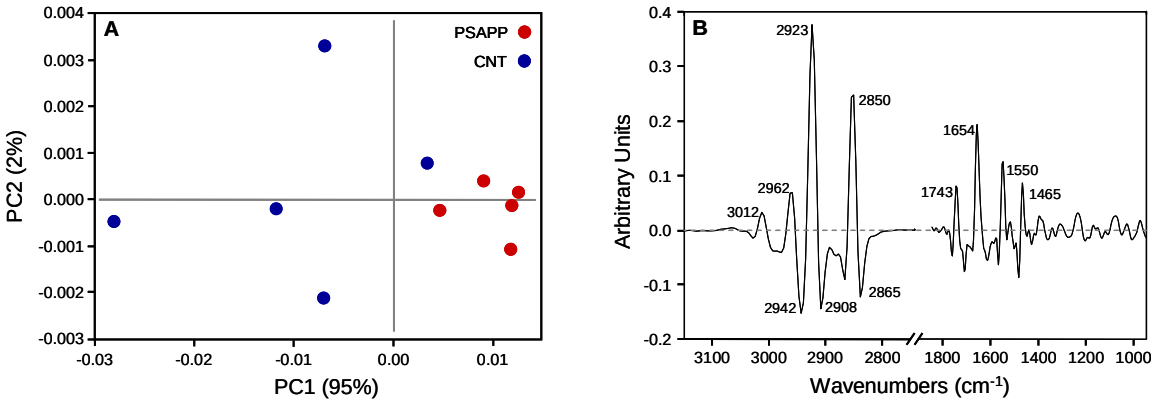

Figure 5.2 (A) Scores plot of average axonal layer spectra from 56 week-old PSAPP and CNT mice; (B) PC1 loadings of average axonal layer spectra from 56 week-old PSAPP and CNT mice.

We then examined lipid unsaturation in each ROI by calculating the integrated area of the olefinic =CH peak (3000 – 3020 cm^{-1}) divided by the integrated area of the total lipid region (2750 – 3020 cm^{-1}). A lower ratio indicates a lower level of lipid unsaturation. In both PSAPP and CNT animals, the olefinic peak at 3012 cm^{-1} was most easily detected in the axonal layer, while the content was below the detection limit in the

other ROIs at all time points. The distribution of unsaturated lipid in the axonal measured by integrated olefinic peak area at each pixel is shown in **Figure 5.3**, where red indicates a large olefinic peak area, demonstrating a high unsaturated lipid content, whereas purple indicates a small olefinic peak area, demonstrating lower lipid unsaturation. In the 13 and 24 week-old CNT mice, a low olefinic content was observed throughout the axonal layer (**Figure 5.3,** top row). However, from 24 to 40 weeks-old, the level of unsaturated lipids increased, as evidenced by a significant increase in the median integrated area of the olefinic peak from 0 at 24 weeks to 0.0005 at 40 weeks ($p < 0.01$). The median integrated olefinic peak area increased even more at 56 weeks-old to 0.0013 ($p < 0.01$), indicating a further increase in unsaturated lipid content. In the 13 and 24 week-old PSAPP mice, the unsaturated lipid content was similar to the CNT mice as the median integrated olefinic areas were identical. However, at 40 and 56 weeks, the median integrated olefinic area remained low and relatively constant, indicating that plaque pathology was keeping the unsaturated lipid content low. Finally, the lipid / protein ratio was similar across all time points in both PSAPP and CNT mice (data not shown).

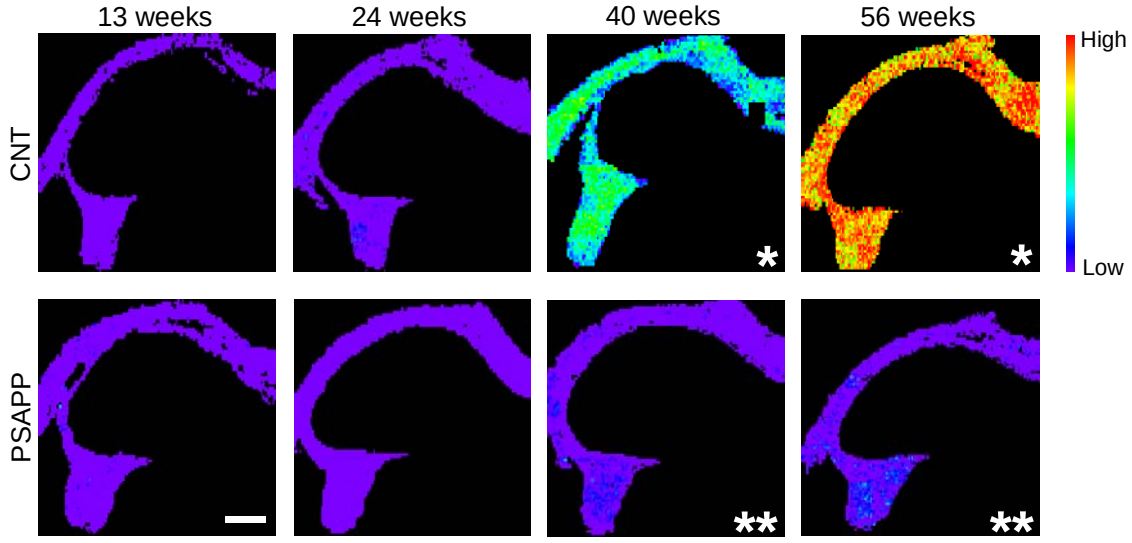

Figure 5.3 Olefinic content as a function of age in CNT mice (top row) and PSAPP (bottom row) in the axonal layer. Red indicates very high olefinic content while purple represents very low olefinic content. * = median is significantly different from 13 and 24 week-old CNT mice ($p < 0.01$); ** = median is significantly different from CNT mice at the same time point ($p < 0.01$).

5.5 DISCUSSION

The hippocampus is a critical structure in the brain responsible for certain aspects of learning and declarative memory and is one of the first and most severely affected regions of the brain by amyloid pathology in AD [120]. The goal of this study was to characterize the unsaturated lipid content and distribution in the intact hippocampus of an aging mouse and to assess changes in unsaturated lipid content in the age-matched PSAPP mouse using FTIRI. We found that regions of the hippocampus containing higher amounts of lipid are affected differently in the PSAPP mice than in normal aging.

In this study, the parameter that was used to assess the amount of unsaturated lipid is the olefinic =CH stretching vibration at 3012 cm^{-1} of the IR spectrum. A decrease in this peak corresponds to a loss of unsaturation in fatty acid chains, mainly arachidonic and docosahexaenoic acids [202, 204]. We observed that this peak is most intense in the white matter-rich axonal layer, while much lower in the other two ROIs. However, the content was low in both young CNT and PSAPP mice from 13 to 24 weeks. We observed a significant increase in olefinic content in the axonal layer of CNT mice as they grew older (i.e. after 24 weeks), while the olefinic content remained low throughout the lifespan of the PSAPP animals. Since the olefinic content was normalized to total lipid content, this implies an increase in unsaturation in the CNT mice with age, but not in the PSAPP mice. Thus, while AD is thought to primarily affect the grey matter, these findings support evidence that white matter regions, including those connected to the hippocampus, are also affected [209].

In rodents, myelination is rapid during post-natal development, but steadily increases throughout aging [210]. Thus, it is possible that the observed increase in unsaturated lipid in the axonal layer of CNT mice represents an increase in myelination since myelin contains unsaturated fatty acids [211]. Though we did not observe any differences between CNT or PSAPP mice across all time points in the total lipid / protein ratio, earlier studies have shown that, while the total lipid content in the myelin of the developing rat brain does not change, the fatty acid composition of the lipid is altered [212, 213]. For example, sphingomyelin, cerebroside, phosphatidic acid, and inositol plasmalogen are all increased [210]. On the contrary, an increase in unsaturation of the longest acyl chains of major myelin glycosphingolipids with aging could represent

decreased myelin stability [214]. The present results further suggest that the total lipid content in the axonal layer remains constant in both PSAPP and CNT mice, and that unsaturated lipids accumulate as the CNT mouse brain develops.

Since unsaturated lipid accumulated in the CNT mice, it is possible that accumulation in the PSAPP mice was inhibited. For example, the unsaturated class of lipids, dolichol, which increase membrane fluidity, increase substantially in the brain during aging [215]. In rats, it has been shown to increase 100-fold from birth to two years of age [216] and appears to be a common feature of the aging process, though through unknown mechanisms [217]. However, in AD brain dolichol is markedly decreased [218]. A decrease in unsaturated lipids could also represent a deficiency in the uptake of the essential fatty acids linoleic and linolenic acids, both of which are required for biosynthesis of long-chain PUFAs [219]. Since mammals cannot produce either of these essential fatty acids, they must be introduced through the diet. Both the CNT and PSAPP mice in this study were fed identical, standard diets that contained linoleic acid. Thus, a dietary deficiency cannot explain the differences, but it is possible that the disease process impaired the normal processing pathways for the synthesis of PUFAs from dietary unsaturated fatty acids and/or the incorporation of them into the brain.

The low unsaturated lipid content in the endstage PSAPP mice may also be a result of Aβ-mediated lipid peroxidation. Polyunsaturated lipids in the brain are readily attacked by free radicals because of their double bond content, becoming oxidized into lipid peroxides [52]. Aβ, the primary component of amyloid plaques, has been implicated in oxidative damage through metal ion reduction [82], lipid peroxidation in synaptic plasma membranes [79, 220], and production of HNE in hippocampal neurons [221]. Indeed, increased lipid peroxidation has been observed in human AD, mild cognitive impairment, and in transgenic mouse models of AD [197, 222, 223], suggesting that antioxidant defenses are impaired in AD [57]. This is consistent with recent work by Petursdottir and colleagues [122] who that demonstrated that 12 month-old senescence-accelerated mice had decreased α-tocopherol, a lipid soluble antioxidant, in the hippocampus and amygdala compared to young mice, which also coincided with a decreased proportion of docosahexaenoic acid and arachidonic acid in these regions.

In addition to lipid peroxidation, gliosis is a common occurrence in AD brain

[224, 225]. Glial cells are not only capable of producing free radicals [226], but glial membranes also contain less unsaturated lipid than neuronal membranes [227]. In AD, astrocytes typically become reactive around amyloid plaques [228]; gliosis accompanied by tissue degeneration has also been observed in the dentate gyrus and subiculum of AD patients in response to lesions of the afferent projection sites [229] and also in the white matter of AD patients [230]. Moreover, an increase in astrocytes is associated with a decrease in oligodendrocytes in the white matter of AD patients [231]. In addition, axonal and oligodendroglial loss is accompanied by deep white matter gliosis, which is independent from grey matter lesions [232]. It is possible that the decreased level of unsaturated lipid observed in the PSAPP mice in the present study may also represent astrocytic gliosis or oligodendroglial or axonal loss in response to the insults caused by plaque formation.

In summary, we found that unsaturated lipid accumulation increases during normal aging but is impaired in PSAPP mice and that this defect occurs at early time points, preferentially in the white matter. It is possible that the effects of AD play a crucial role long before the onset of amyloid plaque pathology and may initiate a cascade of events of which the consequences extend well into the disease process. Taken together, these results indicate that damage to white matter occurs at the beginning stages of amyloid plaque formation in the PSAPP mouse model of AD, and preventing loss of unsaturated lipid early may be critical in avoiding the onset of the disease.

5.6 ACKNOWLEDGMENTS

The authors would like to thank Janelle Collins for her skillful technical assistance with the animal dissection and tissue preparation. We would also like to thank Alvin Acerbo and Randy Smith for assistance with the FTIR microscope. This work is funded by the National Institutes of Health Grants R01-GM66873 and S10-RR023782. The National Synchrotron Light Source is funded by the U.S. Department of Energy, Office of Science, Office of Basic Energy Sciences, under Contract DE-AC02-98CH10886. There are no conflicts of interest associated with this work.

CHAPTER 6

DISCUSSION, CONCLUSIONS, AND OUTLOOK

AD is a devastating neurodegenerative disorder characterized by the decreasing ability to function, the accumulation of neurofibrillary tangles and amyloid plaques in the brain. The eventual result is death. The etiology of AD is very complex and remains largely unknown, but imbalances of naturally occurring metal ions in the brain, such as Fe, Cu, and Zn, are thought to be important contributors to the disease process. However, studies on brain metal content in human AD patients can only be done upon autopsy. Thus, important information on what happens in the brain before disease onset is missing. Therefore, this dissertation was undertaken to examine metal ion content in the brain using a PSAPP mouse model of plaque formation in AD, from pre- to late-stages. **Specific Aim 1** addressed this uncertainty by examining plaque and non-plaque cortical tissue in PSAPP mice as the animals aged. It is also unknown how the chemical composition in terms of unsaturated lipid and metal ion content of the hippocampus, a critical brain region affected by AD, is altered in response to plaque formation. Therefore, **Specific Aim 2** was designed to examine the metal ion content using XFM and unsaturated lipid content using FTIRI in the hippocampus in PSAPP and CNT mice as the mice aged. Our techniques enabled us to examine Fe, Cu, and Zn content simultaneously in the same tissues, in contrast to histology, which only permits the examination of one element, and to bulk techniques, which eliminate spatial orientation. Overall, our studies suggest that Fe is altered early in the disease process, possibly in response to plaque formation, and that Cu may be a factor in the neurodegeneration observed in human AD.

6.1 IRON AND ZINC HOMEOSTASIS IN THE BRAIN

Fe is required in the brain for metabolic processes, as well as DNA synthesis, gene expression, myelination, neurotransmission, and mitochondrial electron transport.

Global Fe homeostasis is regulated at the level of Fe absorption from the gastrointestical tract. After absorption, Fe in the oxidized form (Fe^{3+}) binds to serum transferrin (Tf) and is distributed throughout the general circulation. The blood brain barrier (BBB) tightly regulates the exchange of Fe between the blood and neuropil, which allows the brain to regulate its Fe content independently of other tissues. Fe is thought to cross the BBB by binding to transerrin receptors (TfR) within the luminal membranes of cerebral endothelial cells. Fe^{3+} is dissociated from Tf, reduced to Fe^{2+} and a divalent metal transporter (DMT1) translocates the Fe from the endosome to the cytosol. The Fe-free Tf, bound to TfR, is transported back to the plasma membrane, where it is released back into the circulation. After crossing the BBB, Fe^{2+} is oxidized to Fe^{3+} by the ferroxidase activity of ceruloplasmin, allowing the Fe to be stored in a redox-inactive form. It then either passes into the mitochondria to supply Fe for haem and Fe-sulphur cluster biosynthesis, or is stored in the cytosolic Fe-storage protein ferritin [124].

Within the cytosol, Fe is tightly regulated since Fe is an important source for cytosolic, mitochondrial, and nuclear ferroproteins and because excessive accumulation of free Fe^{2+} is a source of oxidative stress and cytotoxicity. Ferritin serves to detoxify and store Fe in the cytosol. It is also present in axons and may transport Fe to the synapse.

Finally, the major route of Fe export out of the brain is via the CSF and reabsorption back into the blood. Transferrin, lactoferrin, ferritin are all present in the CSF and may contribute to Fe export.

The brain has the highest Zn content with respect to other organs in the body. Zn transport into the brain is thought to occur when Zn binds to albumin or L-histidine in the plasma and CSF which transfers Zn to target sites and regulate its uptake across the BBB [233]. Like Fe, Zn is transferred to DMT1 or other Zn transporters to the brain endothelial cells, which respond to changes in Zn status. However, the mechanism of transfer from the endothelial cells to the brain extracellular fluid is not known [234]. From the extracellular fluid, Zn uptake by neurons and glial cells is mediated by Zip transporters. ZnTs then regulate the transport of Zn from neurons into synaptic vesicles. Alternatively, Zn^{2+} homeostasis could be modulated through uptake by neuronal mitochondria [235].

6.2 THE INVOLVEMENT OF METAL IONS IN AD

The first goal of this dissertation was to examine the metal ion content in the plaques of PSAPP mice as the mice aged. We found that Fe, Cu, and Zn content in the plaques was not elevated until the mice were 56 weeks-old. However, after normalization to protein density, we found that the plaques were elevated only in Zn. We then compared the results from the endstage PSAPP plaques to endstage human AD plaques. We found clear evidence that Cu is lacking from endstage PSAPP plaques, but is abundant in endstage human AD plaques. This difference between the two species is beneficial and suggests a specific role of Cu and Aβ in human AD. For example, Aβ reduces Cu^{2+} to Cu^{+}, an interaction which mediates neurotoxicity through production of H_2O_2 [82, 86]. The abundance of Cu in the human plaques could be one reason why human AD exhibits such severe neurodegeneration, which is not observed in mouse models of AD.

In human AD, metal ion fluctuation in the brain has been demonstrated in regions vulnerable to neurodegeneration, such as the hippocampus and cortex [68, 149]. It is possible that metal ion dyshomeostasis in these regions could lead to increased free radical production, neuron degeneration, and decreased function. However, it is still unclear whether changes in metal ion content are a causative factor or a consequence of the disease. Here, no changes in metal ion content were observed in the CNT mice. We also found no change in Cu levels in both the cortex and hippocampus. However, previous studies have shown that Cu is increased extracellularly and decreased intracellularly in human AD [76], which could imply that the PSAPP mice also followed this trend. On the other hand, Fe content in PSAPP mouse brain increases in the cortex and hippocampus and is higher than in CNT mice starting at 24 weeks-old. Since plaques form in these mice at around this age, it is possible that increased Fe could be a factor in plaque formation. Though the Fe content in the cortex was generally higher than that in the hippocampus, Fe concentrations over time followed the same trend: from 13 to 24 weeks-old Fe content increased by 33.9% (not significant) in the cortex, and by 31.2% in the hippocampus, followed by a decrease at 56 weeks-old. Interestingly, no elevation of Fe was observed in the plaques at any time point and could indicate that the increased Fe in non-plaque tissue may not be associated with Aβ. Although it is still unclear where the

increased Fe in the cortex and hippocampus arises from, it is possible that the expression of Fe regulatory, transport, or storage proteins is disrupted. For example, the Fe storage protein ferritin is a component of senile plaques in AD [149, 236]. In addition, most of the non-heme iron in the brain is bound to ferritin as Fe^{3+}, and is released after being reduced to Fe^{2+} [237]. However, in AD, increased Fe occurs without a concurrent increase in ferritin providing a potential source of neurotoxic Fe^{2+} [182]. It is possible that the increased Fe observed in our studies represents Fe^{2+}, which could increase the risk of oxidative stress [82]. Another possibility is a breakdown in the BBB that allows more Fe to access the brain [124].

Zn is also altered in human AD brain. It has been shown that Zn levels correlate with plaque burden in human AD and is typically a late-stage effect [96]. From our studies, it appears that increased Zn levels in the cortex, hippocampus, and in plaques follow deposition of Aβ since these alterations were not observed until the late-stage time point. Unlike Fe, Zn content in the hippocampus and cortex were similar at 13, 24, and 40 week-old. However, Zn was much higher in the cortex than in the hippocampus at 56 weeks-old, suggesting that the cortex is more susceptible to increases in Zn. Since increases in ZnT 1, 3, 4, 6, and 7 have been observed in PSAPP cortex and hippocampus [190], it is possible that increases in Zn represent increased expression of ZnT proteins. ZnT3, which serves to sequester Zn ions into synaptic vesicles is found primarily the mossy fiber boutons in the hilus of the dentate gyrus [177]. It is also found in plaques in both human AD [148] and in PSAPP mice [190] and supports the notion that ZnT3 or excess synaptic Zn plays a key role in plaque formation [126]. While it may be true that ZnT3 is associated with amyloid plaques, our results demonstrate that Zn is elevated in the plaque only at the latest time point. The possibility that ZnT3 accumulates later in plaques and is not involved in the formation of plaques, as previously suggested, requires further investigation [148]. Furthermore, since the Zn in plaques appears at the same time as increased Zn in the hilus it suggests that excess synaptic Zn may play a different role than in plaque formation. For example, it is possible that the Zn observed in plaques at the late-AD time point in PSAPP mice serves to make the Aβ in plaques redox-inert [59].

Unsaturated lipids are highly vulnerable to oxidative attack because of their

double bond content and the increased degradation of PUFAs in AD may be evidence of lipid peroxidation [196]. Since Fe content was altered in the hippocampus and could be one source of lipid peroxidation, we then examined the unsaturated lipid content in the hippocampus. We found that the white matter of the hippocampus from 56 week-old PSAPP and CNT mice were spectrally different and that the spectral regions of greatest difference between the two groups were in the lipid region. In addition, we observed decreased unsaturated lipid content in the white matter of the hippocampus starting at the same time points as increased Fe, indicating that increased oxidative stress due to increased Fe is a likely possibility, although impairments in antioxidant defenses or defects in myelination are also possible. It also highlights the importance of not only examining grey matter in the brain, but also the white matter regions, an area which is often ignored.

6.3 Implications for Diagnosis and Treatment

The global increases of Fe in both the cortex and hippocampus observed at the beginning stages of plaque formation may have direct clinical relevance for early detection of the pathological symptoms of AD. Currently, AD is most accurately diagnosed in the mid or late stages, but treatment strategies implemented at pre-clinical or early stages are more likely to be effective [2]. Currently, there is considerable interest in optimizing MRI sequences to non-invasively detect and quantify excessive Fe in the brain for the purposes of early diagnosis and treatment monitoring [128-130]. Our results showed that Fe is not only higher in the PSAPP mice than in the CNT mice, but that this difference was already evident at 24-weeks of age, i.e. at the first signs of plaque formation as well as spatial working memory impairments in these mice [143]. This implies that if Fe is in sufficient quantity to be identified by MRI, an increase in Fe could be indicative of a disease state. These results suggest that early Fe accumulation reflects pathological changes related to plaque formation in PSAPP mice, making Fe deposition a promising biomarker to predict the presence of early amyloid plaque deposition. Further advancement of MRI techniques in conjunction with other imaging techniques to identify amyloid plaques (e.g. positron emission tomography) may allow for early diagnosis through sensitive quantification of brain Fe deposition at pre-clinical or early stage AD and related diseases so that more effective treatments can be developed and monitored.

We have also shown that Fe, Cu, and Zn are abundant in human plaques, but only Zn is present in PSAPP plaques. Moreover, PSAPP mice do not show the severe neurodegeneration and cognitive deficits that are a signature of human AD. Since the mice do not show neurodegeneration, this implies that it is the interaction of Aβ with redox-active Cu and Fe, a potential source of neurotoxicity, and not Zn, that could be causing the neurodegeneration that is seen in humans. This suggests a viable target for drug development or metal-targeted therapy for prevention and treatment of AD. Indeed, metal chelation therapy has been considered a promising therapeutic approach to treating AD. However, it is important to remember that chelators do not only remove metal from the plaques, but also from healthy brain tissue, causing potentially harmful metal deficiencies. In the case of Cu, it is not just increased extracellularly, but also decreased intracellularly [140]. Furthermore, while Cu is enriched in the plaques, Fe is more likely to be enriched in the tissue highlighting the importance of chelators selectivity and the complexity of designing an appropriate therapy [33]. Therefore, the best approach seems to be not just metal removal, but disruption of abnormal metal-Aβ interactions and relocation to restore normal metabolism [33, 238].

6.4 LIMITATIONS

There are a number of limitations associated with these studies. First, sample size was limited by time-consuming data acquisition and the small amount of beamtime available for synchrotron techniques. However, due to the high resolution and sensitivity needed, these experiments could not be done using benchtop sources and required a synchrotron source. Next, the spatial resolution was not on the cellular level. Though changes were observed in the present studies, it is possible that that are extensive subcellular changes taking place, which could not be visualized, but should be examined in the future in order to fully understand the involvement of metals in the disease process. Also, the sample preparation consisted of dried tissue sections, which could result in some uncertainty regarding metal ion concentration. Ideally, future advancements in data collection techniques could allow for three dimensional imaging of whole brains at sub-cellular resolution. Finally, and most importantly, a direct correlation of our findings to human aging and AD is limited by fundamental differences between PSAPP mice and the human condition. For example, PSAPP mice do not possess the full spectrum of AD

pathology. They are lacking neurofibrillary tangles, severe cognitive deficits, and neurodegeneration, which are important hallmarks of human AD. Moreover, their metal regulatory mechanisms are likely different than in humans. In addition, since PSAPP mice express genes thought to be involved in familial AD, which is a very small percentage of AD cases, relevance to sporadic cases is not clear. The lifespan of PSAPP mice is also quite different from that of a human AD patient. PSAPP mice may live up to three years and develop plaque pathology very early into their lifespan. Human AD patients with the early onset form of AD develop symptoms at approximately 55-60 years old, which is closer to the end of the human lifespan. Therefore, the equivalent age at onset and duration of the illness is different. It is possible that the mice in our studies were not yet old enough to develop the severe neurodegeneration and debilitating symptoms observed in human AD.

6.5 Conclusion and Future Directions

The studies described in this dissertation were designed to assess the involvement of metal ions in the pathogenesis of AD. We have found a unique role of Fe, Cu, and Zn using the PSAPP mouse model of plaque formation in AD. For example, Fe is elevated in the cortex and hippocampus at the beginning stages of plaque formation and highlights a potential role in early diagnosis through MRI; Cu was absent from PSAPP plaques, in stark contrast to human plaques, indicating a role of Cu in neurodegeneration and a possible therapeutic target; Zn was elevated in plaques, the cortex, and the hilus of the hippocampus at the latest time point, suggesting that Zn is not involved in plaque formation, but may have a protective role. We also observed decreased unsaturated lipid in hippocampal white matter, which coincided with the changes in Fe content in the hippocampus. It is possible that the decreased unsaturation resulted from Fe induced lipid peroxidation. Furthermore, this result shows that though AD is considered a disease of grey matter, white matter damage may also occur and should not be ignored in future studies.

AD is an extremely complex disease with a number of other possible factors involved it its etiology and progression. Thus, future studies are needed to further clarify the role of metal ions in AD. For example, the involvement of neurofibrillary tangles, a vital component to AD, could be addressed in studies using a triple transgenic mouse

model of AD (3×Tg-AD), a model which develops both plaques and tangles. Another mouse model, the 5×FAD mouse, is the one of the few models of plaque pathology which exhibits neurodegeneration. It would be interesting to determine if the plaques in these mice are also lacking in Cu. If they are not, it would provide more evidence that Aβ-Cu interaction may cause neurodegeneration. If they are, however, it would suggest that other factors are contributing to neurodegeneration.

Reduction of Fe^{3+} to Fe^{2+} and Cu^{2+} to Cu^{+} is believed to contribute to the production of neurotoxic reactive oxygen species, which could result in neurodegeneration. Also, ferritin serves to detoxify Fe by converting Fe^{2+} to Fe^{3+} where it is stored within the ferritin molecule. Thus, inadequate storage of storage of Fe by ferritin would result in free Fe^{2+} ions. In addition, some pathological conditions result in the loss of ceruloplasmin, the ferroxidase which oxidizes Fe^{2+} to Fe^{3+}, allowing it to bind to Tf for transport into the cell. Though we have shown increased Fe, which we attributed to dysfunctional Fe transport and storage proteins, such as ferritin, it is still unclear what the chemical species of that Fe is. Similarly, the species of Cu present in the brain and in plaques during AD is also unknown. Metal speciation in plaques and in brain tissue could be examined using XANES. To date, XANES studies on brain tissue have been difficult to perform. The extremely low metal concentration relative to other materials (i.e. geological samples) present in the brain requires very long scan times in order to collect good quality spectra. Not only time-consuming, such long exposure to the X-ray beam may reduce the Fe^{3+} or Cu^{2+}, thereby artificially increasing Fe^{2+} and Cu^{+} in the sample. The new synchrotron at NSLS II would provide enough flux on the sample in order to drastically reduce scan times and minimize tissue damage, making XANES or even speciation mapping studies definite future goal. Not only would the chemical species of the metal ions be known, but the distribution. Additionally, recent evidence also suggests the presence of bioavailable Cu within the mitochondria. Though we saw no changes in Cu content, it is possible that there are changes within the mitochondria. Sub-cellular spatial resolution, attainable with NSLS II, would enable metal concentration in the mitochondria within a cell to be analyzed.

In summary, we have revealed the possible involvement of Fe, Cu, and Zn in the pathogenesis of AD. Extension of these results to the human condition is the final goal.

This underscores the necessity for reliable and specific biomarkers for early diagnosis of AD. In this way, longitudinal studies of AD patients, starting from pre- or early stages of plaque formation, could be possible.

REFERENCES

1. Caughey B. and Lansbury P.T., 2003. Protofibrils, pores, fibrils, and neurodegeneration: separating the responsible protein aggregates from the innocent bystanders. *Annu. Rev. Neurosci.* 26, 267-98.

2. Masters C.L., Cappai R., Barnham K.J., and Villemagne V.L., 2006. Molecular mechanisms for Alzheimer's disease: implications for neuroimaging and therapeutics. *J. Neurochem.* 97, 1700-25.

3. Selkoe D.J., 2001. Alzheimer's disease: genes, proteins, and therapy. *Physiol. Rev.* 81, 741-66.

4. Katzman R., 1976. Editorial: The prevalence and malignancy of Alzheimer disease. A major killer. *Arch. Neurol.* 33, 217-8.

5. Rogers A.B., *Progress Report on Alzheimer's Disease 2004-2005*, P.D. Lynch and K.M. Pocinki, Editors, National Institute on Aging.

6. Ewbank D.C., 1999. Deaths attributable to Alzheimer's disease in the United States. *Am. J. Public Health*. 89, 90-2.

7. Hebert L.E., Scherr P.A., Bienias J.L., Bennett D.A., and Evans D.A., 2003. Alzheimer disease in the US population: prevalence estimates using the 2000 census. *Arch. Neurol.* 60, 1119-22.

8. Ernst R.L. and Hay J.W., 1994. The US economic and social costs of Alzheimer's disease revisited. *Am. J. Public Health*. 84, 1261-4.

9. Arnold S.E., Hyman B.T., Flory J., Damasio A.R., and Van Hoesen G.W., 1991. The topographical and neuroanatomical distribution of neurofibrillary tangles and neuritic plaques in the cerebral cortex of patients with Alzheimer's disease. *Cereb. Cortex*. 1, 103-16.

10. Clark C.M. and Karlawish J.H., 2003. Alzheimer disease: current concepts and emerging diagnostic and therapeutic strategies. *Ann. Intern. Med.* 138, 400-10.

11. Giannakopoulos P., Herrmann F.R., Bussiere T., Bouras C., Kovari E., Perl D.P., Morrison J.H., Gold G., and Hof P.R., 2003. Tangle and neuron numbers, but not amyloid load, predict cognitive status in Alzheimer's disease. *Neurology*. 60, 1495-500.

12. Lovestone S. and Reynolds C.H., 1997. The phosphorylation of tau: a critical stage in neurodevelopment and neurodegenerative processes. *Neuroscience*. 78, 309-24.

13. Roher A.E., Lowenson J.D., Clarke S., Woods A.S., Cotter R.J., Gowing E., and Ball M.J., 1993. β-Amyloid-(1-42) is a major component of cerebrovascular amyloid deposits: implications for the pathology of Alzheimer disease. *Proc. Natl. Acad. Sci. U S A.* 90, 10836-40.

14. Bitan G., Kirkitadze M.D., Lomakin A., Vollers S.S., Benedek G.B., and Teplow D.B., 2003. Amyloid β-protein (Aβ) assembly: Aβ40 and Aβ42 oligomerize through distinct pathways. *Proc. Natl. Acad. Sci. U S A.* 100, 330-5.

15. Iwatsubo T., Odaka A., Suzuki N., Mizusawa H., Nukina N., and Ihara Y., 1994. Visualization of Aβ42(43) and Aβ40 in senile plaques with end-specific Aβmonoclonals: evidence that an initially deposited species is Aβ42(43). *Neuron*. 13, 45-53.

16. Miyata M. and Smith J.D., 1996. Apolipoprotein E allele-specific antioxidant activity and effects on cytotoxicity by oxidative insults and β-amyloid peptides. *Nat. Genet.* 14, 55-61.

17. Strittmatter W.J., Saunders A.M., Schmechel D., Pericak-Vance M., Enghild J., Salvesen G.S., and Roses A.D., 1993. Apolipoprotein E: high-avidity binding to β-amyloid and increased frequency of type 4 allele in late-onset familial Alzheimer disease. *Proc. Natl. Acad. Sci. U S A.* 90, 1977-81.

18. Frey C., Bonert A., Kratzsch T., Rexroth G., Rosch W., Muller-Spahn F., Maurer K., Muller W.E., and Eckert A., 2006. Apolipoprotein E epsilon 4 is associated with an increased vulnerability to cell death in Alzheimer's disease. *J. Neural. Transm.* 113, 1753-61.

19. Higgins G.A. and Jacobsen H., 2003. Transgenic mouse models of Alzheimer's disease: phenotype and application. *Behav. Pharmacol.* 14, 419-38.

20. St George-Hyslop P.H., 2000. Genetic factors in the genesis of Alzheimer's disease. *Ann. N Y Acad. Sci.* 924, 1-7.

21. Maynard C.J., Cappai R., Volitakis I., Cherny R.A., White A.R., Beyreuther K., Masters C.L., Bush A.I., and Li Q.X., 2002. Overexpression of Alzheimer's disease amyloid-β opposes the age-dependent elevations of brain copper and iron. *J. Biol. Chem.* 277, 44670-6.

22. White A.R., Reyes R., Mercer J.F., Camakaris J., Zheng H., Bush A.I., Multhaup G., Beyreuther K., Masters C.L., and Cappai R., 1999. Copper levels are increased in the cerebral cortex and liver of APP and APLP2 knockout mice. *Brain Res.* 842, 439-44.

23. De Strooper B., Saftig P., Craessaerts K., Vanderstichele H., Guhde G., Annaert W., Von Figura K., and Van Leuven F., 1998. Deficiency of presenilin-1 inhibits the normal cleavage of amyloid precursor protein. *Nature*. 391, 387-90.

24. Kimberly W.T., Xia W., Rahmati T., Wolfe M.S., and Selkoe D.J., 2000. The transmembrane aspartates in presenilin 1 and 2 are obligatory for γ-secretase activity and amyloid β-protein generation. *J. Biol. Chem.* 275, 3173-8.

25. Miklossy J., Taddei K., Suva D., Verdile G., Fonte J., Fisher C., Gnjec A., Ghika J., Suard F., Mehta P.D., McLean C.A., Masters C.L., Brooks W.S., and Martins R.N., 2003. Two novel presenilin-1 mutations (Y256S and Q222H) are associated with early-onset Alzheimer's disease. *Neurobiol. Aging*. 24, 655-62.

26. Ramassamy C., Averill D., Beffert U., Theroux L., Lussier-Cacan S., Cohn J.S., Christen Y., Schoofs A., Davignon J., and Poirier J., 2000. Oxidative insults are associated with apolipoprotein E genotype in Alzheimer's disease brain. *Neurobiol. Dis.* 7, 23-37.

27. Hardy J.A. and Higgins G.A., 1992. Alzheimer's disease: the amyloid cascade hypothesis. *Science*. 256, 184-5.

28. Selkoe D.J., 1991. The molecular pathology of Alzheimer's disease. *Neuron*. 6, 487-98.

29. St George-Hyslop P.H. and Petit A., 2005. Molecular biology and genetics of Alzheimer's disease. *C. R. Biol.* 328, 119-30.

30. Reznik-Wolf H., Machado J., Haroutunian V., DeMarco L., Walter G.F., Goldman B., Davidson M., Johnston J.A., Lannfelt L., Dani S.U., and Friedman E., 1998. Somatic mutation analysis of the APP and Presenilin 1 and 2 genes in Alzheimer's disease brains. *J. Neurogenet.* 12, 55-65.

31. Spargo E., Luthert P.J., Janota I., and Lantos P.L., 1992. βA4 deposition in the temporal cortex of adults with Down's syndrome. *J. Neurol. Sci.* 111, 26-32.

32. Small S.A. and Duff K., 2008. Linking Aβ and tau in late-onset Alzheimer's disease: a dual pathway hypothesis. *Neuron*. 60, 534-42.

33. Bush A.I., 2008. Drug development based on the metals hypothesis of Alzheimer's disease. *J Alzheimers Dis*. 15, 223-40.

34. Pike C.J., Walencewicz-Wasserman A.J., Kosmoski J., Cribbs D.H., Glabe C.G., and Cotman C.W., 1995. Structure-activity analyses of β-amyloid peptides: contributions of the β25-35 region to aggregation and neurotoxicity. *J. Neurochem.* 64, 253-65.

35. Dahlgren K.N., Manelli A.M., Stine W.B., Jr., Baker L.K., Krafft G.A., and LaDu M.J., 2002. Oligomeric and fibrillar species of amyloid-β peptides differentially affect neuronal viability. *J. Biol. Chem.* 277, 32046-53.

36. Watson D., Castano E., Kokjohn T.A., Kuo Y.M., Lyubchenko Y., Pinsky D., Connolly E.S., Jr., Esh C., Luehrs D.C., Stine W.B., Rowse L.M., Emmerling M.R., and Roher A.E., 2005. Physicochemical characteristics of soluble oligomeric Aβ and their pathologic role in Alzheimer's disease. *Neurol. Res.* 27, 869-81.

37. Hoshi M., Sato M., Matsumoto S., Noguchi A., Yasutake K., Yoshida N., and Sato K., 2003. Spherical aggregates of β-amyloid (amylospheroid) show high neurotoxicity and activate tau protein kinase I/glycogen synthase kinase-3β. *Proc. Natl. Acad. Sci. U S A.* 100, 6370-5.

38. Stromer T. and Serpell L.C., 2005. Structure and morphology of the Alzheimer's amyloid fibril. *Microsc. Res. Tech.* 67, 210-7.

39. Mastrangelo I.A., Ahmed M., Sato T., Liu W., Wang C., Hough P., and Smith S.O., 2006. High-resolution atomic force microscopy of soluble Aβ42 oligomers. *J. Mol. Biol.* 358, 106-19.

40. Barrow C.J. and Zagorski M.G., 1991. Solution structures of β peptide and its constituent fragments: relation to amyloid deposition. *Science*. 253, 179-82.

41. Shao H., Jao S., Ma K., and Zagorski M.G., 1999. Solution structures of micelle-bound amyloid β-(1-40) and β-(1-42) peptides of Alzheimer's disease. *J. Mol. Biol.* 285, 755-73.

42. Shen C.L. and Murphy R.M., 1995. Solvent effects on self-assembly of β-amyloid peptide. *Biophys. J.* 69, 640-51.

43. Takano K., Endo S., Mukaiyama A., Chon H., Matsumura H., Koga Y., and Kanaya S., 2006. Structure of amyloid β fragments in aqueous environments. *Febs J.* 273, 150-8.

44. Huang T.H., Yang D.S., Plaskos N.P., Go S., Yip C.M., Fraser P.E., and Chakrabartty A., 2000. Structural studies of soluble oligomers of the Alzheimer β-amyloid peptide. *J. Mol. Biol.* 297, 73-87.

45. Salvati S., Attorri L., Di Benedetto R., Di Biase A., and Leonardi F., 2006. Polyunsaturated fatty acids and neurological diseases. *Mini. Rev. Med. Chem.* 6, 1201-11.

46. Tully A.M., Roche H.M., Doyle R., Fallon C., Bruce I., Lawlor B., Coakley D., and Gibney M.J., 2003. Low serum cholesteryl ester-docosahexaenoic acid levels in Alzheimer's disease: a case-control study. *Br. J. Nutr.* 89, 483-9.

47. Soderberg M., Edlund C., Kristensson K., and Dallner G., 1991. Fatty acid composition of brain phospholipids in aging and in Alzheimer's disease. *Lipids*. 26, 421-5.

48. Calon F., Lim G.P., Yang F., Morihara T., Teter B., Ubeda O., Rostaing P., Triller A., Salem N., Jr., Ashe K.H., Frautschy S.A., and Cole G.M., 2004. Docosahexaenoic acid protects from dendritic pathology in an Alzheimer's disease mouse model. *Neuron*. 43, 633-45.

49. Sahlin C., Pettersson F.E., Nilsson L.N., Lannfelt L., and Johansson A.S., 2007. Docosahexaenoic acid stimulates non-amyloidogenic APP processing resulting in reduced Aβ levels in cellular models of Alzheimer's disease. *Eur. J. Neurosci.* 26, 882-9.

50. Lim G.P., Calon F., Morihara T., Yang F., Teter B., Ubeda O., Salem N., Jr., Frautschy S.A., and Cole G.M., 2005. A diet enriched with the omega-3 fatty acid docosahexaenoic acid reduces amyloid burden in an aged Alzheimer mouse model. *J. Neurosci.* 25, 3032-40.

51. Oksman M., Iivonen H., Hogyes E., Amtul Z., Penke B., Leenders I., Broersen L., Lutjohann D., Hartmann T., and Tanila H., 2006. Impact of different saturated fatty acid, polyunsaturated fatty acid and cholesterol containing diets on beta-amyloid accumulation in APP/PS1 transgenic mice. *Neurobiol. Dis.* 23, 563-72.

52. Floyd R.A., 1999. Antioxidants, oxidative stress, and degenerative neurological disorders. *Proc. Soc. Exp. Biol. Med.* 222, 236-45.

53. Nunomura A., Perry G., Aliev G., Hirai K., Takeda A., Balraj E.K., Jones P.K., Ghanbari H., Wataya T., Shimohama S., Chiba S., Atwood C.S., Petersen R.B., and Smith M.A., 2001. Oxidative damage is the earliest event in Alzheimer disease. *J. Neuropathol. Exp. Neurol.* 60, 759-67.

54. Butterfield D.A., Perluigi M., and Sultana R., 2006. Oxidative stress in Alzheimer's disease brain: new insights from redox proteomics. *Eur. J. Pharmacol.* 545, 39-50.

55. Sayre L.M., Moreira P.I., Smith M.A., and Perry G., 2005. Metal ions and oxidative protein modification in neurological disease. *Ann. Ist. Super. Sanita.* 41, 143-64.

56. Holscher C., 1998. Possible causes of Alzheimer's disease: amyloid fragments, free radicals, and calcium homeostasis. *Neurobiol. Dis.* 5, 129-41.

57. Lovell M.A., Ehmann W.D., Butler S.M., and Markesbery W.R., 1995. Elevated thiobarbituric acid-reactive substances and antioxidant enzyme activity in the brain in Alzheimer's disease. *Neurology*. 45, 1594-601.

58. Kuo Y.M., Webster S., Emmerling M.R., De Lima N., and Roher A.E., 1998. Irreversible dimerization/tetramerization and post-translational modifications inhibit proteolytic degradation of Aβ peptides of Alzheimer's disease. *Biochim. Biophys. Acta*. 1406, 291-8.

59. Cuajungco M.P., Goldstein L.E., Nunomura A., Smith M.A., Lim J.T., Atwood C.S., Huang X., Farrag Y.W., Perry G., and Bush A.I., 2000. Evidence that the β-amyloid plaques of Alzheimer's disease represent the redox-silencing and entombment of Aβ by zinc. *J. Biol. Chem.* 275, 19439-42.

60. Holscher C., 1998. β-amyloid induced reduction in synaptic transmission is reversed by inhibitors of nitric oxide synthase. *Neuroreport*. 9, 1245-8.

61. Griffin W.S., Sheng J.G., Royston M.C., Gentleman S.M., McKenzie J.E., Graham D.I., Roberts G.W., and Mrak R.E., 1998. Glial-neuronal interactions in Alzheimer's disease: the potential role of a 'cytokine cycle' in disease progression. *Brain Pathol.* 8, 65-72.

62. Eikelenboom P., Bate C., Van Gool W.A., Hoozemans J.J., Rozemuller J.M., Veerhuis R., and Williams A., 2002. Neuroinflammation in Alzheimer's disease and prion disease. *Glia*. 40, 232-9.

63. Mattiace L.A., Davies P., Yen S.H., and Dickson D.W., 1990. Microglia in cerebellar plaques in Alzheimer's disease. *Acta Neuropathol.* 80, 493-8.

64. Frautschy S.A., Yang F., Irrizarry M., Hyman B., Saido T.C., Hsiao K., and Cole G.M., 1998. Microglial response to amyloid plaques in APPsw transgenic mice. *Am. J. Pathol.* 152, 307-17.

65. Bornemann K.D., Wiederhold K.H., Pauli C., Ermini F., Stalder M., Schnell L., Sommer B., Jucker M., and Staufenbiel M., 2001. Aβ-induced inflammatory processes in microglia cells of APP23 transgenic mice. *Am. J. Pathol.* 158, 63-73.

66. Hu J., Akama K.T., Krafft G.A., Chromy B.A., and Van Eldik L.J., 1998. Amyloid-β peptide activates cultured astrocytes: morphological alterations, cytokine induction and nitric oxide release. *Brain Res.* 785, 195-206.

67. Bush A.I., 2003. The metallobiology of Alzheimer's disease. *Trends Neurosci.* 26, 207-14.

68. Lovell M.A., Robertson J.D., Teesdale W.J., Campbell J.L., and Markesbery W.R., 1998. Copper, iron and zinc in Alzheimer's disease senile plaques. *J. Neurol. Sci.* 158, 47-52.

69. Cuajungco M.P. and Lees G.J., 1997. Zinc and Alzheimer's disease: is there a direct link? *Brain Res. Brain. Res. Rev.* 23, 219-36.

70. Danielsson J., Pierattelli R., Banci L., and Gräslund A., 2007. High-resolution NMR studies of the zinc-binding site of the Alzheimer's amyloid β-peptide. *Febs J.* 274, 46-59.

71. Streltsov V., 2008. X-ray absorption and diffraction studies of the metal binding sites in amyloid β-peptide. *Eur. Biophys. J.* 37, 257-63.

72. Miura T., Suzuki K., Kohata N., and Takeuchi H., 2000. Metal binding modes of Alzheimer's amyloid β-peptide in insoluble aggregates and soluble complexes. *Biochemistry*. 39, 7024-31.

73. Tõugu V., Karafin A., and Palumaa P., 2008. Binding of zinc(II) and copper(II) to the full-length Alzheimer's amyloid-β peptide. *J. Neurochem.* 104, 1249-59.

74. Opazo C., Huang X., Cherny R.A., Moir R.D., Roher A.E., White A.R., Cappai R., Masters C.L., Tanzi R.E., Inestrosa N.C., and Bush A.I., 2002. Metalloenzyme-like activity of Alzheimer's disease β-amyloid. Cu-dependent catalytic conversion of dopamine, cholesterol, and biological reducing agents to neurotoxic H_2O_2. *J. Biol. Chem.* 277, 40302-8.

75. Cuajungco M.P. and Faget K.Y., 2003. Zinc takes the center stage: its paradoxical role in Alzheimer's disease. *Brain Res. Brain. Res. Rev.* 41, 44-56.

76. Maynard C.J., Bush A.I., Masters C.L., Cappai R., and Li Q.X., 2005. Metals and amyloid-β in Alzheimer's disease. *Int. J. Exp. Pathol.* 86, 147-59.

77. Bush A.I., Pettingell W.H., Multhaup G., d. Paradis M., Vonsattel J.P., Gusella J.F., Beyreuther K., Masters C.L., and Tanzi R.E., 1994. Rapid induction of Alzheimer Aβ amyloid formation by zinc. *Science*. 265, 1464-7.

78. Atwood C.S., Scarpa R.C., Huang X., Moir R.D., Jones W.D., Fairlie D.P., Tanzi R.E., and Bush A.I., 2000. Characterization of copper interactions with alzheimer amyloid β peptides: identification of an attomolar-affinity copper binding site on amyloid β1-42. *J. Neurochem.* 75, 1219-33.

79. Murray I.V., Sindoni M.E., and Axelsen P.H., 2005. Promotion of oxidative lipid membrane damage by amyloid β proteins. *Biochemistry*. 44, 12606-13.

80. Koppaka V., Paul C., Murray I.V., and Axelsen P.H., 2003. Early synergy between Aβ42 and oxidatively damaged membranes in promoting amyloid fibril formation by Aβ40. *J. Biol. Chem.* 278, 36277-84.

81. Smith D.G., Cappai R., and Barnham K.J., 2007. The redox chemistry of the Alzheimer's disease amyloid β peptide. *Biochim. Biophys. Acta*. 1768, 1976-90.

82. Huang X., Atwood C.S., Hartshorn M.A., Multhaup G., Goldstein L.E., Scarpa R.C., Cuajungco M.P., Gray D.N., Lim J., Moir R.D., Tanzi R.E., and Bush A.I., 1999. The Aβ peptide of Alzheimer's disease directly produces hydrogen peroxide through metal ion reduction. *Biochemistry*. 38, 7609-16.

83. Nunomura A., Perry G., Pappolla M.A., Wade R., Hirai K., Chiba S., and Smith M.A., 1999. RNA oxidation is a prominent feature of vulnerable neurons in Alzheimer's disease. *J. Neurosci.* 19, 1959-64.

84. Zou K., Gong J.S., Yanagisawa K., and Michikawa M., 2002. A novel function of monomeric amyloid β-protein serving as an antioxidant molecule against metal-induced oxidative damage. *J. Neurosci.* 22, 4833-41.

85. Stellato F., Menestrina G., Serra M.D., Potrich C., Tomazzolli R., Meyer-Klaucke W., and Morante S., 2006. Metal binding in amyloid β-peptides shows intra- and inter-peptide coordination modes. *Eur. Biophys. J.* 35, 340-51.

86. Dong J., Atwood C.S., Anderson V.E., Siedlak S.L., Smith M.A., Perry G., and Carey P.R., 2003. Metal binding and oxidation of amyloid-β within isolated senile plaque cores: Raman microscopic evidence. *Biochemistry*. 42, 2768-73.

87. Syme C.D., Nadal R.C., Rigby S.E., and Viles J.H., 2004. Copper binding to the amyloid-β (Aβ) peptide associated with Alzheimer's disease: folding, coordination

geometry, pH dependence, stoichiometry, and affinity of Aβ-(1-28): insights from a range of complementary spectroscopic techniques. *J. Biol. Chem.* 279, 18169-77.

88. Garai K., Sengupta P., Sahoo B., and Maiti S., 2006. Selective destabilization of soluble amyloid β oligomers by divalent metal ions. *Biochem. Biophys. Res. Commun.* 345, 210-5.

89. Cardoso S.M., Rego A.C., Pereira C., and Oliveira C.R., 2005. Protective effect of zinc on amyloid-β 25-35 and 1-40 mediated toxicity. *Neurotox. Res.* 7, 273-81.

90. Huang X., Atwood C.S., Moir R.D., Hartshorn M.A., Vonsattel J.P., Tanzi R.E., and Bush A.I., 1997. Zinc-induced Alzheimer's Aβ1-40 aggregation is mediated by conformational factors. *J. Biol. Chem.* 272, 26464-70.

91. Atwood C.S., Moir R.D., Huang X., Scarpa R.C., Bacarra N.M., Romano D.M., Hartshorn M.A., Tanzi R.E., and Bush A.I., 1998. Dramatic aggregation of Alzheimer Aβ by Cu(II) is induced by conditions representing physiological acidosis. *J. Biol. Chem.* 273, 12817-26.

92. Frederickson C.J., Koh J.Y., and Bush A.I., 2005. The neurobiology of zinc in health and disease. *Nat. Rev. Neurosci.* 6, 449-62.

93. Lee J.Y., Mook-Jung I., and Koh J.Y., 1999. Histochemically reactive zinc in plaques of the Swedish mutant β-amyloid precursor protein transgenic mice. *J. Neurosci.* 19, RC10.

94. Suh S.W., Jensen K.B., Jensen M.S., Silva D.S., Kesslak P.J., Danscher G., and Frederickson C.J., 2000. Histochemically-reactive zinc in amyloid plaques, angiopathy, and degenerating neurons of Alzheimer's diseased brains. *Brain Res.* 852, 274-8.

95. Miller L.M., Wang Q., Telivala T.P., Smith R.J., Lanzirotti A., and Miklossy J., 2006. Synchrotron-based infrared and X-ray imaging shows focalized accumulation of Cu and Zn co-localized with β-amyloid deposits in Alzheimer's disease. *J. Struct. Biol.* 155, 30-7.

96. Religa D., Strozyk D., Cherny R.A., Volitakis I., Haroutunian V., Winblad B., Naslund J., and Bush A.I., 2006. Elevated cortical zinc in Alzheimer disease. *Neurology*. 67, 69-75.

97. Corrigan F.M., Reynolds G.P., and Ward N.I., 1993. Hippocampal tin, aluminum and zinc in Alzheimer's disease. *Biometals*. 6, 149-54.

98. Deibel M.A., Ehmann W.D., and Markesbery W.R., 1996. Copper, iron, and zinc imbalances in severely degenerated brain regions in Alzheimer's disease: possible relation to oxidative stress. *J. Neurol. Sci.* 143, 137-42.

99. Phinney A.L., Drisaldi B., Schmidt S.D., Lugowski S., Coronado V., Liang Y., Horne P., Yang J., Sekoulidis J., Coomaraswamy J., Chishti M.A., Cox D.W., Mathews P.M., Nixon R.A., Carlson G.A., St George-Hyslop P., and Westaway D., 2003. In vivo reduction of amyloid-β by a mutant copper transporter. *Proc. Natl. Acad. Sci. U S A.* 100, 14193-8.

100. Spires T.L. and Hyman B.T., 2005. Transgenic models of Alzheimer's disease: learning from animals. *NeuroRx*. 2, 423-37.

101. Mineur Y.S., McLoughlin D., Crusio W.E., and Sluyter F., 2005. Genetic mouse models of Alzheimer's disease. *Neural Plast.* 12, 299-310.

102. Borchelt D.R., Ratovitski T., van Lare J., Lee M.K., Gonzales V., Jenkins N.A., Copeland N.G., Price D.L., and Sisodia S.S., 1997. Accelerated amyloid deposition in the brains of transgenic mice coexpressing mutant presenilin 1 and amyloid precursor proteins. *Neuron*. 19, 939-45.

103. Garcia-Alloza M., Robbins E.M., Zhang-Nunes S.X., Purcell S.M., Betensky R.A., Raju S., Prada C., Greenberg S.M., Bacskai B.J., and Frosch M.P., 2006. Characterization of amyloid deposition in the APPswe/PS1dE9 mouse model of Alzheimer disease. *Neurobiol. Dis.* 24, 516-24.

104. Jankowsky J.L., Slunt H.H., Ratovitski T., Jenkins N.A., Copeland N.G., and Borchelt D.R., 2001. Co-expression of multiple transgenes in mouse CNS: a comparison of strategies. *Biomol. Eng.* 17, 157-65.

105. Santacruz K., Lewis J., Spires T., Paulson J., Kotilinek L., Ingelsson M., Guimaraes A., DeTure M., Ramsden M., McGowan E., Forster C., Yue M., Orne J., Janus C., Mariash A., Kuskowski M., Hyman B., Hutton M., and Ashe K.H., 2005. Tau suppression in a neurodegenerative mouse model improves memory function. *Science*. 309, 476-81.

106. Allen B., Ingram E., Takao M., Smith M.J., Jakes R., Virdee K., Yoshida H., Holzer M., Craxton M., Emson P.C., Atzori C., Migheli A., Crowther R.A., Ghetti B., Spillantini M.G., and Goedert M., 2002. Abundant tau filaments and nonapoptotic neurodegeneration in transgenic mice expressing human P301S tau protein. *J. Neurosci.* 22, 9340-51.

107. Oddo S., Caccamo A., Shepherd J.D., Murphy M.P., Golde T.E., Kayed R., Metherate R., Mattson M.P., Akbari Y., and LaFerla F.M., 2003. Triple-transgenic

model of Alzheimer's disease with plaques and tangles: intracellular Aβand synaptic dysfunction. *Neuron*. 39, 409-21.

108. Oddo S., Caccamo A., Kitazawa M., Tseng B.P., and LaFerla F.M., 2003. Amyloid deposition precedes tangle formation in a triple transgenic model of Alzheimer's disease. *Neurobiol. Aging*. 24, 1063-70.

109. Radde R., Duma C., Goedert M., and Jucker M., 2008. The value of incomplete mouse models of Alzheimer's disease. *Eur. J. Nucl. Med. Mol. Imaging*. 35 Suppl 1, S70-4.

110. Miller L.M. and Dumas P., 2006. Chemical imaging of biological tissue with synchrotron infrared light. *Biochim. Biophys. Acta*. 1758, 846-57.

111. Petter C.H., Heigl N., Rainer M., Bakry R., Pallua J., Bonn G.K., and Huck C.W., 2009. Development and application of Fourier-transform infrared chemical imaging of tumour in human tissue. *Curr. Med. Chem.* 16, 318-26.

112. Wang Q., Sanad W., Miller L.M., Voigt A., Klingel K., Kandolf R., Stangl K., and Baumann G., 2005. Infrared imaging of compositional changes in inflammatory cardiomyopathy. *Vib. Spectrosc.* 38, 217-222.

113. Huang R.Y., Miller L.M., Carlson C.S., and Chance M.R., 2003. In situ chemistry of osteoporosis revealed by synchrotron infrared microspectroscopy. *Bone*. 33, 514-21.

114. Boskey A. and Mendelsohn R., 2005. Infrared analysis of bone in health and disease. *J. Biomed. Opt.* 10, 031102.

115. Choo L.P., Jackson M., Halliday W.C., and Mantsch H.H., 1993. Infrared spectroscopic characterisation of multiple sclerosis plaques in the human central nervous system. *Biochim. Biophys. Acta*. 1182, 333-7.

116. Sayre L.M., Perry G., and Smith M.A., 1999. In situ methods for detection and localization of markers of oxidative stress: application in neurodegenerative disorders. *Methods. Enzymol.* 309, 133-52.

117. Saeed S.M. and Fine G., 1967. Thioflavin-T for amyloid detection. *Am. J. Clin. Pathol.* 47, 588-93.

118. Westermark G.T., Johnson K.H., and Westermark P., 1999. Staining methods for identification of amyloid in tissue. *Methods. Enzymol.* 309, 3-25.

119. Sun A., Nguyen X.V., and Bing G., 2002. Comparative analysis of an improved thioflavin-s stain, Gallyas silver stain, and immunohistochemistry for neurofibrillary tangle demonstration on the same sections. *J. Histochem. Cytochem.* 50, 463-72.

120. Braak H. and Braak E., 1991. Neuropathological stageing of Alzheimer-related changes. *Acta Neuropathol.* 82, 239-59.

121. Levenson C.W., 2005. Trace metal regulation of neuronal apoptosis: from genes to behavior. *Physiol. Behav.* 86, 399-406.

122. Petursdottir A.L., Farr S.A., Morley J.E., Banks W.A., and Skuladottir G.V., 2007. Lipid peroxidation in brain during aging in the senescence-accelerated mouse (SAM). *Neurobiol. Aging*. 28, 1170-8.

123. Donnelly P.S., Xiao Z., and Wedd A.G., 2007. Copper and Alzheimer's disease. *Curr. Opin. Chem. Biol.* 11, 128-33.

124. Zecca L., Youdim M.B., Riederer P., Connor J.R., and Crichton R.R., 2004. Iron, brain ageing and neurodegenerative disorders. *Nat. Rev. Neurosci.* 5, 863-73.

125. Leskovjan A.C., Lanzirotti A., and Miller L.M., 2009. Amyloid plaques in PSAPP mice bind less metal than plaques in human Alzheimer's disease. *Neuroimage*. 47, 1215-20.

126. Lee J.Y., Cole T.B., Palmiter R.D., Suh S.W., and Koh J.Y., 2002. Contribution by synaptic zinc to the gender-disparate plaque formation in human Swedish mutant APP transgenic mice. *Proc. Natl. Acad. Sci. U S A*. 99, 7705-10.

127. Price J.L. and Morris J.C., 1999. Tangles and plaques in nondemented aging and "preclinical" Alzheimer's disease. *Ann Neurol*. 45, 358-68.

128. Brass S.D., Chen N.K., Mulkern R.V., and Bakshi R., 2006. Magnetic resonance imaging of iron deposition in neurological disorders. *Top. Magn. Reson. Imaging*. 17, 31-40.

129. Stankiewicz J., Panter S.S., Neema M., Arora A., Batt C.E., and Bakshi R., 2007. Iron in chronic brain disorders: imaging and neurotherapeutic implications. *Neurotherapeutics*. 4, 371-86.

130. Haacke E.M., Cheng N.Y., House M.J., Liu Q., Neelavalli J., Ogg R.J., Khan A., Ayaz M., Kirsch W., and Obenaus A., 2005. Imaging iron stores in the brain using magnetic resonance imaging. *Magn. Reson. Imaging*. 23, 1-25.

131. Thomas L.O., Boyko O.B., Anthony D.C., and Burger P.C., 1993. MR detection of brain iron. *Am. J. Neuroradiol.* 14, 1043-8.

132. Gelman N., Gorell J.M., Barker P.B., Savage R.M., Spickler E.M., Windham J.P., and Knight R.A., 1999. MR imaging of human brain at 3.0 T: preliminary report on transverse relaxation rates and relation to estimated iron content. *Radiology*. 210, 759-67.

133. Michaeli S., Oz G., Sorce D.J., Garwood M., Ugurbil K., Majestic S., and Tuite P., 2007. Assessment of brain iron and neuronal integrity in patients with Parkinson's disease using novel MRI contrasts. *Mov. Disord.* 22, 334-40.

134. Helpern J.A., Jensen J., Lee S.P., and Falangola M.F., 2004. Quantitative MRI assessment of Alzheimer's disease. *J Mol Neurosci*. 24, 45-8.

135. Guntern R., Bouras C., Hof P.R., and Vallet P.G., 1992. An improved thioflavine S method for staining neurofibrillary tangles and senile plaques in Alzheimer's disease. *Experientia*. 48, 8-10.

136. Schenck J.F., Zimmerman E.A., Li Z., Adak S., Saha A., Tandon R., Fish K.M., Belden C., Gillen R.W., Barba A., Henderson D.L., Neil W., and O'Keefe T., 2006. High-field magnetic resonance imaging of brain iron in Alzheimer disease. *Top Magn Reson Imaging*. 17, 41-50.

137. Bartzokis G., Sultzer D., Cummings J., Holt L.E., Hance D.B., Henderson V.W., and Mintz J., 2000. In vivo evaluation of brain iron in Alzheimer disease using magnetic resonance imaging. *Arch Gen Psychiatry*. 57, 47-53.

138. Danscher G., Jensen K.B., Frederickson C.J., Kemp K., Andreasen A., Juhl S., Stoltenberg M., and Ravid R., 1997. Increased amount of zinc in the hippocampus and amygdala of Alzheimer's diseased brains: a proton-induced X-ray emission spectroscopic analysis of cryostat sections from autopsy material. *J. Neurosci. Methods*. 76, 53-9.

139. Stoltenberg M., Bush A.I., Bach G., Smidt K., Larsen A., Rungby J., Lund S., Doering P., and Danscher G., 2007. Amyloid plaques arise from zinc-enriched cortical layers in APP/PS1 transgenic mice and are paradoxically enlarged with dietary zinc deficiency. *Neuroscience*. 150, 357-69.

140. Crouch P.J., White A.R., and Bush A.I., 2007. The modulation of metal bio-availability as a therapeutic strategy for the treatment of Alzheimer's disease. *Febs J.* 274, 3775-83.

141. McCrea R.P., Harder S.L., Martin M., Buist R., and Nichol H., 2008. A comparison of rapid-scanning X-ray fluorescence mapping and magnetic resonance imaging to localize brain iron distribution. *Eur J Radiol*. 68, S109-13.

142. Zhu W.Z., Zhong W.D., Wang W., Zhan C.J., Wang C.Y., Qi J.P., Wang J.Z., and Lei T., 2009. Quantitative MR phase-corrected imaging to investigate increased brain iron deposition of patients with Alzheimer disease. *Radiology*. 253, 497-504.

143. Trinchese F., Liu S., Battaglia F., Walter S., Mathews P.M., and Arancio O., 2004. Progressive age-related development of Alzheimer-like pathology in APP/PS1 mice. *Ann. Neurol.* 55, 801-14.

144. Pfefferbaum A., Adalsteinsson E., Rohlfing T., and Sullivan E.V., 2009. MRI estimates of brain iron concentration in normal aging: comparison of field-dependent (FDRI) and phase (SWI) methods. *Neuroimage*. 47, 493-500.

145. Clements A., Allsop D., Walsh D.M., and Williams C.H., 1996. Aggregation and metal-binding properties of mutant forms of the amyloid Aβ peptide of Alzheimer's disease. *J. Neurochem.* 66, 740-7.

146. White A.R., Barnham K.J., and Bush A.I., 2006. Metal homeostasis in Alzheimer's disease. *Expert. Rev. Neurother.* 6, 711-22.

147. Smith J.L., Xiong S., Markesbery W.R., and Lovell M.A., 2006. Altered expression of zinc transporters-4 and -6 in mild cognitive impairment, early and late Alzheimer's disease brain. *Neuroscience*. 140, 879-88.

148. Zhang L.H., Wang X., Stoltenberg M., Danscher G., Huang L., and Wang Z.Y., 2008. Abundant expression of zinc transporters in the amyloid plaques of Alzheimer's disease brain. *Brain Res. Bull.* 77, 55-60.

149. Quintana C., Bellefqih S., Laval J.Y., Guerquin-Kern J.L., Wu T.D., Avila J., Ferrer I., Arranz R., and Patino C., 2006. Study of the localization of iron, ferritin, and hemosiderin in Alzheimer's disease hippocampus by analytical microscopy at the subcellular level. *J. Struct. Biol.* 153, 42-54.

150. Lopes K.O., Sparks D.L., and Streit W.J., 2008. Microglial dystrophy in the aged and Alzheimer's disease brain is associated with ferritin immunoreactivity. *Glia*. 56, 1048-60.

151. Schwab C., Hosokawa M., and McGeer P.L., 2004. Transgenic mice overexpressing amyloid beta protein are an incomplete model of Alzheimer disease. *Exp. Neurol.* 188, 52-64.

152. Wirths O., Breyhan H., Schäfer S., Roth C., and Bayer T.A., 2008. Deficits in working memory and motor performance in the APP/PS1ki mouse model for Alzheimer's disease. *Neurobiol. Aging*. 29, 891-901.

153. German D.C. and Eisch A.J., 2004. Mouse models of Alzheimer's disease: insight into treatment. *Rev. Neurosci.* 15, 353-69.

154. Takeuchi A., Irizarry M.C., Duff K., Saido T.C., Hsiao Ashe K., Hasegawa M., Mann D.M., Hyman B.T., and Iwatsubo T., 2000. Age-related amyloid β deposition in transgenic mice overexpressing both Alzheimer mutant presenilin 1 and amyloid β precursor protein Swedish mutant is not associated with global neuronal loss. *Am. J. Pathol.* 157, 331-9.

155. Pype S., Moechars D., Dillen L., and Mercken M., 2003. Characterization of amyloid β peptides from brain extracts of transgenic mice overexpressing the London mutant of human amyloid precursor protein. *J. Neurochem.* 84, 602-9.

156. van Groen T., Kiliaan A.J., and Kadish I., 2006. Deposition of mouse amyloid β in human APP/PS1 double and single AD model transgenic mice. *Neurobiol. Dis.* 23, 653-62.

157. Johnstone E.M., Chaney M.O., Norris F.H., Pascual R., and Little S.P., 1991. Conservation of the sequence of the Alzheimer's disease amyloid peptide in dog, polar bear and five other mammals by cross-species polymerase chain reaction analysis. *Brain Res. Mol. Brain Res.* 10, 299-305.

158. Liu S.T., Howlett G., and Barrow C.J., 1999. Histidine-13 is a crucial residue in the zinc ion-induced aggregation of the Aβ peptide of Alzheimer's disease. *Biochemistry*. 38, 9373-8.

159. Liao L., Cheng D., Wang J., Duong D.M., Losik T.G., Gearing M., Rees H.D., Lah J.J., Levey A.I., and Peng J., 2004. Proteomic characterization of postmortem amyloid plaques isolated by laser capture microdissection. *J. Biol. Chem.* 279, 37061-8.

160. Atwood C.S., Martins R.N., Smith M.A., and Perry G., 2002. Senile plaque composition and posttranslational modification of amyloid-beta peptide and associated proteins. *Peptides*. 23, 1343-50.

161. Choo L.P., Wetzel D.L., Halliday W.C., Jackson M., LeVine S.M., and Mantsch H.H., 1996. In situ characterization of β-amyloid in Alzheimer's diseased tissue by synchrotron Fourier transform infrared microspectroscopy. *Biophys. J.* 71, 1672-9.

162. Kalback W., Watson M.D., Kokjohn T.A., Kuo Y.M., Weiss N., Luehrs D.C., Lopez J., Brune D., Sisodia S.S., Staufenbiel M., Emmerling M., and Roher A.E., 2002. APP transgenic mice Tg2576 accumulate Aβ peptides that are distinct from the chemically modified and insoluble peptides deposited in Alzheimer's disease senile plaques. *Biochemistry*. 41, 922-8.

163. Khachaturian Z.S., 1987. Hypothesis on the regulation of cytosol calcium concentration and the aging brain. *Neurobiol. Aging*. 8, 345-6.

164. Green K.N. and LaFerla F.M., 2008. Linking calcium to Aβ and Alzheimer's disease. *Neuron*. 59, 190-4.

165. Cheung K.H., Shineman D., Muller M., Cárdenas C., Mei L., Yang J., Tomita T., Iwatsubo T., Lee V.M., and Foskett J.K., 2008. Mechanism of Ca^{2+} disruption in Alzheimer's disease by presenilin regulation of $InsP_3$ receptor channel gating. *Neuron*. 58, 871-83.

166. Kuchibhotla K.V., Goldman S.T., Lattarulo C.R., Wu H.Y., Hyman B.T., and Bacskai B.J., 2008. Aβ plaques lead to aberrant regulation of calcium homeostasis in vivo resulting in structural and functional disruption of neuronal networks. *Neuron*. 59, 214-25.

167. Arispe N., Pollard H.B., and Rojas E., 1994. The ability of amyloid β-protein [AβP (1-40)] to form Ca^{2+} channels provides a mechanism for neuronal death in Alzheimer's disease. *Ann. N Y Acad. Sci.* 747, 256-66.

168. Amaral D. and Lavenex P., *Hippocampal Neuroanatomy*, in *The Hippocampus Book*, P. Anderson, et al., Editors. 2007, Oxford University Press. p. 38.

169. West M.J., Kawas C.H., Martin L.J., and Troncoso J.C., 2000. The CA1 region of the human hippocampus is a hot spot in Alzheimer's disease. *Ann. N Y Acad. Sci.* 908, 255-9.

170. Calhoun M.E., Kurth D., Phinney A.L., Long J.M., Hengemihle J., Mouton P.R., Ingram D.K., and Jucker M., 1998. Hippocampal neuron and synaptophysin-positive bouton number in aging C57BL/6 mice. *Neurobiol. Aging*. 19, 599-606.

171. Jones L.C., Beard J.L., and Jones B.C., 2008. Genetic analysis reveals polygenic influences on iron, copper, and zinc in mouse hippocampus with neurobiological implications. *Hippocampus*. 18, 398-410.

172. Bastian C. and Li Y.V., 2007. Fluorescence imaging study of extracellular zinc at the hippocampal mossy fiber synapse. *Neurosci. Lett.* 419, 119-24.

173. Huang X., Cuajungco M.P., Atwood C.S., Moir R.D., Tanzi R.E., and Bush A.I., 2000. Alzheimer's disease, β-amyloid protein and zinc. *J. Nutr.* 130, 1488S-92S.

174. Schlief M.L., Craig A.M., and Gitlin J.D., 2005. NMDA receptor activation mediates copper homeostasis in hippocampal neurons. *J. Neurosci.* 25, 239-46.

175. Frederickson C.J., Suh S.W., Silva D., Frederickson C.J., and Thompson R.B., 2000. Importance of zinc in the central nervous system: the zinc-containing neuron. *J. Nutr.* 130, 1471S-83S.

176. Zhang L.H., Wang X., Zheng Z.H., Ren H., Stoltenberg M., Danscher G., Huang L., Rong M., and Wang Z.Y., 2008. Altered expression and distribution of zinc transporters in APP/PS1 transgenic mouse brain. *Neurobiol Aging*.

177. Wenzel H.J., Cole T.B., Born D.E., Schwartzkroin P.A., and Palmiter R.D., 1997. Ultrastructural localization of zinc transporter-3 (ZnT-3) to synaptic vesicle membranes within mossy fiber boutons in the hippocampus of mouse and monkey. *Proc. Natl. Acad. Sci. U S A.* 94, 12676-81.

178. Frederickson C.J., Klitenick M.A., Manton W.I., and Kirkpatrick J.B., 1983. Cytoarchitectonic distribution of zinc in the hippocampus of man and the rat. *Brain Res.* 273, 335-9.

179. Vogt S., 2003. MAPS: A set of software tools for analysis and visualization of 3D X-ray fluorescence data sets. *Journal De Physique Iv*. 104, 635-638.

180. Magaki S., Raghavan R., Mueller C., Oberg K.C., Vinters H.V., and Kirsch W.M., 2007. Iron, copper, and iron regulatory protein 2 in Alzheimer's disease and related dementias. *Neurosci. Lett.* 418, 72-6.

181. Morris C.M., Kerwin J.M., and Edwardson J.A., 1994. Non-haem iron histochemistry of the normal and Alzheimer's disease hippocampus. *Neurodegeneration*. 3, 267-75.

182. Connor J.R., Snyder B.S., Beard J.L., Fine R.E., and Mufson E.J., 1992. Regional distribution of iron and iron-regulatory proteins in the brain in aging and Alzheimer's disease. *J. Neurosci. Res.* 31, 327-35.

183. House M.J., St Pierre T.G., Foster J.K., Martins R.N., and Clarnette R., 2006. Quantitative MR imaging R2 relaxometry in elderly participants reporting memory loss. *AJNR Am J Neuroradiol*. 27, 430-9.

184. El Tannir El Tayara N., Delatour B., Le Cudennec C., Guegan M., Volk A., and Dhenain M., 2006. Age-related evolution of amyloid burden, iron load, and MR relaxation times in a transgenic mouse model of Alzheimer's disease. *Neurobiol. Dis.* 22, 199-208.

185. Takahashi S., Takahashi I., Sato H., Kubota Y., Yoshida S., and Muramatsu Y., 2001. Age-related changes in the concentrations of major and trace elements in the brain of rats and mice. *Biol Trace Elem Res*. 80, 145-58.

186. Gorter J.A., Mesquita A.R., van Vliet E.A., da Silva F.H., and Aronica E., 2005. Increased expression of ferritin, an iron-storage protein, in specific regions of the parahippocampal cortex of epileptic rats. *Epilepsia*. 46, 1371-9.

187. Bartzokis G., Tishler T.A., Shin I.S., Lu P.H., and Cummings J.L., 2004. Brain ferritin iron as a risk factor for age at onset in neurodegenerative diseases. *Ann N Y Acad Sci*. 1012, 224-36.

188. Griffiths P.D., Dobson B.R., Jones G.R., and Clarke D.T., 1999. Iron in the basal ganglia in Parkinson's disease. An in vitro study using extended X-ray absorption fine structure and cryo-electron microscopy. *Brain*. 122 (Pt 4), 667-73.

189. Gutteridge J.M., 1992. Iron and oxygen radicals in brain. *Ann Neurol*. 32 Suppl, S16-21.

190. Zhang L.H., Wang X., Zheng Z.H., Ren H., Stoltenberg M., Danscher G., Huang L., Rong M., and Wang Z.Y., 2008. Altered expression and distribution of zinc transporters in APP/PS1 transgenic mouse brain. *Neurobiol. Aging*.

191. Linkous D.H., Flinn J.M., Koh J.Y., Lanzirotti A., Bertsch P.M., Jones B.F., Giblin L.J., and Frederickson C.J., 2008. Evidence that the ZNT3 protein controls the total amount of elemental zinc in synaptic vesicles. *J Histochem Cytochem*. 56, 3-6.

192. Itoh T., Saito T., Fujimura M., Watanabe S., and Saito K., 1993. Restraint stress-induced changes in endogenous zinc release from the rat hippocampus. *Brain Res*. 618, 318-22.

193. Vandenberg R.J., Mitrovic A.D., and Johnston G.A., 1998. Molecular basis for differential inhibition of glutamate transporter subtypes by zinc ions. *Mol Pharmacol*. 54, 189-96.

194. Leskovjan A.C., Kretlow A., and Miller L.M., 2009. Unsaturated lipid content is reduced in the hippocampus of the PSAPP transgenic mouse model of Alzheimer's disease. *Anal. Chem.* Submitted.

195. Sastry P.S., 1985. Lipids of nervous tissue: composition and metabolism. *Prog. Lipid. Res.* 24, 69-176.

196. Montine T.J., Neely M.D., Quinn J.F., Beal M.F., Markesbery W.R., Roberts L.J., and Morrow J.D., 2002. Lipid peroxidation in aging brain and Alzheimer's disease. *Free Radic. Biol. Med.* 33, 620-6.

197. Sayre L.M., Zelasko D.A., Harris P.L., Perry G., Salomon R.G., and Smith M.A., 1997. 4-Hydroxynonenal-derived advanced lipid peroxidation end products are increased in Alzheimer's disease. *J. Neurochem.* 68, 2092-7.

198. Williams T.I., Lynn B.C., Markesbery W.R., and Lovell M.A., 2006. Increased levels of 4-hydroxynonenal and acrolein, neurotoxic markers of lipid peroxidation, in the brain in Mild Cognitive Impairment and early Alzheimer's disease. *Neurobiol. Aging*. 27, 1094-9.

199. Abdul H.M., Sultana R., St Clair D.K., Markesbery W.R., and Butterfield D.A., 2008. Oxidative damage in brain from human mutant APP/PS-1 double knock-in mice as a function of age. *Free Radic. Biol. Med.* 45, 1420-5.

200. Pratico D., Uryu K., Leight S., Trojanoswki J.Q., and Lee V.M., 2001. Increased lipid peroxidation precedes amyloid plaque formation in an animal model of Alzheimer amyloidosis. *J. Neurosci.* 21, 4183-7.

201. Hensley K., Hall N., Subramaniam R., Cole P., Harris M., Aksenov M., Aksenova M., Gabbita S.P., Wu J.F., Carney J.M., and et al., 1995. Brain regional correspondence between Alzheimer's disease histopathology and biomarkers of protein oxidation. *J. Neurochem.* 65, 2146-56.

202. Sills R.H., Moore D.J., and Mendelsohn R., 1994. Erythrocyte peroxidation: quantitation by Fourier transform infrared spectroscopy. *Anal. Biochem.* 218, 118-23.

203. Liu K.Z., Bose R., and Mantsch H.H., 2002. Infrared spectroscopic study of diabetic platelets. *Vib. Spectrosc.* 28, 131-136.

204. Severcan F., Gorgulu G., Gorgulu S.T., and Guray T., 2005. Rapid monitoring of diabetes-induced lipid peroxidation by Fourier transform infrared spectroscopy: evidence from rat liver microsomal membranes. *Anal. Biochem.* 339, 36-40.

205. Humecki J., ed. *Practical Guide to Infrared Microspectroscopy*. Practical Spectroscopy Series. Vol. 19. 1995, CRC Press: New York.

206. Stuart B., *Biological Applications of Infrared Spectroscopy*. 1997, Chichester: John Wiley & Sons, Ltd.

207. Pidgeon C., Apostol G., and Markovich R., 1989. Fourier transform infrared assay of liposomal lipids. *Anal. Biochem.* 181, 28-32.

208. Roher A.E., Weiss N., Kokjohn T.A., Kuo Y.M., Kalback W., Anthony J., Watson D., Luehrs D.C., Sue L., Walker D., Emmerling M., Goux W., and Beach T., 2002. Increased Aβ peptides and reduced cholesterol and myelin proteins characterize white matter degeneration in Alzheimer's disease. *Biochemistry*. 41, 11080-90.

209. Salat D.H., Tuch D.S., van der Kouwe A.J., Greve D.N., Pappu V., Lee S.Y., Hevelone N.D., Zaleta A.K., Growdon J.H., Corkin S., Fischl B., and Rosas H.D., 2008. White matter pathology isolates the hippocampal formation in Alzheimer's disease. *Neurobiol. Aging*.

210. Wells M.A. and Dittmer J.C., 1967. A comprehensive study of the postnatal changes in the concentration of the lipids of developing rat brain. *Biochemistry*. 6, 3169-75.

211. Zabelinskii S.A., Chebotareva M.A., Kostkin V.B., and Krivchenko A.I., 1999. Phospholipids and their fatty acids in mitochondria, synaptosomes and myelin from the liver and brain of trout and rat: a new view on the role of fatty acids in membranes. *Comp. Biochem. Physiol. B Biochem. Mol. Biol.* 124, 187-93.

212. Norton W.T. and Poduslo S.E., 1973. Myelination in rat brain: changes in myelin composition during brain maturation. *J. Neurochem.* 21, 759-73.

213. Oulton M.R. and Mezei C., 1976. Characterization of myelin of chick sciatic nerve during development. *J. Lipid Res.* 17, 167-75.

214. Malone M.J. and Szoke M.C., 1982. Neurochemical studies in aging brain. I. Structural changes in myelin lipids. *J Gerontol*. 37, 262-7.

215. Soderberg M., Edlund C., Kristensson K., and Dallner G., 1990. Lipid compositions of different regions of the human brain during aging. *J. Neurochem.* 54, 415-23.

216. Zhang Y., Appelkvist E.L., Kristensson K., and Dallner G., 1996. The lipid compositions of different regions of rat brain during development and aging. *Neurobiol. Aging*. 17, 869-75.

217. Pallottini V., Marino M., Cavallini G., Bergamini E., and Trentalance A., 2003. Age-related changes of isoprenoid biosynthesis in rat liver and brain. *Biogerontology*. 4, 371-8.

218. Edlund C., Soderberg M., and Kristensson K., 1994. Isoprenoids in aging and neurodegeneration. *Neurochem Int*. 25, 35-8.

219. Youdim K.A., Martin A., and Joseph J.A., 2000. Essential fatty acids and the brain: possible health implications. *Int. J. Dev. Neurosci.* 18, 383-99.

220. Avdulov N.A., Chochina S.V., Igbavboa U., O'Hare E.O., Schroeder F., Cleary J.P., and Wood W.G., 1997. Amyloid β-peptides increase annular and bulk fluidity and induce lipid peroxidation in brain synaptic plasma membranes. *J. Neurochem.* 68, 2086-91.

221. Mark R.J., Lovell M.A., Markesbery W.R., Uchida K., and Mattson M.P., 1997. A role for 4-hydroxynonenal, an aldehydic product of lipid peroxidation, in disruption of ion homeostasis and neuronal death induced by amyloid beta-peptide. *J. Neurochem.* 68, 255-64.

222. Markesbery W.R., Kryscio R.J., Lovell M.A., and Morrow J.D., 2005. Lipid peroxidation is an early event in the brain in amnestic mild cognitive impairment. *Ann. Neurol.* 58, 730-735.

223. Gu F., Zhu M., Shi J., Hu Y., and Zhao Z., 2008. Enhanced oxidative stress is an early event during development of Alzheimer-like pathologies in presenilin conditional knock-out mice. *Neurosci. Lett.* 440, 44-8.

224. Sturchler-Pierrat C., Abramowski D., Duke M., Wiederhold K.H., Mistl C., Rothacher S., Ledermann B., Burki K., Frey P., Paganetti P.A., Waridel C., Calhoun M.E., Jucker M., Probst A., Staufenbiel M., and Sommer B., 1997. Two amyloid precursor protein transgenic mouse models with Alzheimer disease-like pathology. *Proc. Natl. Acad. Sci. U S A*. 94, 13287-92.

225. McGowan E., Sanders S., Iwatsubo T., Takeuchi A., Saido T., Zehr C., Yu X., Uljon S., Wang R., Mann D., Dickson D., and Duff K., 1999. Amyloid phenotype characterization of transgenic mice overexpressing both mutant amyloid precursor protein and mutant presenilin 1 transgenes. *Neurobiol. Dis.* 6, 231-44.

226. Davis E.J., Foster T.D., and Thomas W.E., 1994. Cellular forms and functions of brain microglia. *Brain Res. Bull.* 34, 73-8.

227. Norton W.T., Abe T., Poduslo S.E., and DeVries G.H., 1975. The lipid composition of isolated brain cells and axons. *J. Neurosci. Res.* 1, 57-75.

228. Pike C.J., Cummings B.J., and Cotman C.W., 1995. Early association of reactive astrocytes with senile plaques in Alzheimer's disease. *Exp. Neurol.* 132, 172-9.

229. Casanova M.F., Stevens J.R., and Kleinman J.E., 1990. Astrocytosis in the molecular layer of the dentate gyrus: a study in Alzheimer's disease and schizophrenia. *Psychiatry Res.* 35, 149-66.

230. Chalmers K., Wilcock G., and Love S., 2005. Contributors to white matter damage in the frontal lobe in Alzheimer's disease. *Neuropathol. Appl. Neurobiol.* 31, 623-31.

231. Sjobeck M. and Englund E., 2003. Glial levels determine severity of white matter disease in Alzheimer's disease: a neuropathological study of glial changes. *Neuropathol. Appl. Neurobiol.* 29, 159-69.

232. Brun A. and Englund E., 1986. A white matter disorder in dementia of the Alzheimer type: a pathoanatomical study. *Ann. Neurol.* 19, 253-62.

233. Takeda A., Suzuki M., and Oku N., 2002. Possible involvement of plasma histidine in differential brain permeability to zinc and cadmium. *Biometals*. 15, 371-5.

234. Takeda A., 2001. Zinc homeostasis and functions of zinc in the brain. *Biometals*. 14, 343-51.

235. Mocchegiani E., Bertoni-Freddari C., Marcellini F., and Malavolta M., 2005. Brain, aging and neurodegeneration: role of zinc ion availability. *Prog. Neurobiol.* 75, 367-90.

236. Grundke-Iqbal I., Fleming J., Tung Y.C., Lassmann H., Iqbal K., and Joshi J.G., 1990. Ferritin is a component of the neuritic (senile) plaque in Alzheimer dementia. *Acta Neuropathol.* 81, 105-10.

237. Bishop G.M. and Robinson S.R., 2001. Quantitative analysis of cell death and ferritin expression in response to cortical iron: implications for hypoxia-ischemia and stroke. *Brain Res*. 907, 175-87.

238. Hegde M.L., Bharathi P., Suram A., Venugopal C., Jagannathan R., Poddar P., Srinivas P., Sambamurti K., Rao K.J., Scancar J., Messori L., Zecca L., and Zatta P., 2009. Challenges Associated with Metal Chelation Therapy in Alzheimer's Disease. *J Alzheimers Dis*.